Doctoral Thesis

Biomechanical Study on Mechanisms Underlying Hyperosmotic Responses of Tubular Epithelial Cells

Department of Mechanical Systems Engineering,

Graduate School of Systems Design,

Tokyo Metropolitan University

TAKASHI MIYANO

September 2023

Biomechanical Study on Mechanisms

Underlying Hyperosmotic Responses of Tubular Epithelial Cells

Takashi Miyano

Abstract

Chronic kidney disease (CKD) has been recognized as a leading public health problem worldwide, and about 13% of the Japanese adult population is predicted to have CKD. CKD can progress to end-stage chronic renal disease, which requires dialysis or kidney transplants in life-threatening conditions. Renal fibrosis is the final common pathway for nearly all forms of CKD, and the progression of tubular interstitial fibrosis coincides with the degree of renal dysfunction. Therefore, the identification of effective therapeutic targets for renal fibrosis has been required.

Because the proximal tubule is a major site for the reabsorption of water and solutes, proximal tubular epithelial cells are constantly exposed to various levels of osmotic stress that generates not only osmotic but also mechanical stresses in cells. Higher urine osmolarity has been found to be associated with a higher risk of initiating dialysis, and increased water intake lowers urine osmolality retards the progression of CKD. These results suggest dysfunctions of tubular epithelial cells induced by hyperosmotic conditions play an important role in the pathogenesis and the progression of tubular interstitial fibrosis; however, the effects of hyperosmotic stress on tubular epithelial cells remain unclear.

The purpose of this dissertation is to propose new therapeutic targets for the treatment of CKD by revealing the cellular responses to hyperosmotic conditions and the underlying mechanisms from the perspective of cell biomechanics. The author examined the effects of hyperosmotic stress on epithelial-mesenchymal transition (EMT) and autophagy of proximal tubular epithelial cells, which have been identified as key events involved in the progression and suppression of renal fibrosis. I also investigated the molecular mechanisms of cellular hyperosmotic responses to identify key molecules that could lead to new drug targets.

Firstly, the author observed the effects of hyperosmotic stress using mannitol and urea as osmolytes on the morphology and cytoskeletal structure of cultured tubular epithelial cells, which play a crucial role in determining the mechanical properties and behaviors of cells. The hyperosmotic condition above a threshold concentration of mannitol, which is believed to be between 100 and 200 mM in this study, causes an obvious decrease in cell volume and actin cytoskeleton alterations, and induces a decrease or inhibition of cell growth without altering cell viability in proximal tubular epithelial cells. On the other hand, treatment with urea did not cause any significant changes in the cell volume and the actin cytoskeleton. These results indicate hyperosmotic mannitol stress could cause cell shrinkage concomitant with changes in the actin cytoskeleton.

Secondly, since calcium ion (Ca^{2+}) is an important intracellular signaling factor in the process of converting mechanical forces into biochemical signals within a cell, I focused on the effect of hyperosmotic stress on the dynamics of intracellular concentrations of Ca^{2+} in tubular epithelial cells. Hyperosmotic mannitol stress caused a transient Ca^{2+} influx, and a similar phenomenon was observed with disruption of the actin cytoskeleton using cytochalasin D. Furthermore, an antagonist of TRP vanilloid 4 (TRPV4) calcium

channels, which act as a sensor of mechanical stimuli, significantly inhibited Ca^{2+} influx in response to hyperosmotic stress. Thus, hyperosmotic mannitol stress induces a transient Ca^{2+} influx, implying the involvement of TRPV4 channel activation.

A growing body of evidence suggests that renal tubular EMT plays an important role in the progression of acute and chronic kidney damage. To investigate the mechanisms involved in hyperosmolarity-induced EMT, the author examined the effects of hyperosmotic stress on α-smooth muscle actin (α-SMA) expression and focal adhesions (FA) dynamics, which connect the actin cytoskeleton and extracellular matrix and play important roles in the mechanotransduction of cells. Hyperosmotic stress reduced the expression of an epithelial cell marker, E-cadherin, and enhanced the expression of a mesenchymal cell marker, α-SMA protein, indicating the initiation of EMT. I also confirmed that the FA rearrangement in response to hyperosmotic stress is one of the mechanisms responsible for the EMT of proximal tubular epithelial cells. Furthermore, an antagonist of the TRPV4 channel was found to prevent the EMT induction. These results suggest that TRPV4 channels, which are involved in the initial step of Ca^{2+} influx, could be potential therapeutic targets for controlling the progression of EMT.

Finally, the effects of hyperosmotic stress on autophagy, which regulates intracellular homeostasis, were examined. Hyperosmotic stress elevated protein levels of the autophagosome marker LC3-II in proximal tubular epithelial cells, indicating induction of autophagy. The prevention of the reorganization of the actin cytoskeleton by cytochalasin D impaired the increase in the LC3-II levels. However, inhibition of the microtubule dynamics by nocodazole did not alter the expression of LC3-II. Thus, the reorganization of the actin cytoskeleton plays a critical role in the induction of hyperosmotic stress-induced autophagy. I also confirmed that nuclear translocation of

transcription factor EB (TFEB), known as a master regulator of autophagy, contributes to hyperosmotic stress-induced autophagy, and this phenomenon was regulated by the activation of transient receptor potential mucolipin 1 (TRPML1) channel, a lysosomal specific Ca^{2+}-permeable ion channel. These findings suggest that activation of the TRPML1 channel of tubular epithelial cells is a potential therapeutic target for renal protection by autophagy under hyperosmotic conditions.

In this dissertation, the author attempted to propose new therapeutic targets for the treatment of CKD by revealing the cellular responses to hyperosmotic conditions and their mechanisms from the perspective of cell biomechanics. The main findings of this study are as follows: Increased proximal tubular hyperosmotic stress responds to mechanical stress promotes reorganization of FAs in proximal tubular epithelial cells and induces EMT. The mechanism of EMT involves Ca^{2+} influx from outside the cell through TRPV4 channels, which are known as mechanosensing receptors. Furthermore, changes in the actin cytoskeleton induced by hyperosmotic stress are important for the induction of autophagy, a cytoprotective mechanism, and the activation of calcineurin-TFEB pathway through TRPML1 channels-mediated Ca^{2+} release from lysosomes is thought to be partly involved in the mechanism for the autophagy.

The author believes that the results of this dissertation open up possibilities of targeted interventions to treat CKD by modulating the activity of TRPV4 and TRPML1 channels.

Contents

Chapter 1

Introduction

1.1 Kidney function and structure

The kidneys are a pair of bean-shaped organs located in the back of the abdomen. They play a crucial role in maintaining the body's fluid balance, electrolyte balance, and acid-base balance, as well as regulating blood pressure, producing hormones, and autacoids that stimulate the production of red blood cells.

Figure 1-1 shows the kidney structure [1]. The structure of the kidney is complex, consisting of several parts that work together to perform functions. The outer layer of the kidney is called the renal cortex, which contains millions of small filtering units called nephrons. Each nephron is composed of a glomerulus and a tubule. The glomerulus is a network of tiny blood vessels that filter waste products and excess fluid from the blood, while the tubule reabsorbs nutrients and water back into the bloodstream and excretes waste products and excess fluid as urine. The renal tubule has 3 components: the proximal tubule, the Loop of Henle, and the distal tubule.

The proximal tubule is the first section of the renal tubule and is responsible for the majority of reabsorption that occurs in the nephron. The proximal tubule reabsorbs nutrients such as glucose and amino acids, ions like sodium, potassium, and chloride, and water from the filtrate. This reabsorption occurs due to the presence of transporters and channels on the basolateral (facing the interstitial) and apical membranes (facing the tubular lumen) of tubular epithelial cells lining renal tubules.

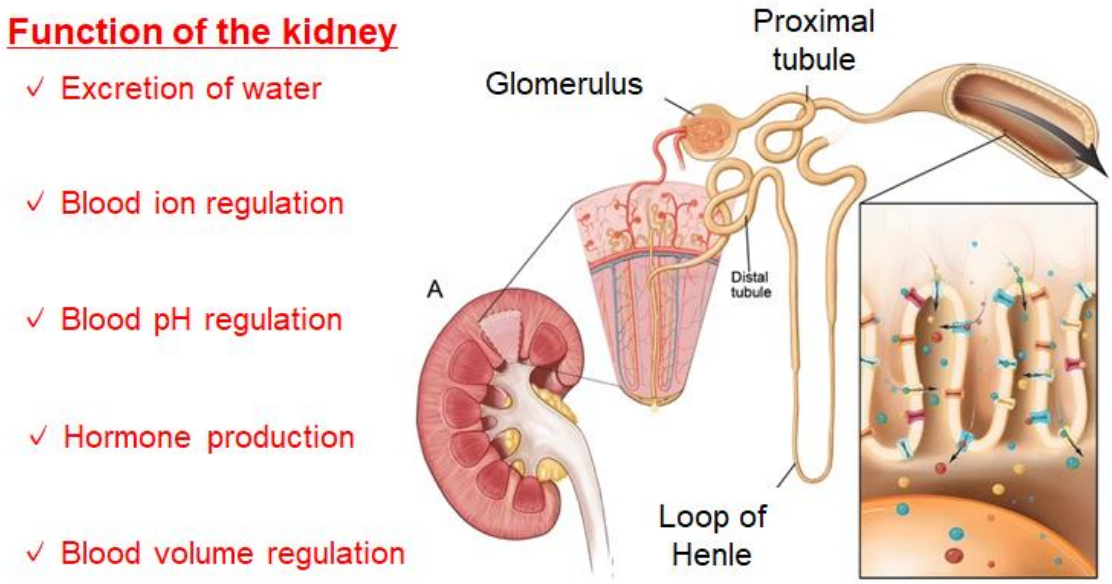

Fig. 1-1 Illustration of kidney structure (Modified from Wessely et al., 2014 [1]).

1.2 Chronic kidney disease (CKD) and Acute kidney injury (AKI)

1.2.1 CKD

Chronic kidney disease (CKD) describes the progressive renal dysfunction that leads to a permanent and irremediable loss of renal function [2]. CKD is usually caused by unhealthy conditions, such as high blood pressure, diabetes, or autoimmune diseases [2]. CKD has been recognized as a leading public health problem worldwide (the world's fifth major cause of mortality by 2040) and the number of CKD patients in Japan is estimated at about 13 million (about 13% of the Japanese adult population) [3-5]. Progression of CKD may lead to end-stage renal disease (ESRD), which requires renal replacement therapy such as dialysis or transplantation. Since current therapies have limited effectiveness and only delay CKD progression, it is desirable to identify novel attractive targets for the prevention and treatment of CKD.

1.2.2 AKI to CKD

Acute kidney injury (AKI) is a pathologic condition characterized by a steep decrease in glomerular filtration and results in the dysfunction or death of proximal tubule cells [6]. The main clinical causes include renal ischemia-reperfusion, nephrotoxins, and obstruction [6]. AKI is usually reversible if the underlying cause is identified and treated promptly.

Notably, while CKD and AKI are different conditions that affect the kidneys, they can sometimes occur together. AKI can occur as a complication of CKD, and CKD can also increase the risk of AKI. Indeed, approximately 50% of AKI patients who had recovered successfully from AKI were newly diagnosed with CKD during the median follow-up period of 3.3 years [7]. The hazard ratio of chronic dialysis in patients who had recovered from dialysis-requiring AKI was 3.23, compared to patients without dialysis-requiring AKI [8]. Thus, AKI is recognized as a risk factor for CKD.

In the progression from AKI to CKD, tubular epithelial cells undergo various changes, including necrosis, apoptosis, and G_2/M cell cycle arrest (Fig. 1-2) [9]. In the initial stages of AKI, tubular epithelial cells can undergo necrosis, which is a form of cell death characterized by rapid loss of cell membrane integrity and release of cellular contents into the surrounding tissue. Necrotic cells release damage-associated molecular pattern molecules, which activate identical pattern recognition receptors on dendritic cells or recruit leukocytes [10], causing them to secrete proinflammatory cytokines and chemokines [11]. Apoptosis, or programmed cell death, is another mechanism that plays a role in the transition from AKI to CKD [12]. Excessive or prolonged apoptosis can contribute to tubular cell loss and the development of interstitial fibrosis in CKD. G2/M cell cycle arrest refers to a temporary cell cycle arrest at the transition from the G_2 phase

to the M phase. This arrest can occur in response to cellular stress or DNA damage. Injured tubular epithelial cells may activate DNA damage response pathways and undergo cell cycle arrest to allow time for DNA repair or prevent the transmission of genetic abnormalities. However, prolonged or unresolved G_2/M cell cycle arrest can impair tubular cell regeneration and contribute to the progression of tubular injury toward CKD [13,14].

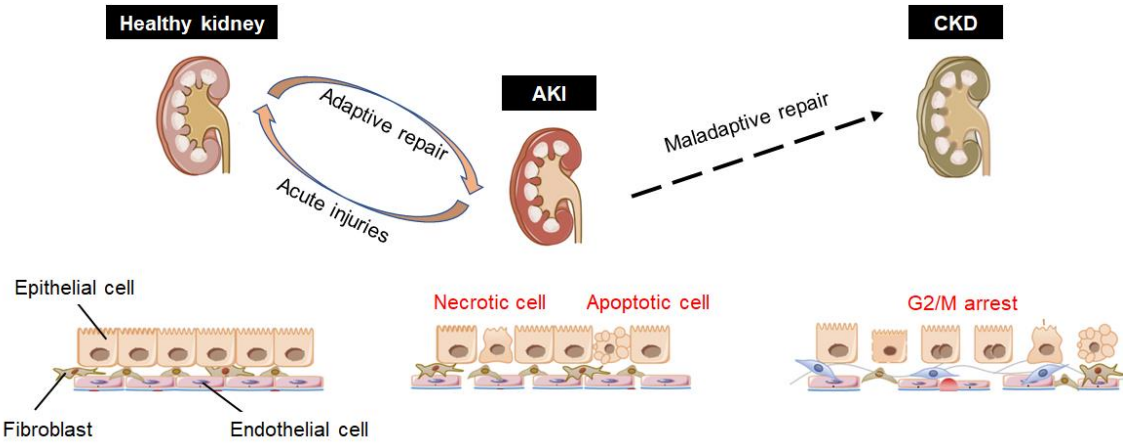

Fig. 1-2 Schematic illustration of pathophysiological processes involved in the AKI to CKD (Modified from Jiang et al., 2020 [9]).

Proximal tubules are susceptible to various kinds of cellular stress as described above and are therefore considered a main therapeutic target of AKI. Interestingly, previous studies showed that proximal tubular injury is both a primary trigger of AKI as well as a potential determinant of CKD progression [15-17]. These studies indicate that proximal tubular injury is both a primary trigger of AKI as well as a potential determinant of later disease progression, and that the protection of proximal tubules is essential to preventing the development of AKI and its progression to CKD [18].

1.2.3 Mannitol-induced AKI and hyperosmolarity

Elevation of blood plasma osmolality by administration of osmolytes, including mannitol ($C_6H_{14}O_6$), is clinically performed to reduce intracranial and intraocular pressures, but excessive administration is known to be an incidence and risk factor for AKI [19-21]. Mannitol-induced AKI is characterized by the structural changes that occur at the cellular level in the proximal tubule, including intracytoplasmic vacuolization and swelling of cells [22,23]. Excessive mannitol is not reabsorbed and leads to an increase in the osmolality in the proximal tubular fluid. The exact mechanism of mannitol-induced AKI has not been clarified but changes in tubular osmolarity and the osmolar gap may be the contributing factors [23].

There is increasing evidence linking high fluid intake, vasopressin suppression, and urine osmolarity control with the degree of renal dysfunction [24,25]. The Consortium for Radiologic Imaging Studies of Polycystic Kidney Disease (CRISP) reported that high urine osmolality was associated with a greater baseline glomerular filtration rate (GFR) but a steeper decline in GFR in patients with polycystic kidney disease [26]. Another retrospective clinical research also demonstrated that higher urine osmolarity is associated with a higher risk of initiating dialysis (Fig. 1-3) [27].

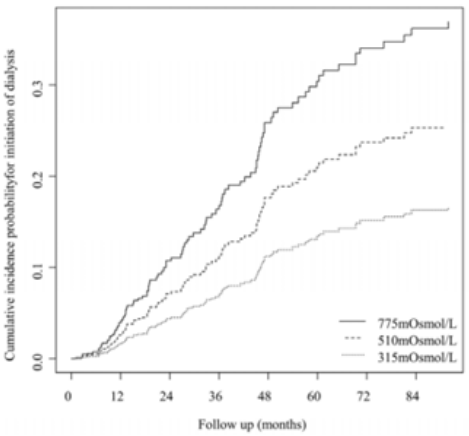

Fig. 1-3 Cumulative morbidity of dialysis initiation for urine osmolarity. Cumulative morbidity probabilities of dialysis initiation for a baseline urine osmolarity of 315, 510, or 775 mOsm/L, estimated from the proportional sub-distribution hazards model [27].

1.3 Renal fibrosis and associated cellular processes

Renal fibrosis, which is characterized by the accumulation of the extracellular matrix (ECM) such as collagen, connective tissue growth factor (CTGF), and fibronectin, is a final common pathway to end-stage renal disease of CKD progression (Fig. 1-4) [28,29]. The severity of renal fibrosis, especially tubulointerstitial fibrosis, closely correlated to the future appearance of renal failure and has therefore been associated with poor long-term prognosis [30,31]. Therefore, preventing the progression of tubulointerstitial fibrosis is recognized as an effective strategy for preventing CKD progression [32,33].

Epithelial-mesenchymal transition (EMT) and autophagy are two famous cellular processes that have been implicated in the development and protection of renal fibrosis. Understanding the molecular mechanisms underlying their interactions may provide insights into the development of therapeutic strategies for managing kidney fibrosis and preserving renal function.

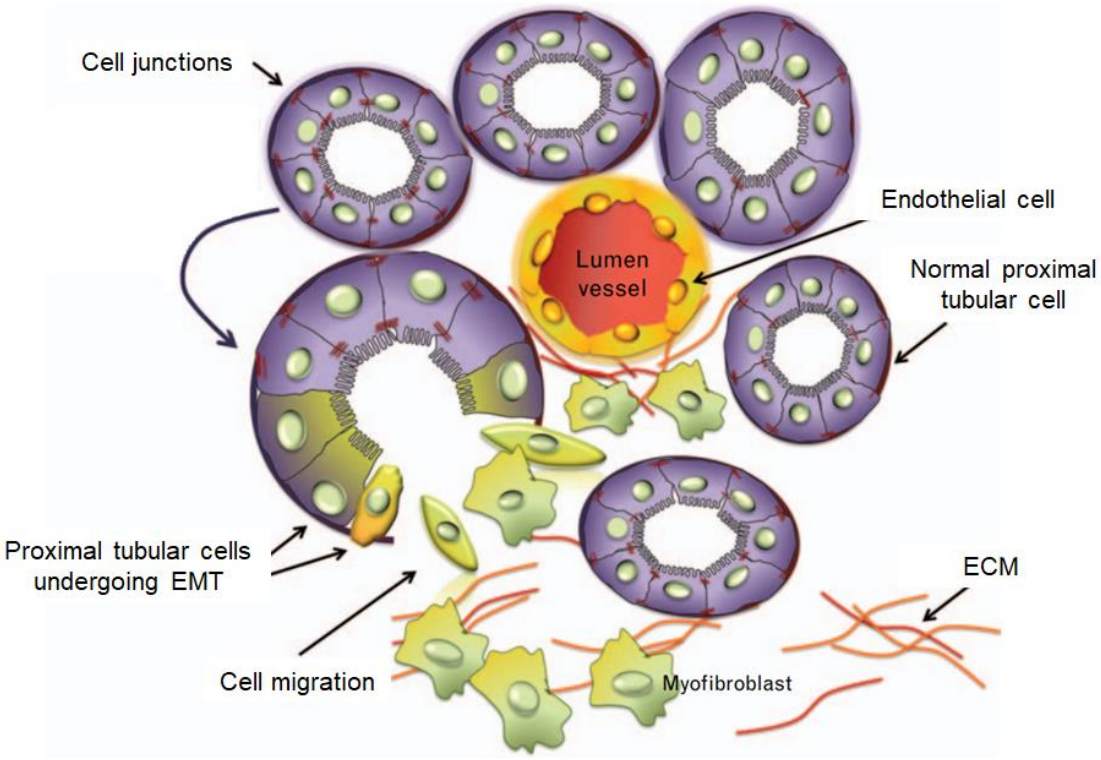

Fig. 1-4 Schematic illustration of renal fibrosis during the progression of CKD (Modified from Seccia et al., 2017 [34]). Extracellular matrices such as collagen and fibronectin are excessively accumulated in the renal tubulointerstitial during the progression of CKD. EMT, epithelial-mesenchymal transition; ECM, extracellular matrix.

1.3.1 Epithelial-mesenchymal transition (EMT)

Epithelial-mesenchymal transition (EMT) is a widely accepted mechanism by which injured tubular epithelial cells transform into myofibroblasts, and is involved in the pathogenesis of not only CKD but also in AKI [35,36]. Epithelial cells are characterized by apical, lateral, and basal plasma membrane domains and the lateral domain contains an adhesive structure that contributes to the establishment of apical-basal polarity [37]. Under physiologic conditions, tubular epithelial cells express epithelial markers, including E-cadherin, which is the major component of adherent junctions and tightly connects between cells. During EMT, the tubular epithelial cells lose their epithelial characteristics and acquire mesenchymal features, concomitant with the downregulation of E-cadherin, and the upregulation of mesenchymal markers, including α-smooth muscle actin (α-SMA) and vimentin (Fig. 1-5) [38]. α-SMA-positive myofibroblasts are known to induce the expression of profibrotic factors such as collagen, CTGF, fibronectin, and plasminogen activator inhibitor type 1 (PAI-1) in organ fibrosis [2,39,40].

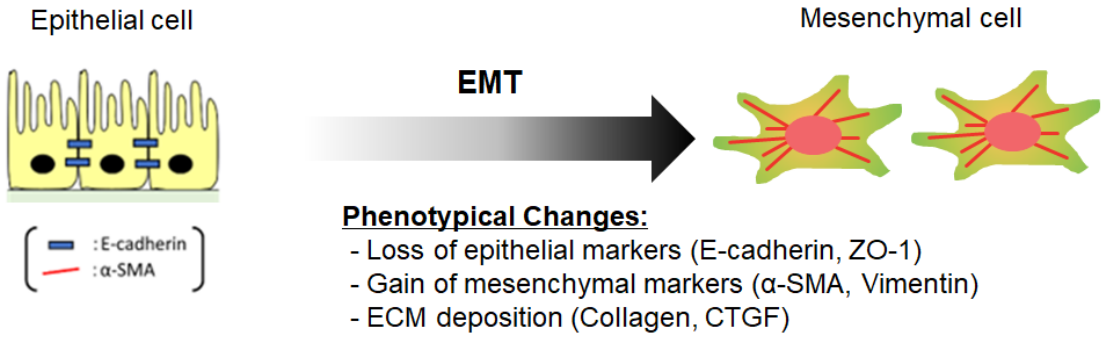

Fig. 1-5 Schematic illustration of changes in the molecular markers during EMT. E-cadherin is cell-cell contact proteins that are lost during EMT. α-SMA are mesenchymal markers that are gained during EMT.

Several cell types can differentiate into myofibroblasts, which are key contributors to tissue fibrosis. Experiments with genetically engineered mice have revealed that about half of myofibroblasts emerge through proliferation, and the rest are recruited through differentiation [41]. The total pool of myofibroblasts in kidney fibrosis is split (Fig. 1-6), with 50% derived through proliferation from resident fibroblasts. Non-proliferative myofibroblasts are 35% differentiated from bone marrow-derived cells, 10% arise from endothelial-mesenchymal transition, and 5% through EMT [41].

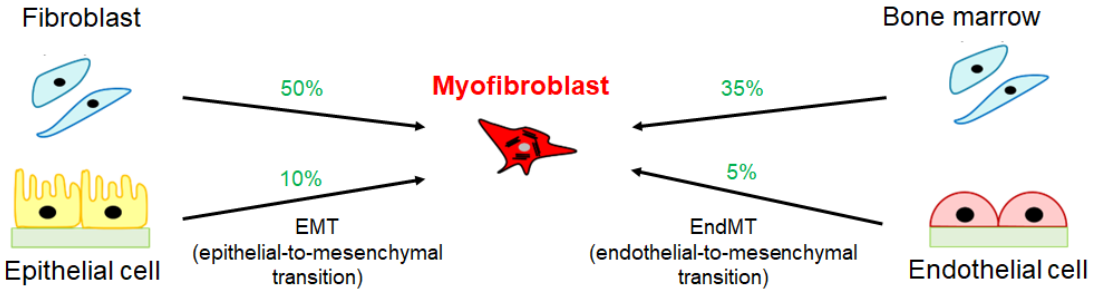

Fig. 1-6 Summary of cells that differentiate into myofibroblasts. Distinct cell types are involved in intestinal fibrosis, such as ECM-producing cells derived from fibroblasts, epithelial cells, bone marrow-derived fibroblasts, and endothelial cells.

Many inhibitors against EMT exerted profound therapeutic effects on renal diseases by suppressing differentiation into myofibroblasts and the production of ECM [42,43]. This is because EMT leads to the loss of epithelial cell-cell adhesion and disruption of the epithelial barrier, and this disruption allows for increased permeability, which can lead to the leakage of proteins, electrolytes, and other solutes into the interstitial space. Therefore, although the proportion of EMT-derived myofibroblasts is small, the EMT program is believed to play an important role in the progression of renal disease.

1.3.2 Autophagy

1.3.2.1 Autophagosome and LC3

Autophagy is a highly conserved "self-eating" pathway that eliminates damaged proteins and organelles and can be activated by pathophysiological stressors [44-46]. Figure 1-7 shows the autophagy process. The autophagic process initiates the formation of omegasomes, which expand into double-membrane-bound autophagic vesicles (autophagosomes). Autophagosomes fuse with lysosomes to generate autolysosomes, deleting harmful cellular components and restoring intracellular homeostasis [47,48]. The resulting breakdown products, such as amino acids and nucleotides, can be recycled and reused by the cell. Autophagosomes are tagged by a protein called lipid-conjugated microtubule-associated protein 1 light chain 3 (LC3) [49]. The conversion of soluble LC3-I to lipid-bound LC3-II is considered as an indicator of autophagosome formation [50]. Therefore, the amount of LC3-II correlates with the number of autophagosomes, and is usually used as a marker of autophagy [50].

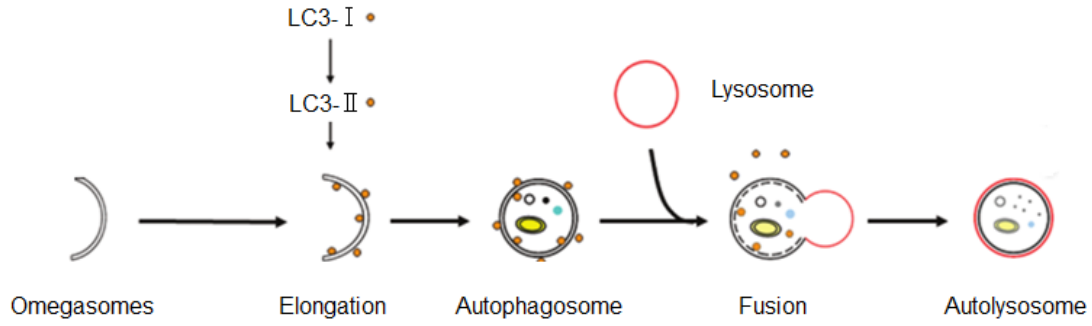

Fig. 1-7 Schematic illustration of the process of autophagy. Autophagy begins with the formation of the omegasomes, which leads to the expansion of the phagophore into an autophagosome (vesicle elongation). The autophagosome contains some different damaged organelles, which can fuse with a lysosome forming an autolysosome.

1.3.2.2 Transcriptional factor EB (TFEB)

The transcription factor EB (TFEB) is a member of the microphthalmia family of basic helix-loop-helix-leucine-zipper (bHLH-Zip) transcription factors [51]. TFEB is known as a major transcriptional regulator of autophagy-lysosome pathways and positively regulates the expression of autophagy and lysosomal gene [52,53].

TFEB activity is significantly regulated by phosphorylation events [54] (Fig. 1-8). While phosphorylated TFEB is retained in the cytoplasm binding to 14-3-3 proteins, dephosphorylated TFEB travels to the nucleus. Phosphorylation of TFEB is mainly mediated by the mammalian target of rapamycin complex 1 (mTORC1) kinase, a major kinase complex that is a negative regulator of autophagy [55]. When mTORC1 activity is inhibited, TFEB is dephosphorylated and translocated into the nucleus [56]. In parallel, the activity of the calcium-dependent protein phosphatase calcineurin is induced by lysosomal specific Ca^{2+}-permeable ion channels, TRPML1, which contribute to the nuclear translocation of TFEB [56].

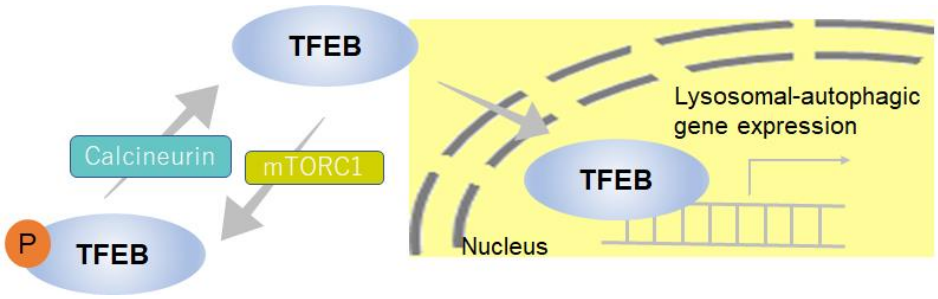

Fig. 1-8 Schematic illustration of the mechanism of TFEB activation. TFEB activity (nuclear translocation) is mainly regulated by its phosphorylation status that can be modulated by dephosphorylation by calcineurin and phosphorylation by mTORC1.

1.4 Cell biomechanics

Current research on diseases mainly focuses on the molecular, immunological, and pathological aspects of pathogenesis. However, the development of some diseases is usually accompanied by not only biological alterations, but also physical and structural (biomechanical) property changes in cells [57-59]. The biomechanical alterations in cells also play an important role in the genesis and development of disease and can also be a promising therapeutic target [57-59]. Indeed, some studies on the pathophysiology of a wide range of human diseases have suggested that their etiology might have resulted from deviation in the structural and mechanical properties of cells as well as from abnormal mechanotransduction [60,61]. This suggests that in disease states, cells sense abnormal mechanical signals, which disrupt or deregulate the molecular mechanisms by which cells sense mechanical signals and convert them into a chemical or electrical response [61]. Thus, molecules that mediate mechanotransduction, including extracellular matrix molecules, transmembrane receptors, cytoskeletal structures and associated signal transduction components, may therefore represent targets for therapeutic intervention in a variety of diseases.

These relationships among cell structure, biomechanics, and disease states are schematically illustrated in Fig. 1-9. This paradigm is interesting for considering mechanisms of pathological conditions and therapeutic targets from the perspective of cell biomechanics.

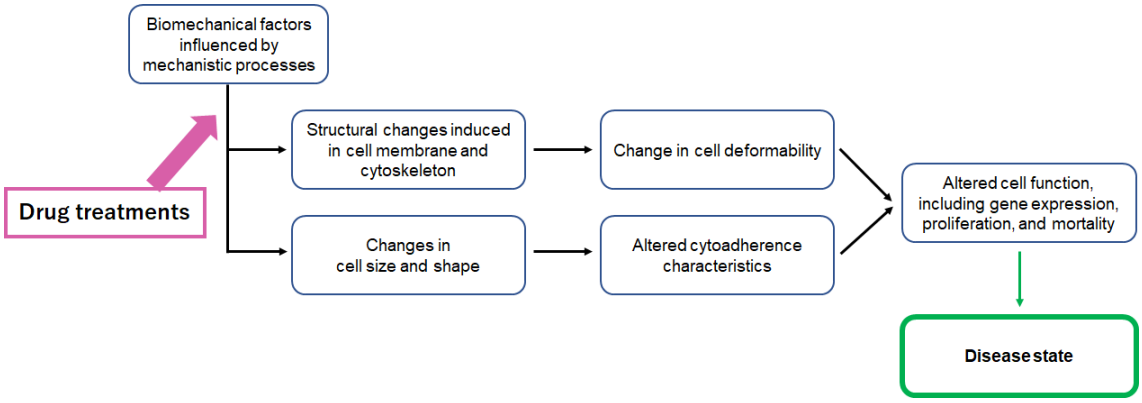

Fig. 1-9. Schematic of biomechanical pathways influencing connections among cellular structure, cell biomechanics, and disease (Modified from Suresh, 2007 [62]**).**

1.4.1 Tissue fibrosis and cell biomechanics

Different organs have distinct mechanical environments, and several studies have shown how mechanical stress impacts fibrosis in specific tissues [63,63] (Fig. 1-10). In organ fibrosis, it is clear from clinical practice that tissue stiffness varies with the disease state. Tissue stiffness is measured as the elastic modulus, and the values of fibrotic lung have been shown to range from approximately 2 kPa in normal tissue to about 17 kPa in fibrotic tissue [65]. The elastic modulus of fibrotic liver has also been reported to range from 3 kPa to 22 kPa [66]. Tissues are subject to wall shear stress caused by fluid flow through the vasculature, tubules, and interstitium. In particular, the effects of shear stress on vascular flow have been shown to be associated with cardiovascular disease and tissue remodeling. Tissues such as the kidney, liver, and lungs have large amounts of flow through specialized vessels, such as the glomerulus, sinusoid, and pulmonary, respectively. Changes in shear stress due to altered flow through these vessels are both a cause and a consequence of tissue remodeling and fibrosis [67]. Furthermore, fluid flowing in ducts such as bile ducts, pancreatic ducts, and renal tubules is another source

of shear stress in tissues that may be associated with fibrosis [68]. Other mechanical stresses that may act on fibrosis include hydrostatic pressure and stretching stimuli. Obstruction of the bile ducts and pancreatic ducts causes fibrosis, which may be at least partially due to changes in hydrostatic pressure [69]. Cyclic mechanical stretch is particularly important in the lungs, which undergo periodic stretching during respiration [70].

There are many unexplored aspects regarding the role of mechanical stresses in tissue fibrosis and mechanotransduction. Future work will need to expand our understanding of the effects of mechanical stress on fibrosis in biological tissues and may eventually lead to attractive targets based on the biomechanical characteristics of fibrosis.

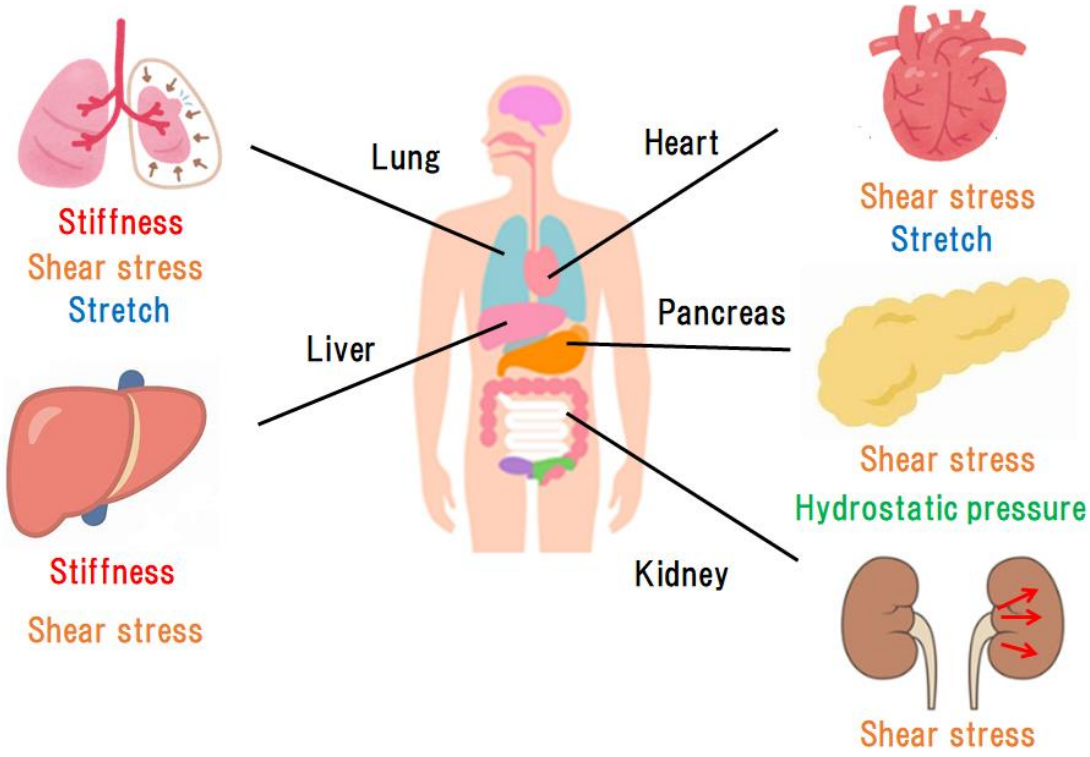

Fig. 1-10. Schematic diagram of mechanical stresses involved in tissue fibrosis.

1.5 Cellular response to hyperosmotic stresses

Biomechanics research often studies the mechanical properties and behaviors of cells, and it encompasses a wide range of cellular phenomena. The focus on specific cellular phenomena such as the changes in cell morphology, cytoskeleton structure, and calcium dynamics, is driven by their significant roles in cell biomechanics.

1.5.1 Actin cytoskeleton

The actin cytoskeleton is a network of protein fibers that provides structural support to the cell and helps maintain and change the cell shape. Actin filaments are involved in a variety of cellular responses, including cell migration, morphogenesis, endocytosis, phagocytosis and organelle dynamics [71]. Consequently, aberrant actin cytoskeleton dynamics are linked to various diseases, including cancer, as well as immunological and neurological disorders [72].

Rho-associated coiled-coil-containing protein kinase (ROCK) and myosin light chain kinase (MLCK) are factors that play important roles in the formation of actin filaments (Fig. 1-11). ROCK is a serine/tyrosine kinase activated by Rho and phosphorylates the myosin light chain (MLC) [73]. ROCK also promotes the phosphorylation of myosin light chain phosphatase (MLCP), thereby inhibiting the activity of MLCP and promoting MLC phosphorylation [74,75]. ROCK activation by Rho induces the formation of thick actin filament fibers (stress fibers) containing myosin II, tropomyosin, and MLC-kinase, and consequently of focal adhesions, which are immature integrin-based adhesion points with the extracellular substrate (described below) [76,77].

A previous study has shown that the actin filaments were disassembled and then reorganized into thick stress fibers in response to hyperosmotic stress [78]. The

mechanism is that hyperosmotic stress induces rapid activation of Rho and promotes phosphorylation of MLC by ROCK signaling [79,80]. It is also reported that hyperosmotic stress activates Rho/ROCK signaling and shrinkage-induced cofilin phosphorylation, which induces the reorganization of the actin cytoskeleton upon osmotic stress [81].

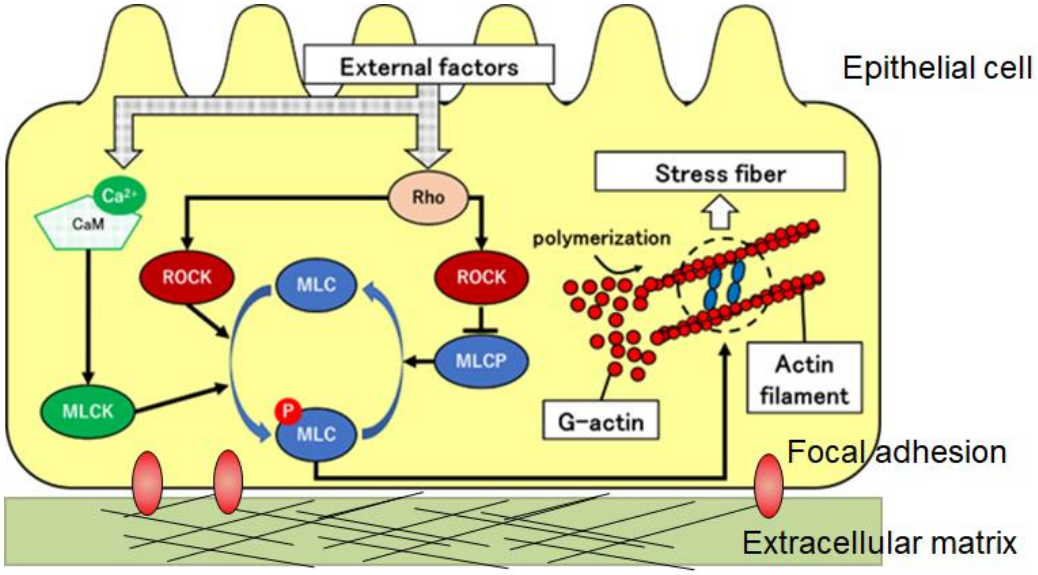

Fig. 1-11 Schematic illustration of the formation of actin stress fibers by ROCK and MLCK signaling. The process begins with the activation of Rho, which can be triggered by various extracellular factors. Activated Rho binds and activates ROCK, a downstream effector molecule. ROCK phosphorylates various target proteins involved in actin cytoskeletal dynamics.

1.5.2 Focal adhesion

Focal adhesions (FAs) are large, dynamic protein complexes that link the extracellular matrix to the actin cytoskeleton in the cell. The formation of FAs plays a critical role in cell adhesion, migration, and signaling. FAs are composed of several different proteins,

including integrins, talin, vinculin, and focal adhesion kinase (FAK) [82], and highly dynamic structures that undergo constant assembly and disassembly concomitant with cell movement. The FAs are also highly regulated by a variety of signaling pathways, including Rho signaling [71].

To the best of our knowledge, there are no studies regarding the effects of hyperosmotic stress on FAs. FAK may play an important role in mediating the transforming growth factor β (TGF-β) -induced EMT, suggesting FAs may be involved in EMT [83]. It has also been proposed that the size of FAs controls the recruitment of α-SMA to actin stress fibers [84-86] (Fig. 1-12). Therefore, FAs could be involved in the induction of EMT by controlling the expression of α-SMA.

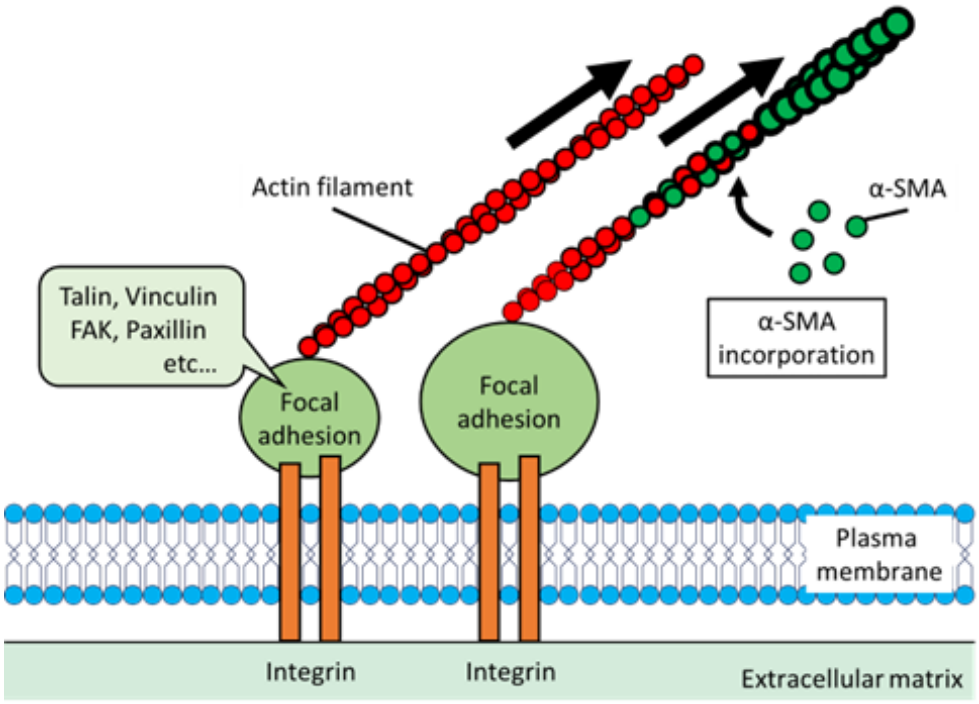

Fig. 1-12 Schematic illustration of the relationship between FAs and the recruitment of α-SMA. Actin filaments bind to the extracellular matrix via FAs. Larger focal adhesions may control the recruitment of α-SMA to actin filaments.

1.5.3 Ca^{2+} dynamics

The calcium ion (Ca^{2+}) is a ubiquitous intracellular second messenger to couple extracellular stimuli to their characteristic intracellular responses and to coordinate a wide range of endogenous processes [87]. The regulation of Ca^{2+} signaling is complex and involves a variety of ion channels and transporters that control the intracellular concentration of Ca^{2+} [87]. Increases of intracellular Ca^{2+} are known to mediate (A) voltage-gated and receptor-mediated channels, (B) mitochondrial Ca^{2+} uniporter (MCU) (C) store-operated channels which include the inositol trisphosphate receptor and ryanodine receptor, and (D) lysosomal channels [88] (Fig. 1-13).

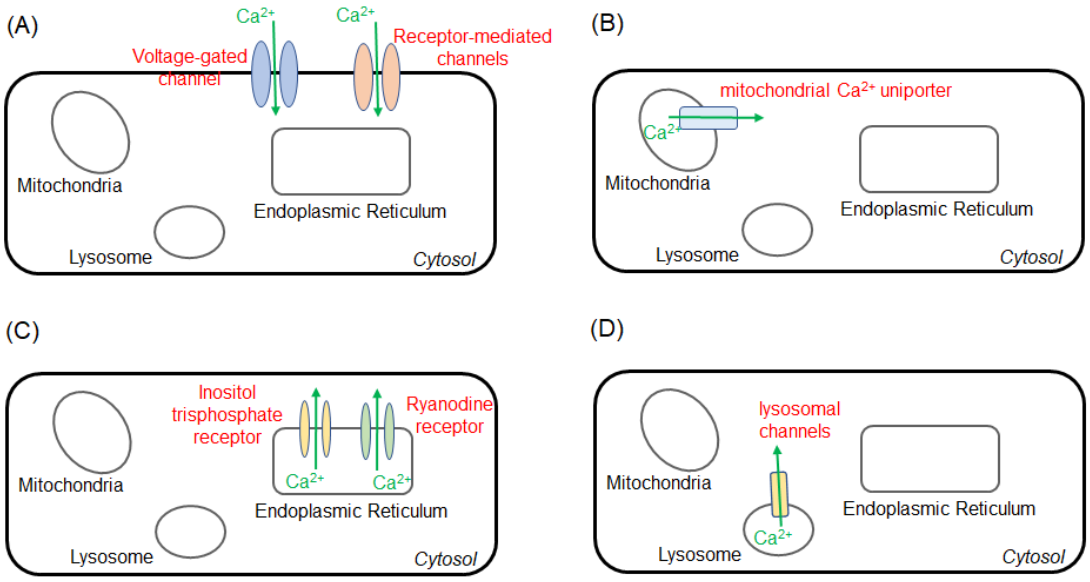

Fig. 1-13 Schematic illustration of the mechanisms of intracellular Ca^{2+} increases. (A) Ca^{2+} influx via Ca^{2+} channels on the plasma membrane. (B) Ca^{2+} release from the mitochondria. (C) Ca^{2+} release from the endoplasmic reticulum. (D) Ca^{2+} release from the lysosome.

Mechanosensing refers to the ability of cells and tissues to detect and respond to mechanical forces in their environment. The transient receptor potential (TRP) superfamily of channels comprises a diverse group of cation channels that can be directly or indirectly activated by mechanical forces, such as stretching, compression, or shear stress [81]. Modulating TRP channel activity provides an important way to impact cellular function by regulating both membrane excitability and intracellular calcium levels [89]. These channels respond to multiple types of stimuli and, in turn, allow cation entry.

TRP vanilloid 4 (TRPV4) is a nonselective cationic channel permeable to Ca^{2+}, Na^{+}, and Mg^{2+}, which can be activated by several stimuli, including changes in osmolarity, the temperature in the range of 25°C–37°C, and mechanical forces [90-92]. TRPV4 is widely expressed in various tissues, including the kidney, bladder, lung, and musculoskeletal system and is involved in the regulation of intracellular Ca^{2+} levels [93,94]. It is also known that TRPV4 interacts with the actin cytoskeletal network [95,96]. Although TRPV4 is known to be activated by hypoosmotic stress, recent studies suggest that TRPV4 could also be involved in hyperosmotic stress [97].

TRPML1 is an intracellular channel present in the membranes of both the lysosome and endosome, where it serves as the key regulator of Ca^{2+} efflux [98,99]. Ion flux mediated by TRPML1 may regulate lysosomal dynamics. Since the over-expression of TRPML1 results in a significant increase of the autophagic flux, whereas its mutations can affect the accumulation of autophagosome, TRPML1 has some role in the early steps of autophagy [100].

1.6 Objective and outline of the dissertation

Although CKD is increasingly recognized as a leading public health problem, current therapies have limited effectiveness and only delay CKD progression, and the identification of more effective therapeutic targets for CKD has been required. Considering the impact of AKI, which results in the dysfunction or death of proximal tubule cells, on an increased risk of progression to CKD, appropriate management of proximal tubular damage during AKI could suppress the progression of widespread nephron damage in CKD. As described above, since changes in cellular biomechanical properties caused by pathological environments play an important role in the genesis and development of diseases, studies on the effects of hyperosmotic stress as a biomechanical factor on tubular epithelial cells can lead to identification of novel therapeutic targets for kidney diseases.

In this dissertation, the author hypothesized that hyperosmotic stress induced by an overdose of mannitol, known as a risk factor for AKI, has effects on the proximal tubular epithelial cells and examined its effects focusing on the cytoskeleton, calcium dynamics, and protein expression changes from the perspective of cell biomechanics. By examining hyperosmotic stress on EMT and autophagy of proximal tubular epithelial cells, which have been identified as key mechanisms involved in the progression and suppression of renal fibrosis, the author clarified the molecular mechanism of cellular hyperosmotic responses to identify key molecules that could lead to new drug targets.

The dissertation is organized as follows:

Chapter 1 is introduction.

In Chapter 2, the author shows the effects of hyperosmotic stress using mannitol and urea as osmolytes on the cell morphology, cytoskeletal structure, and cell proliferation of

cultured proximal tubular epithelial cells.

In Chapter 3, the author presents the effect of hyperosmotic stress on the dynamics of intracellular concentrations of Ca^{2+} in proximal tubular epithelial cells. The authors also examined the mechanism of hyperosmotic stress-induced Ca^{2+} influx, focusing on TRPV4 channels.

In Chapter 4, the author describes the effect of hyperosmotic stress on the EMT of tubular epithelial cells and its mechanism. I examined the effects of hyperosmotic stress on EMT markers expression and FA dynamics in proximal tubular epithelial cells. Moreover, based on the Chapter 3 results, I investigated the effects of TRPV4-mediated calcium influx on EMT to better understand the mechanisms of hyperosmolarity-induced EMT.

In Chapter 5, the author investigates the mechanisms involved in hyperosmolarity-induced autophagy. For this purpose, I examined the relationship between the LC3 upregulation in response to hyperosmotic stress and the reorganization of the actin cytoskeleton. Moreover, I also examined the effects of hyperosmotic stress on TFEB nuclear translocation and its mechanism to better understand the mechanisms of hyperosmolarity-induced autophagy, focusing on TRPML1 channels.

In Chapter 6, this dissertation is concluded.

References

1. Wessely O, Cerqueira DM, Tran U, Kumar V, Hassey JM, Romaker D. The bigger the better: Determining nephron size in kidney. Pediatric Nephrology. 2014;29: 525–530.
2. Kalantar-Zadeh K, Jafar TH, Nitsch D, Neuen BL, Perkovic V. Chronic kidney disease. The Lancet. 2021;398: 786–802.
3. Jha V, Garcia-Garcia G, Iseki K, Li Z, Naicker S, Plattner B, et al. Chronic kidney disease: Global dimension and perspectives. The Lancet. 2013;382: 260–272.
4. Bikbov B, Purcell CA, Levey AS, Smith M, Abdoli A, Abebe M, et al. Global, regional, and national burden of chronic kidney disease, 1990–2017: a systematic analysis for the Global Burden of Disease Study 2017. The Lancet. 2020;395: 709–733.
5. Nagai K, Asahi K, Iseki K, Yamagata K. Estimating the prevalence of definitive chronic kidney disease in the Japanese general population. Clinical and Experimental Nephrology. 2021;25: 885–892.
6. Lameire NH, Bagga A, Cruz D, De Maeseneer J, Endre Z, Kellum JA, et al. Acute kidney injury: An increasing global concern. The Lancet. 2013;382: 170–179.
7. Bucaloiu ID, Kirchner HL, Norfolk ER, Hartle JE, Perkins RM. Increased risk of death and de novo chronic kidney disease following reversible acute kidney injury. Kidney International. 2012;81: 477–485.
8. Ireland R. Acute kidney injury: Risk of chronic dialysis and death in survivors of acute kidney injury. Nature Reviews Nephrology. 2009;5: 667.
9. Jiang M, Bai M, Lei J, Xie Y, Xu S, Jia Z, et al. Mitochondrial dysfunction and the AKI-to-CKD transition. AJP - Renal Physiology. 2020;319: F1105–F1116.

10. Leaf IA, Nakagawa S, Johnson BG, Cha JJ, Mittelsteadt K, Guckian KM, et al. Pericyte MyD88 and IRAK4 control inflammatory and fibrotic responses to tissue injury. The Journal of clinical investigation. 2017;127: 321–334.

11. Kurts C, Panzer U, Anders H-J, Rees AJ. The immune system and kidney disease: basic concepts and clinical implications. Nature reviews Immunology. 2013;13: 738–753.

12. Anders H-J, Ryu M. Renal microenvironments and macrophage phenotypes determine progression or resolution of renal inflammation and fibrosis. Kidney international. 2011;80: 915–925.

13. Yang L, Besschetnova TY, Brooks CR, Shah J V, Bonventre J V. Epithelial cell cycle arrest in G2/M mediates kidney fibrosis after injury. Nature medicine. 2010;16: 535–543.

14. Wu C-F, Chiang W-C, Lai C-F, Chang F-C, Chen Y-T, Chou Y-H, et al. Transforming growth factor β-1 stimulates profibrotic epithelial signaling to activate pericyte-myofibroblast transition in obstructive kidney fibrosis. The American journal of pathology. 2013;182: 118–131.

15. Grgic I, Campanholle G, Bijol V, Wang C, Sabbisetti VS, Ichimura T, et al. Targeted proximal tubule injury triggers interstitial fibrosis and glomerulosclerosis. Kidney International. 2012;82: 172–183.

16. Endo T, Nakamura J, Sato Y, Asada M, Yamada R, Takase M, et al. Exploring the origin and limitations of kidney regeneration. Journal of Pathology. 2015;236: 251–263.

17. Takaori K, Nakamura J, Yamamoto S, Nakata H, Sato Y, Takase M, et al. Severity and frequency of proximal tubule injury determines renal prognosis. Journal of the

American Society of Nephrology. 2016;27: 2393–2406.

18. Liu BC, Tang TT, Lv LL, Lan HY. Renal tubule injury: a driving force toward chronic kidney disease. Kidney international. 2018;93: 568–579.

19. Dorman HR, Sondheimer JH, Cadnapaphornchai P. Mannitol-Induced Acute Renal Failure. Medicine (Baltimore). 1990;69:153–159.

20. Kelly AM, Dwamena B, Cronin P, Bernstein SJ, Carlos RC. Meta-analysis: Effectiveness of Drugs for Preventing Contrast-Induced Nephropathy. Annals of Internal Medicine. 2008;148: 284-294.

21. Majumdar SR, Kjellstrand CM, Tymchak WJ, Hervas-Malo M, Taylor DA, Teo KK. Forced Euvolemic Diuresis With Mannitol and Furosemide for Prevention of Contrast-Induced Nephropathy in Patients With CKD Undergoing Coronary Angiography: A Randomized Controlled Trial. Am J Kidney Dis. 2009;54: 602-609.

22. Bragadottir G, Redfors B, Ricksten S-E. Mannitol increases renal blood flow and maintains filtration fraction and oxygenation in postoperative acute kidney injury: a prospective interventional study. Critical care (London, England). 2012;16: R159.

23. Rello J, Triginer C, Sánchez JM, Net A. Acute Renal Failure following Massive Mannitol Infusion. Nephron. 1989;53: 377-378.

24. Bouby N, Hassler C, Bankir L. Contribution of vasopressin to progression of chronic renal failure: study in Brattleboro rats. Life sciences. 1999;65: 991–1004.

25. Sugiura T, Yamauchi A, Kitamura H, Matsuoka Y, Horio M, Imai E, et al. High water intake ameliorates tubulointerstitial injury in rats with subtotal nephrectomy: possible role of TGF-beta. Kidney international. 1999;55: 1800–1810.

26. Torres VE, Grantham JJ, Chapman AB, Mrug M, Bae KT, King BFJ, et al. Potentially modifiable factors affecting the progression of autosomal dominant polycystic kidney disease. Clinical journal of the American Society of Nephrology : CJASN. 2011;6: 640–647.

27. Plischke M, Kohl M, Bankir L, Shayganfar S, Handisurya A, Heinze G, et al. Urine osmolarity and risk of dialysis initiation in a chronic kidney disease cohort--a possible titration target? PloS one. 2014;9: e93226.

28. Eddy AA. Progression in Chronic Kidney Disease. Advances in Chronic Kidney Disease. 2005;12: 353-365.

29. Boor P, Ostendorf T, Floege J. Renal fibrosis: novel insights into mechanisms and therapeutic targets. Nature reviews Nephrology. 2010;6: 643–656.

30. Servais A, Meas-Yedid V, Buchler M, Morelon E, Olivo-Marin J-C, Lebranchu Y, et al. Quantification of interstitial fibrosis by image analysis on routine renal biopsy in patients receiving cyclosporine. Transplantation. 2007;84: 1595–1601.

31. Servais A, Meas-Yedid V, Noël LH, Martinez F, Panterne C, Kreis H, et al. Interstitial fibrosis evolution on early sequential screening renal allograft biopsies using quantitative image analysis. American journal of transplantation : official journal of the American Society of Transplantation and the American Society of Transplant Surgeons. 2011;11: 1456–1463.

32. Gewin LS. Renal fibrosis: Primacy of the proximal tubule. Matrix biology : journal of the International Society for Matrix Biology. 2018;68–69: 248–262.

33. Yanagita M. Inhibitors/antagonists of TGF-β system in kidney fibrosis. Nephrology, dialysis, transplantation : official publication of the European Dialysis and Transplant Association - European Renal Association. England; 2012.

3686–3691.

34. Seccia TM, Caroccia B, Gioco F, Piazza M, Buccella V, Guidolin D, et al. Endothelin-1 Drives Epithelial-Mesenchymal Transition in Hypertensive Nephroangiosclerosis. Journal of the American Heart Association. 2016;5: e003888.

35. Ferenbach DA, Bonventre J V. Mechanisms of maladaptive repair after AKI leading to accelerated kidney ageing and CKD. Nature Reviews Nephrology. 2015;11: 264-276.

36. Humphreys BD. Mechanisms of Renal Fibrosis. Annual Review of Physiology. 2018;80: 309-326.

37. Nelson WJ. Remodeling epithelial cell organization: transitions between front-rear and apical-basal polarity. Cold Spring Harbor perspectives in biology. 2009;1: a000513.

38. Lamouille S, Xu J, Derynck R. Molecular mechanisms of epithelial–mesenchymal transition. Nature Reviews Molecular Cell Biology. 2014;15: 178-196.

39. Burns WC, Thomas MC. The molecular mediators of type 2 epithelial to mesenchymal transition (EMT) and their role in renal pathophysiology. Expert Reviews in Molecular Medicine. 2010;12: e17.

40. Eddy AA. Serine proteases, inhibitors and receptors in renal fibrosis. Thromb Haemost. 2009;10: 656-664.

41. LeBleu VS, Taduri G, O'Connell J, Teng Y, Cooke VG, Woda C, et al. Origin and function of myofibroblasts in kidney fibrosis. Nature Medicine. 2013;19: 1047-1053.

42. Ruiz-Ortega M, Rayego-Mateos S, Lamas S, Ortiz A, Rodrigues-Diez RR.

Targeting the progression of chronic kidney disease. Nature reviews Nephrology. 2020;16: 269–288.

43. Feng Y-L, Wang W-B, Ning Y, Chen H, Liu P. Small molecules against the origin and activation of myofibroblast for renal interstitial fibrosis therapy. Biomedicine & pharmacotherapy = Biomedecine & pharmacotherapie. 2021;139: 111386.

44. Mazure NM, Pouysségur J. Hypoxia-induced autophagy: cell death or cell survival? Current Opinion in Cell Biology. 2010;22: 177–180.

45. Galluzzi L, Pietrocola F, Levine B, Kroemer G. Metabolic control of autophagy. Cell. 2014;159: 1263–1276.

46. Russell RC, Yuan HX, Guan KL. Autophagy regulation by nutrient signaling. Cell research. 2014;24: 42–57.

47. Mehrpour M, Esclatine A, Beau I, Codogno P. Overview of macroautophagy regulation in mammalian cells. Cell research. 2010;20: 748–762.

48. Yorimitsu T, Klionsky DJ. Autophagy: molecular machinery for self-eating. Cell death and differentiation. 2005;12 Suppl 2: 1542–1552.

49. Kabeya Y, Mizushima N, Ueno T, Yamamoto A, Kirisako T, Noda T, et al. LC3, a mammalian homologue of yeast Apg8p, is localized in autophagosome membranes after processing. The EMBO journal. 2000;19: 5720–5728.

50. Ravikumar B, Sarkar S, Davies JE, Futter M, Garcia-Arencibia M, Green-Thompson ZW, et al. Regulation of mammalian autophagy in physiology and pathophysiology. Physiological reviews. 2010;90: 1383–1435.

51. Steingrímsson E, Copeland NG, Jenkins NA. Melanocytes and the microphthalmia transcription factor network. Annual review of genetics. 2004;38: 365–411.

52. Sardiello M, Palmieri M, Ronza A Di, Medina DL, Valenza M, Gennarino VA, et

al. A gene network regulating lysosomal biogenesis and function. Scienc3. 2009;325: 473–477.

53. Settembre C, Di Malta C, Polito VA, Arencibia MG, Vetrini F, Erdin S, et al. TFEB links autophagy to lysosomal biogenesis. Science. 2011;332: 1429–1433.

54. Settembre C, Zoncu R, Medina DL, Vetrini F, Erdin S, Erdin S, et al. A lysosome-to-nucleus signalling mechanism senses and regulates the lysosome via mTOR and TFEB. The EMBO journal. 2012;31: 1095–1108.

55. Peña-Llopis S, Vega-Rubin-De-Celis S, Schwartz JC, Wolff NC, Tran TAT, Zou L, et al. Regulation of TFEB and V-ATPases by mTORC1. The EMBO journal. 2011;30: 3242–3258.

56. Puertollano R, Ferguson SM, Brugarolas J, Ballabio A. The complex relationship between TFEB transcription factor phosphorylation and subcellular localization. The EMBO journal. 2018;37.

57. Lee GYH, Lim CT. Biomechanics approaches to studying human diseases. Trends in biotechnology. 2007;25: 111–118.

58. Phillip JM, Aifuwa I, Walston J, Wirtz D. The Mechanobiology of Aging. Annual review of biomedical engineering. 2015;17: 113–141.

59. Bajpai A, Li R, Chen W. The cellular mechanobiology of aging: from biology to mechanics. Annals of the New York Academy of Sciences. 2021;1491: 3–24.

60. Lim CT, Zhou EH, Quek ST. Mechanical models for living cells--a review. Journal of biomechanics. 2006;39: 195–216.

61. Ingber DE. Mechanobiology and diseases of mechanotransduction. Annals of medicine. 2003;35: 564–577.

62. Suresh S. Biomechanics and biophysics of cancer cells. Acta biomaterialia.

2007;3: 413–438.

63. Wells RG. Tissue mechanics and fibrosis. Biochimica et biophysica acta. 2013;1832: 884–890.

64. Davidson MD, Burdick JA, Wells RG. Engineered Biomaterial Platforms to Study Fibrosis. Advanced healthcare materials. 2020;9: e1901682.

65. Brown AC, Fiore VF, Sulchek TA, Barker TH. Physical and chemical microenvironmental cues orthogonally control the degree and duration of fibrosis-associated epithelial-to-mesenchymal transitions. The Journal of pathology. 2013;229: 25–35.

66. Georges PC, Hui J-J, Gombos Z, McCormick ME, Wang AY, Uemura M, et al. Increased stiffness of the rat liver precedes matrix deposition: implications for fibrosis. AJP Gastrointestinal and liver physiology. 2007;293: G1147-G1154.

67. Kim MY, Baik SK, Lee SS. Hemodynamic alterations in cirrhosis and portal hypertension. The Korean journal of hepatology. 2010;16: 347–352.

68. Rohatgi R, Flores D. Intratubular hydrodynamic forces influence tubulointerstitial fibrosis in the kidney. Curr Opin Nephrol Hypertens. 2010;19:65-71.

69. Guyot C, Combe C, Desmoulière A. The common bile duct ligation in rat: A relevant in vivo model to study the role of mechanical stress on cell and matrix behaviour. Histochemistry and cell biology. 2006;126: 517–523.

70. Tschumperlin DJ, Boudreault F, Liu F. Recent advances and new opportunities in lung mechanobiology. Journal of biomechanics. 2010;43: 99–107.

71. Dominguez R, Holmes KC. Actin structure and function. Annual review of biophysics. 2011;40: 169–186.

72. Lappalainen P, Kotila T, Jégou A, Romet-Lemonne G. Biochemical and

mechanical regulation of actin dynamics. Nature reviews Molecular cell biology. 2022;23: 836–852.

73. Amano M, Ito M, Kimura K, Fukata Y, Chihara K, Nakano T, et al. Phosphorylation and activation of myosin by Rho-associated kinase (Rho-kinase). The Journal of biological chemistry. 1996;271: 20246–20249.

74. Uehata M, Ishizaki T, Satoh H, Ono T, Kawahara T, Morishita T, et al. Calcium sensitization of smooth muscle mediated by a Rho-associated protein kinase in hypertension. Nature. 1997;389: 990–994.

75. Maekawa M, Ishizaki T, Boku S, Watanabe N, Fujita A, Iwamatsu A, et al. Signaling from Rho to the actin cytoskeleton through protein kinases ROCK and LIM-kinase. Science. 1999;285: 895–898.

76. Riento K, Ridley AJ. Rocks: multifunctional kinases in cell behaviour. Nature reviews Molecular cell biology. 2003;4: 446–456.

77. Wang Y, Zheng XR, Riddick N, Bryden M, Baur W, Zhang X, et al. ROCK isoform regulation of myosin phosphatase and contractility in vascular smooth muscle cells. Circulation research. 2009;104: 531–540.

78. Desforges B, Savarin P, Bounedjah O, Delga S, Hamon L, Curmi PA, et al. Gap junctions favor normal rat kidney epithelial cell adaptation to chronic hypertonicity. AJP-Cell Physiology. 2011;301: C705-C716.

79. Di Ciano-Oliveira C, Sirokmány G, Szászi K, Arthur WT, Masszi A, Peterson M, et al. Hyperosmotic stress activates Rho: differential involvement in Rho kinase-dependent MLC phosphorylation and NKCC activation. AJP Cell physiology. 2003;285: C555-C566.

80. Lewis A, Di Ciano C, Rotstein OD, Kapus A. Osmotic stress activates Rac and

Cdc42 in neutrophils: role in hypertonicity-induced actin polymerization. AJP Cell physiology. 2002;282: C271-C279.

81. Thirone ACP, Speight P, Zulys M, Rotstein OD, Szászi K, Pedersen SF, et al. Hyperosmotic stress induces Rho/Rho kinase/LIM kinase-mediated cofilin phosphorylation in tubular cells: Key role in the osmotically triggered F-actin response. AJP - Cell Physiology. 2009;296: C463-C475.

82. Kanchanawong P, Shtengel G, Pasapera AM, Ramko EB, Davidson MW, Hess HF, et al. Nanoscale architecture of integrin-based cell adhesions. Nature. 2010;468: 580–584.

83. Deng B, Yang X, Liu J, He F, Zhu Z, Zhang C. Focal adhesion kinase mediates TGF-beta1-induced renal tubular epithelial-to-mesenchymal transition in vitro. Molecular and cellular biochemistry. 2010;340: 21–29.

84. Goffin JM, Pittet P, Csucs G, Lussi JW, Meister J-J, Hinz B. Focal adhesion size controls tension-dependent recruitment of $α$-smooth muscle actin to stress fibers. Journal of Cell Biology. 2006;172: 259-268.

85. Hinz B, Celetta G, Tomasek JJ, Gabbiani G, Chaponnier C. Alpha-Smooth Muscle Actin Expression Upregulates Fibroblast Contractile Activity. Molecular Biology of the Cell. 2001;12: 2730-2741.

86. Hinz B, Dugina V, Ballestrem C, Wehrle-Haller B, Chaponnier C. Alpha-smooth muscle actin is crucial for focal adhesion maturation in myofibroblasts. Molecular biology of the cell. 2003;14: 2508–2519.

87. Carafoli E, Krebs J. Why calcium? How calcium became the best communicator. Journal of Biological Chemistry. 2016;291: 20849–20857.

88. Satheesh NJ, Büsselberg D. The role of intracellular calcium for the development

and treatment of neuroblastoma. Cancers. 2015;7: 823–848.

89. Wissenbach U, Niemeyer BA, Flockerzi V. TRP channels as potential drug targets. Biology of the cell. 2004;96: 47–54.

90. O'Neil RG, Heller S. The mechanosensitive nature of TRPV channels. Pflugers Archiv European Journal of Physiology. 2005.193–203.

91. Thodeti CK, Matthews B, Ravi A, Mammoto A, Ghosh K, Bracha AL, et al. TRPV4 channels mediate cyclic strain-induced endothelial cell reorientation through integrin-to-integrin signaling. Circulation Research. 2009;104: 1123–1130.

92. Grace MS, Bonvini SJ, Belvisi MG, McIntyre P. Modulation of the TRPV4 ion channel as a therapeutic target for disease. Pharmacology & therapeutics. 2017;177: 9–22.

93. Berrout J, Jin M, Mamenko M, Zaika O, Pochynyuk O, O'Neil RG. Function of transient receptor potential cation channel subfamily V member 4 (TRPV4) as a mechanical transducer in flow-sensitive segments of renal collecting duct system. Journal of Biological Chemistry. 2012;287: 8782–8791.

94. Delany NS, Hurle M, Facer P, Alnadaf T, Plumpton C, Kinghorn I, et al. Identification and characterization of a novel human vanilloid receptor-like protein, VRL-2. Physiol Genomics. 2001;4:165-174.

95. Goswami C, Kuhn J, Heppenstall PA, Hucho T. Importance of non-selective cation channel TRPV4 interaction with cytoskeleton and their reciprocal regulations in cultured cells. PLoS ONE. 2010;5: 19–21.

96. Jiao R, Cui D, Wang SC, Li D, Wang YF. Interactions of the Mechanosensitive Channels with Extracellular Matrix, Integrins, and Cytoskeletal Network in

Osmosensation. Frontiers in molecular neuroscience. 2017;10: 96.

97. Mizuno A, Matsumoto N, Imai M, Suzuki M. Impaired osmotic sensation in mice lacking TRPV4. AJP Cell physiology. 2003;285: C96-C101.

98. Dong XP, Cheng X, Mills E, Delling M, Wang F, Kurz T, et al. The type IV mucolipidosis-associated protein TRPML1 is an endolysosomal iron release channel. Nature. 2008;455: 992–996.

99. Shen D, Wang X, Li X, Zhang X, Yao Z, Dibble S, et al. Lipid storage disorders block lysosomal trafficking by inhibiting a TRP channel and lysosomal calcium release. Nature communications. 2012;3: 731.

100. Medina DL, Di Paola S, Peluso I, Armani A, De Stefani D, Venditti R, et al. Lysosomal calcium signalling regulates autophagy through calcineurin and TFEB. Nature cell biology. 2015;17: 288–299.

Chapter 2

The effects of hyperosmotic stress on the morphology and cytoskeletal structure of renal tubular epithelial cells

2.1 Introduction

Biomechanics research often focuses on changes in cell morphology and cytoskeleton first because they play a crucial role in determining the mechanical properties and behaviors of cells. In addition, because cell morphology and the cytoskeleton are intimately connected to cellular functions, these changes could affect cellular functions such as adhesion, proliferation and signaling.

Tubular cells are exposed to much higher levels of hyperosmolarity than the other cells anywhere else in the body. The effects of osmotic stress have been examined with many mammalian cell types, and a variety of cellular responses have been observed in them [1]. These phenomena include perturbations, like changes in cell morphology, cell cycle arrest, and inhibition of transcription and translation, which would be considered pathological events.

Previous studies have reported that hyperosmotic mannitol stress injures tubular epithelial cells. Animal studies revealed that, after administration of mannitol with high dose, structural changes that occur at the cellular level in the proximal tubules, including intracytoplasmic vacuolation and cellular swelling are observed [2-4]. A high concentration of mannitol could inhibit renal tubular epithelial cell proliferation in vitro [5]. However, there is no information on how hyperosmotic mannitol stress affects NRK-52E cells.

This chapter aimed to elucidate the short-term (-0.5 h) and longer-term (12-h) effects of hyperosmotic stress on proximal tubular epithelial cells. Using cultured proximal tubular epithelial cells, the author investigated the changes in cellular morphology (cell area and volume), actin cytoskeletal structure, and cell proliferation in response to hyperosmotic stress.

2.2 Materials and methods

2.2.1 Cell lines

Normal rat kidney cells (NRK-52E), a proximal tubular epithelial cell line derived from rat kidney, were directly purchased from the Japanese Collection of Research Bioresources (JCRB No. IFO50480, Osaka, Japan). Both mannitol and urea for adjusting the osmolarity in the medium were purchased from FUJIFILM Wako Pure Chemical (Osaka, Japan).

2.2.2 Cell culture and hyperosmotic stimulation

NRK-52E cells were maintained in Dulbecco's modified Eagle's medium (DMEM; FUJIFILM Wako Pure Chemical) supplemented with 10% fetal bovine serum (FBS; Cosmo Bio, Tokyo, Japan), 1 U/mL penicillin–streptomycin (FUJIFILM Wako Pure Chemical) and cultured at 37°C in 5% CO_2 atmosphere. For providing hyperosmotic stress to the cells, the medium was switched to DMEM supplemented with 0.5% FBS and cultured for 24 h and then to a hyperosmotic medium containing mannitol or urea. Cells reaching about 80% confluence were used for the experiments.

The hyperosmotic medium was prepared by adding mannitol or urea to DMEM (0 mM: 313 ± 1.5 mOsmol/L, 100 mM: 428 ± 2.4 mOsmol/L, 200 mM: 531 ± 4.8 mOsmol/L

(mean ± S.E.)) (Fig. 2-1). The dose of 200 mM mannitol (amount to 36 g/L) used in this study exceeded the plasma mannitol concentration (29 g/L) after administration high dose of mannitol (4 g/kg/h) clinically reported side effects of acute renal failure [6].

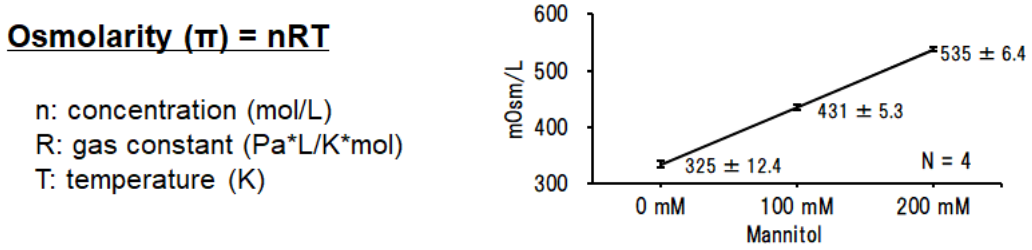

Fig. 2-1 Relationship between osmolality and mannitol concentration.

2.2.3 Cell area measurements

Projected cell areas were measured by manually outlining the cells on fluorescent images of F-actin. For immunofluorescence staining, cells were fixed with 4% paraformaldehyde for 15 min and then permeabilized with 0.5% Triton X-100 for 15 min at room temperature. After blocking with 3% BSA (Sigma-Aldric, Kyoto, Japan) in PBS for 1 h, cells were incubated with Alexa Fluor 546-conjugated phalloidin (Invitrogen, Carlsbad, CA) for 15 min. All samples of immunofluorescence staining were imaged by confocal microscopy (Olympus, Tokyo, Japan). The ImageJ Fiji software (version 1.52b, NIH) was used for the processing of images.

2.2.4 Cell volume measurements

The molecular probe CellMask™ Green Plasma Membrane Stain (Thermo Fisher Scientific, Tokyo, Japan) was incubated in a serum-free medium for 10 min, according to the manufacturer's protocol. Immediately after the hyperosmotic treatment with either

mannitol or urea, the cells were fixed with 4% paraformaldehyde (FUJIFILM Wako Pure Chemical). A confocal laser scanning microscope (Olympus) was used to record optical cross-section images with a 0.10-μm z-axis interval. The cell volume was calculated by counting the number of voxels after area processing for each stack, and the relative cell volume change (normalized to the initial cell volume) after hyperosmotic stimulation was evaluated.

2.2.5 Cell viability assay

After the stimulation of hyperosmotic stress, the morphology of NRK-52E cells was observed under the phase-contrast microscope (Olympus). Cell proliferation and cell viability were evaluated by trypan blue staining (FUJIFILM Wako Pure Chemical). As dead cells are stained as blue color, the number of viable cells was calculated by counting the unstained cells using a hemocytometer.

Cell viability was calculated as the ratio of the number of viable cells to the number of total cells. Cell proliferation was calculated as the ratio of the number of viable cells to the control (untreated cells) at the same time point.

2.2.6 Statistical analysis

All results were analyzed using the GraphPad Prism 5 ver. 5.0 software (GraphPad Software). Summary data are presented as mean ± standard error (S.E.) of at least three separate experiments. For multiple group comparisons, one-way analysis of variance (ANOVA), followed by Steel or Dunnett's post hoc test was used to compare groups with nonparametric and parametric data, respectively.

2.3 Results

2.3.1 Hyperosmolarity induces changes in cell area and volume

Mannitol and urea are osmolytes with different properties; the former is non-ionic and membrane-impermeable, whereas the latter is non-ionic and membrane-permeable.

When the projected cell area was quantified, treatment with 200 mM mannitol resulted in a temporary decrease in cell areas at 0.25 h (3762 ± 383 μm^2) and 0.5 h (2726 ± 166 μm^2), which recovered at 2 h (7310 ± 826 μm^2) to the initial level (7346 ± 524 μm^2; Fig. 2-22A), but the urea treatment did not cause significant changes (0.25 h, 7176 ± 729 μm^2; 0.5 h, 6215 ± 404 μm^2; 2 h, 6683 ± 638 μm^2; 12 h, 7147 ± 610 μm^2) to the initial level (6870 ± 441 μm^2; Fig. 2-2B).

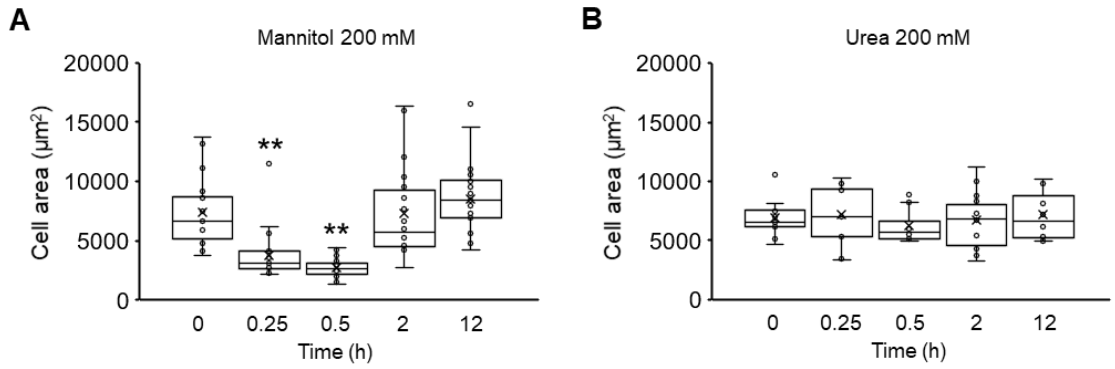

Fig. 2-2 Effects of hyperosmolarity on cell area of NRK-52E cells. (A, B) NRK-52E cells were treated with mannitol (200 mM) (A) or urea (200 mM) (B) for 0, 0.25, 0.5, 2, and 12 h (mannitol; 0 h (n = 25), 0.25 h (n = 26), 0.5 h (n = 28), 2 h (n = 22), 12 h (n = 29): urea; 0 h (n = 12), 0.25 h (n = 13), 0.5 h (n = 12), 2 h (n = 14), 12 h (n = 12)). Data are presented as box and whisker plots with average (×), median, IQR and minimum and maximum values. The n indicates the number of cells analyzed. **P < 0.01 from the data of 0 h (Dunnett's test).

The changes in the cell volume after hyperosmotic mannitol stress were similar to those of the projected cell areas. Treatment with 200 mM mannitol resulted in a significant ($P < 0.01$) decrease in cell volume after 0.25 h (0.60 ± 0.02) and 0.5 h (0.71 ± 0.03), followed by a recovery at 2 h (0.91 ± 0.03), and a significant ($P < 0.01$) increase at 12 h (1.27 ± 0.05) when compared to that observed during the initial state (Fig. 2-3A). On the other hand, treatment with 200 mM urea did not cause any significant changes in the cell volume (0.25 h, 0.94 ± 0.05; 0.5 h, 0.93 ± 0.04; 2 h, 0.87 ± 0.04; 12 h, 0.89 ± 0.03; Fig. 2-3B).

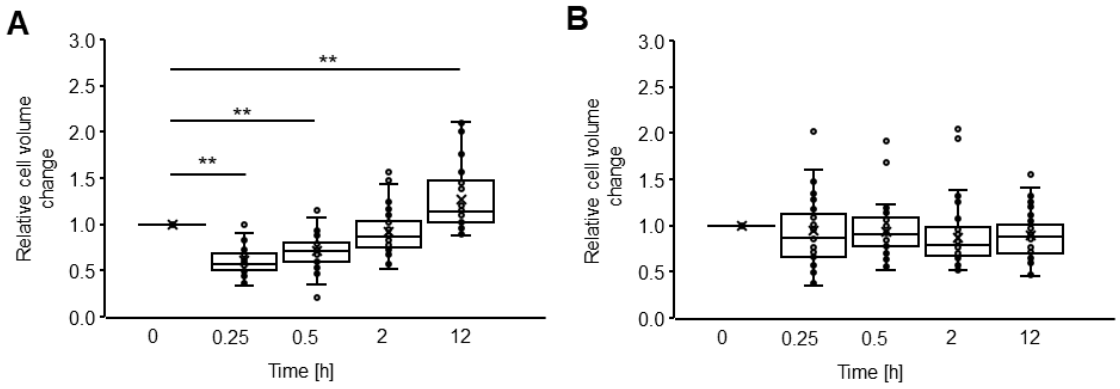

Fig. 2-3 Effects of hyperosmotic stress on cell volume of NRK-52E cells. (A, B) NRK-52E cells were treated with 200 mM mannitol (A) or urea (B) for 0, 0.25, 0.5, 2, and 12 h (mannitol: 0 h (n = 41), 0.25 h (n = 51), 0.5 h (n = 42), 2 h (n = 59), 12 h (n = 49); urea: 0 h (n = 41), 0.25 h (n = 43), 0.5 h (n = 50), 2 h (n = 55), 12 h (n = 55)). The relative cell volume changes were normalized by the cell volume at 0 h. Data are presented as box and whisker plots with average (×), median, IQR, and minimum and maximum values. **$P < 0.01$ from the data at 0 h (Steel test).

2.3.2 Hyperosmolarity induces changes in the actin cytoskeleton

The author hypothesized that the cell shrinkage caused by hyperosmotic stress interferes with the structure and organization of the cytoskeletal network by limiting the intracellular space. I focused on the effect of hyperosmotic stress on actin cytoskeletal structures, which are known to be responsible for mediating various important cellular processes such as cell structural support and functional regulation.

Although there was no change in the actin cytoskeleton cultured with 200 mM urea, the actin cytoskeletal structure exhibited drastic changes after being treated with 200 mM mannitol (Fig. 2-4); the actin filaments were disassembled by treatment with 200 mM mannitol for 0.5 h and then reorganized into thick stress fibers at 12 h.

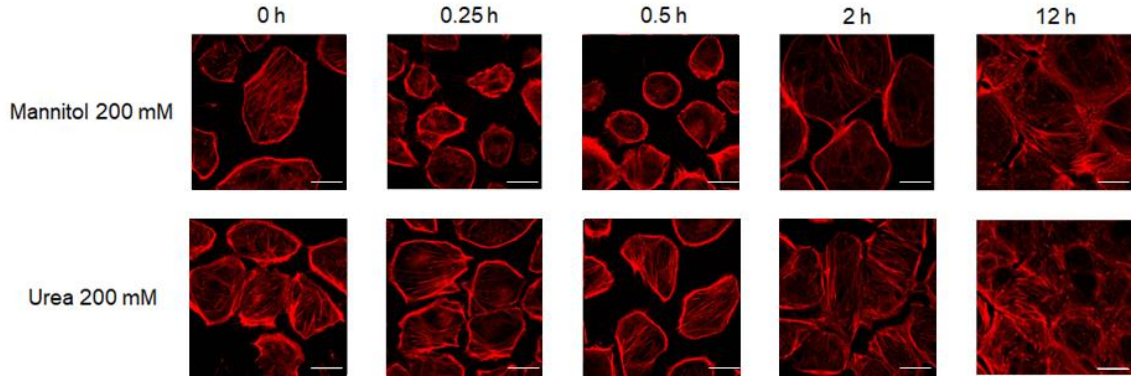

Fig. 2-4 Effects of hyperosmolarity on actin cytoskeleton of NRK-52E cells. Cells were cultured with 200 mM mannitol or urea for 0, 0.25, 0.5, 2, and 12 h. Typical fluorescence images of F-actin. Bar, 25 μm.

2.3.3 Hyperosmolarity inhibits cell growth

Since changes in cell volume and cytoskeleton may affect cell growth, the effects of mannitol stress on cell viability and cell proliferation were examined. Figure 2-5A showed the effect of mannitol-induced hyperosmotic stress on cellular morphology. The control NRK-52E cells (0 mM mannitol) exhibited a typical epithelial cuboidal shape with cobblestone morphology. Treatment with 100 mM mannitol-containing medium for up to 24 h did not cause any detectable changes in cell morphology compared to the control. In contrast, cells exposed to 200 mM mannitol exhibited reduced cell density and lost cell-to-cell contact. Figure 2-5B showed the cytotoxic effects of concentrations and incubation periods of mannitol on NRK-52E cells. Treatment with up to 200 mM mannitol had no significant effects on cell viability. However, treatment of cells with 200 mM mannitol-added medium suppressed cell proliferation in a time-dependent manner (4, 8, 18, and 24 h) (Fig. 2-5C). Compared with the untreated control, cell proliferation was significantly decreased by 24% even 4 h after the beginning of treatment with 200 mM mannitol ($P < 0.01$) (Fig. 2-5C).

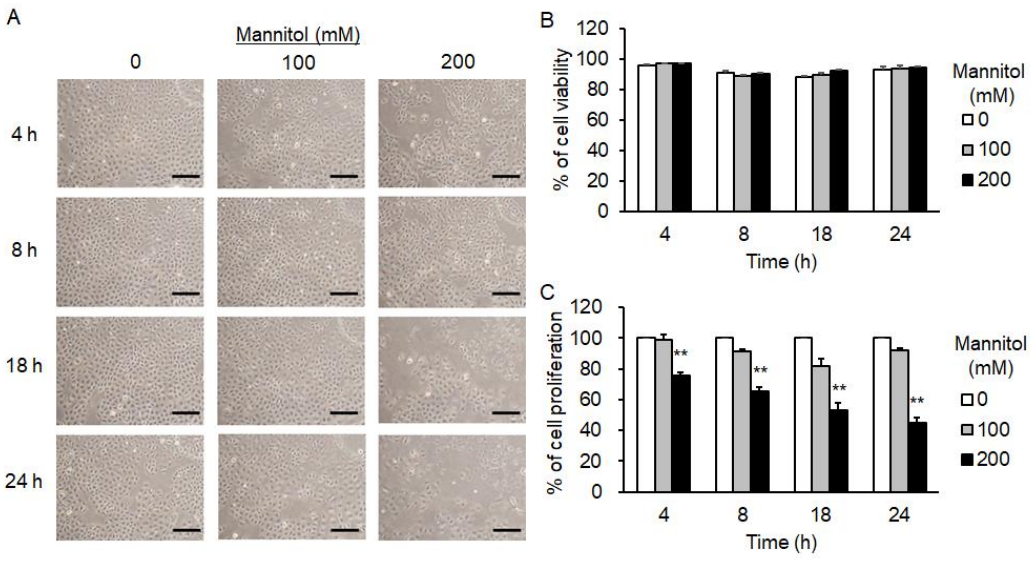

Fig. 2-5 Effects of hyperosmotic stress on cell morphology and cytotoxicity of NRK-52E cells. (A) For assessment of NRK-52E cell morphology, cells were examined by phase-contrast microscopy. NRK-52E cells were cultured with 100 and 200 mM of mannitol for 4, 8, 18, and 24 h. Bar, 50 μm. (B and C) Determination of cell viability (B) and cell proliferation (C) by trypan blue staining. NRK-52E cells were cultured with 100 and 200 mM of mannitol for 4, 8, 18, and 24 h (n = 6). The % of cell proliferation was calculated considering mannitol (0 mM) at the same time point as 100% and plotted (mean ± SEM.). **P < 0.01 from the data of mannitol (0 mM) at the same time point (Steel test).

2.4 Discussion

Tubular epithelial cells are routinely exposed to severe osmotic stresses in our body. The proximal tubule is the first segment of the kidney tubule, and excessive mannitol, administrated to the patients, such as cerebral edema and intracranial hypertension, is not reabsorbed and leads to increase the osmolality in the proximal tubular fluid. Retrospective clinical research demonstrated that higher urine osmolarity is associated with a higher risk of initiating dialysis [7]. In this research, the hyperosmotic urine group has been set at ≥510 mOsmol/L. Taking account for these studies, 200 mM mannitol (531 ± 4.8 mOsmol/L) was used as a hyperosmotic condition. However, since the osmolarity values in the proximal tubule cannot be measured, it should be noted that the results of this study cannot be directly extrapolated the *in vivo* situation. Furthermore, in order to generalize the effects of the osmotic gradient between the intracellular and extracellular compartments on the biomechanics of cells, it is necessary to investigate other membrane-impermeable osmolytes except mannitol (e.g., sorbitol and trehalose).

Hyperosmolarity refers to a higher concentration of solutes outside the cell compared to inside the cell. This osmotic imbalance induces changes in cell area and volume as the cell responds to maintain homeostasis. Previous studies have reported that when proximal tubules were exposed to hyperosmotic urea, the reduction in cell volume was markedly smaller than that under hyperosmotic mannitol treatment [8,9]. Present results (Figs. 2-2 and 2-3) are consistent with those of previous studies. Hyperosmolarity can also trigger intracellular signaling pathways that regulate the cytoskeleton, leading to changes in cell shape and area [10]. Present results (Fig. 2-4) are consistent with those of previous studies that demonstrated hyperosmolarity-induced depolymerization and reorganization of the actin cytoskeleton for adaptive responses [11].

The relationship between hyperosmolarity and cell proliferation is complex and context-dependent [1]. In some cases, hyperosmolarity can stimulate cell proliferation [12], while in others, it can inhibit or even induce cell death [13-16]. One mechanism by which this occurs is through the activation of mitogenic signaling pathways [17]. Hyperosmolarity can activate growth factor receptors, such as the epidermal growth factor receptor (EGFR), leading to downstream signaling events that promote cell cycle progression and proliferation [18]. Additionally, hyperosmolarity can induce the production of cytokines that facilitate cell growth and division [19]. Conversely, hyperosmolarity can also cause cell cycle arrest, preventing cell proliferation. Hyperosmotic conditions can activate stress response pathways, such as the p38 MAPK (mitogen-activated protein kinase) pathway [20,21] and the stress-activated protein kinase/c-Jun N-terminal kinase (SAPK/JNK) pathway [22,23]. These pathways can trigger cell cycle checkpoint activation, leading to cell cycle arrest at various stages, such as the G1/S and G2/M transition phases [24-26]. The purpose of this arrest is to allow

cells to repair any damage and restore homeostasis before resuming proliferation. In extreme cases, hyperosmolarity can induce cell death [27]. The excessive loss of water from the cells can lead to severe dehydration and irreversible damage to cellular structures [1]. This can trigger apoptotic or necrotic cell death pathways, ultimately leading to cell demise. Taken together, the relationship between hyperosmolarity and cell proliferation is multifaceted. While hyperosmolarity can stimulate cell proliferation through mitogenic signaling pathways in some cases, it can also induce cell cycle arrest or cell death under certain conditions. In the present study, the author confirmed that hyperosmotic mannitol stress induced a decrease in cell growth without altering cell viability in NRK-52E cells. Further study is needed to fully understand the mechanisms of this relationship in different cell types and physiological contexts.

2.5 Conclusion

In the present chapter, the author confirmed that the hyperosmotic condition above a threshold concentration of mannitol, which is believed to be 100 and 200 mM in this study, causes obvious actin cytoskeleton alterations and induces a decrease or inhibition of cell growth without altering cell viability in NRK-52E cells.

Reference

1. Burg MB, Ferraris JD, Dmitrieva NI. Cellular response to hyperosmotic stresses. Physiological Reviews. 2007;87: 1441–1474.
2. Bragadottir G, Redfors B, Ricksten S-E. Mannitol increases renal blood flow and maintains filtration fraction and oxygenation in postoperative acute kidney injury: a prospective interventional study. Critical care (London, England). 2012;16: R159.
3. Gutschenritter PW, Newcomer KL, Dahlberg PJ. Mannitol-induced renal insufficiency. Wisconsin medical journal. 1985;84: 16–17.
4. Rello J, Triginer C, Sánchez J M, Net A. Acute renal failure following massive mannitol infusion. Nephron. 1989; 53: 377–378.
5. Shi J, Qian J, Li H, Luo H, Luo W, Lin Z. Renal tubular epithelial cells injury induced by mannitol and its potential mechanism. Renal Failure. 2018;40: 85–91.
6. Dorman HR, Sondheimer JH, Cadnapaphornchai P. Mannitol-induced acute renal failure. Medicine (Baltimore). 1990; 69:153-159.
7. Plischke M, Kohl M, Bankir L, Shayganfar S, Handisurya A, Heinze G, et al. Urine osmolarity and risk of dialysis initiation in a chronic kidney disease cohort--a possible titration target? PloS one. 2014;9: e93226.
8. Miyata Y, Asano Y, Muto S. Effects of P-glycoprotein on cell volume regulation in mouse proximal tubule. AJP - Renal Physiology. 2001;280: 829–837.
9. Miyata Y, Asano Y, Muto S. Hyperosmotic urea activates basolateral NHE in proximal tubule from P-gp null and wild-type mice. AJP Renal physiology. 2002;283: F771-F783.
10. Pedersen SF, Hoffmann EK, Mills JW. The cytoskeleton and cell volume regulation. Comparative Biochemistry and Physiology - A Molecular and

Integrative Physiology. 2001;130: 385–399.

11. Ciano C Di, Nie Z, Szászi K, Lewis A, Uruno T, Zhan X, et al. Osmotic stress-induced remodeling of the cortical cytoskeleton. AJP - Cell Physiology. 2002;283: 850–865.
12. Madonna R, Geng Y-J, Shelat H, Ferdinandy P, De Caterina R. High glucose-induced hyperosmolarity impacts proliferation, cytoskeleton remodeling and migration of human induced pluripotent stem cells via aquaporin-1. Biochimica et biophysica acta. 2014;1842: 2266–2275.
13. Bortner CD, Cidlowski JA. Absence of volume regulatory mechanisms contributes to the rapid activation of apoptosis in thymocytes. The AJP. 1996;271: C950-C961.
14. Galvez A, Morales MP, Eltit JM, Ocaranza P, Carrasco L, Campos X, et al. A rapid and strong apoptotic process is triggered by hyperosmotic stress in cultured rat cardiac myocytes. Cell and Tissue Research. 2001;304: 279–285.
15. Michea L, Ferguson DR, Peters EM, Andrews PM, Kirby MR, Burg MB. Cell cycle delay and apoptosis are induced by high salt and urea in renal medullary cells. AJP - Renal Physiology. 2000;278: 209–218.
16. Santos BC, Chevaile A, Hébert MJ, Zagajeski J, Gullans SR. A combination of NaCl and urea enhances survival of IMCD cells to hyperosmolality. The AJP. 1998;274: F1167-F1173.
17. Zhang Z, Wei T, Cohen DM. Urea protects from the proapoptotic effect of NaCl in renal medullary cells. AJP - Renal Physiology. 2000;279: 345–352.
18. Zhao H, Tian W, Xu H, Cohen DM. Urea signalling to immediate-early gene transcription in renal medullary cellsrequires transactivation of the epidermal growth factor receptor. The Biochemical journal. 2003;370: 479–487.

19. Meier R, Rouse J, Cuenda A, Nebreda AR, Cohen P. Cellular stresses and cytokines activate multiple mitogen-activated-protein kinase kinase homologues in PC12 and KB cells. European Journal of Biochemistry. 1996;236: 796–805.

20. Kramer HJ, Hashemi T, Bäcker A, Bokemeyer D. Hyperosmolality induced by betaine or urea stimulates endothelin synthesis by differential activation of ERK and p38 MAP kinase in MDCK cells. Kidney & blood pressure research. 2002;25: 65–70.

21. Roger F, Martin PY, Rousselot M, Favre H, Féraille E. Cell shrinkage triggers the activation of mitogen-activated protein kinases by hypertonicity in the rat kidney medullary thick ascending limb of the Henle's loop. Requirement of p38 kinase for the regulatory volume increase response. Journal of Biological Chemistry. 1999;274: 34103–34110.

22. Li DQ, Luo L, Chen Z, Kim HS, Song XJ, Pflugfelder SC. JNK and ERK MAP kinases mediate induction of IL-1β, TNF-α and IL-8 following hyperosmolar stress in human limbal epithelial cells. Experimental Eye Research. 2006;82: 588–596.

23. Chen Z, Tong L, Li Z, Yoon KC, Qi H, Farley W, et al. Hyperosmolarity-induced cornification of human corneal epithelial cells is regulated by JNK MAPK. Investigative Ophthalmology and Visual Science. 2008;49: 539–549.

24. Thornton TM, Rincon M. Non-classical p38 map kinase functions: cell cycle checkpoints and survival. International journal of biological sciences. 2009;5: 44–51.

25. Cuenda A, Rousseau S. p38 MAP-Kinases pathway regulation, function and role in human diseases. Biochimica et Biophysica Acta - Molecular Cell Research. 2007;1773: 1358–1375.

26. Zhong W, Xie Y, Wang Y, Lewis J, Trostinskaia A, Wang F, et al. Use of hyperosmolar stress to measure stress-activated protein kinase activation and function in human HTR cells and mouse trophoblast stem cells. Reproductive sciences (Thousand Oaks, Calif). 2007;14: 534–547.

27. Jin Z, El-Deiry WS. Overview of cell death signaling pathways. Cancer Biology and Therapy. 2005;4: 147–171.

Chapter 3

The effects of hyperosmotic stress on the Ca^{2+} influx of renal tubular epithelial cells

3.1 Introduction

Intracellular Ca^{2+} is a universal second messenger involved in the control of various cellular events [1]. Although the intracellular Ca^{2+} concentration is significantly lower than the extracellular level when at rest, various cell stimuli promote a transient increase in intracellular Ca^{2+} concentration [2]. This increase results from either the influx of extracellular Ca^{2+} through Ca^{2+} channels or the discharge from intracellular Ca^{2+} stores [2]. Hyperosmotic stimuli have been shown to increase Ca^{2+} influx in renal inner medullary collecting duct cells [3].

TRP vanilloid 4 (TRPV4), a member of the TRP superfamily, is a nonselective cationic channel permeable to Ca^{2+}, Na^{+}, and Mg^{2+}, which can be activated by several stimuli, including changes in osmolarity, the temperature in the range of 25°C–37°C, and mechanical forces [4-6]. TRPV4 is found in various cell types and tissues and is involved in regulating intracellular Ca^{2+} levels [7]. In addition, cytoskeletal networks, such as actin filaments are directly molecularly bound to the C-terminus of the TRPV4 channel [8]. Although previous researches have shown that hyperosmotic stress can stimulate Ca^{2+} influx in a variety of cell lines [9-12], it is unknown whether hyperosmotic mannitol stress can induce a transient Ca^{2+} influx in NRK-52E cells.

Based on results of the Chapter 2, the author hypothesized that the actin cytoskeletal disruption caused by hyperosmotic mannitol stress could trigger an increase in

intracellular Ca^{2+} concentrations. The aim of this chapter was to elucidate the effects of hyperosmotic mannitol stress on the Ca^{2+} influx of proximal tubular epithelial cells.

3.2 Materials and methods

3.2.1 Cell lines and reagents

NRK-52E cells and mannitol were obtained as described in Section 2.2.1. Both HC-067047, a TRPV4 antagonist, and GSK-1016790A, a TRPV4 agonist, were purchased from Abcam (Cambridge, MA). The actin-depolymerizing agent, cytochalasin D, was obtained from FUJIFILM Wako Pure Chemical.

3.2.2 Cell culture and hyperosmotic stimulation

Culture of NRK-52E cells and application of hyperosmotic mannitol were performed as described in Section 2.2.2. For the inhibitor experiments, cells were pre-treated for 15 min with EGTA or HC-06704 before being stimulated with hyperosmotic mannitol.

3.2.3 Ca^{2+} influx assay

NRK-52E cells were loaded in DMEM medium with the Fluo-4/AM probe (Dojindo; Kumamoto, Japan) for 30 min. Fluorescence images of Fluo-4 were captured at 5-sec intervals for 600 sec with a fluorescence microscope (IX81, Olympus). After 50 sec, the medium was replaced with a hyperosmotic medium or a medium containing a TRPV4 agonist GSK-1016790A (Abcam). The fluorescence signal of Fluo-4 for each cell was analyzed by ImageJ Fiji software. Changes in intracellular Ca^{2+} levels were expressed as the relative fluorescence F/F_0, where F and F_0 represent the intensity of the fluorescence at each time point and the initial fluorescence value (at 0 sec), respectively.

3.2.4 Statistical analysis

Statistical analyses were performed as described in Section 2.2.6. A comparison of the two groups was performed using Student's t-test. To compare multiple groups, a one-way analysis of variance was used, followed by Dunnett's post hoc test. $P < 0.05$ was considered to represent a statistically significant difference. All results were analyzed using the GraphPad Prism 5 ver. 5.0 software (GraphPad Software).

3.3 Results

3.3.1 Hyperosmotic stress promotes Ca^{2+} influx

Ca^{2+} imaging with Fluo-4 was used to assess changes in intracellular Ca^{2+} concentrations in cells cultured with 0, 100, and 200 mM mannitol (Fig. 3-1).

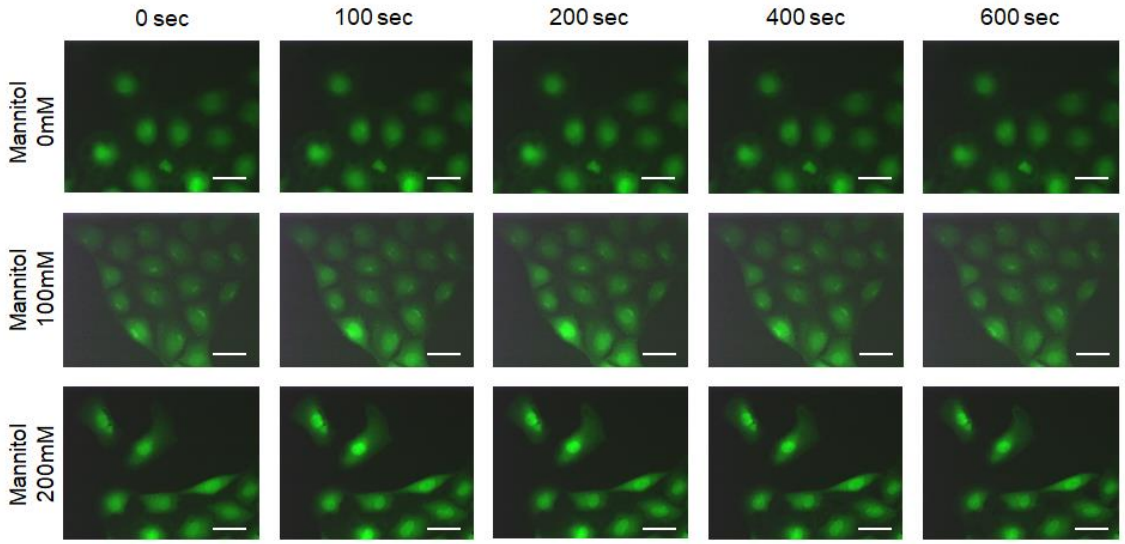

Fig. 3-1 Calcium imaging in response to hyperosmotic stress in NRK-52E cells. Typical time-lapse fluorescence images of Fluo-4/AM cultured with 0, 100, and 200 mM mannitol for 0, 100, 200, 400, and 600 sec. Bar, 50 μm.

When compared to 0 mM mannitol, hyperosmotic mannitol stress resulted in a dose-dependent increase in intracellular Ca^{2+} concentration (Fig. 3-2A). The fluorescence intensity tended to increase slightly after the start of the 0 mM mannitol condition, probably due to physical stress associated with the medium exchange. Although there was no statistically significant difference in the average peak fluorescent intensity for cells cultured with 100 mM mannitol, the peak intensity for cells treated with 200 mM mannitol showed a significant increase compared with 0 mM mannitol (0 mM, 1.18 ± 0.02; 100 mM, 1.25 ± 0.04; 200 mM, 1.46 ± 0.06 ($P < 0.01$)) (Figs. 3-2A, B). The average of fluorescence levels for 0 mM conditions returned to the initial levels at 600 sec after stimulation, but those of 200 mM mannitol did not (0 mM, 1.02 ± 0.02; 100 mM, 1.01 ± 0.02; 200 mM, 1.21 ± 0.05) (Figs. 3-2A, C).

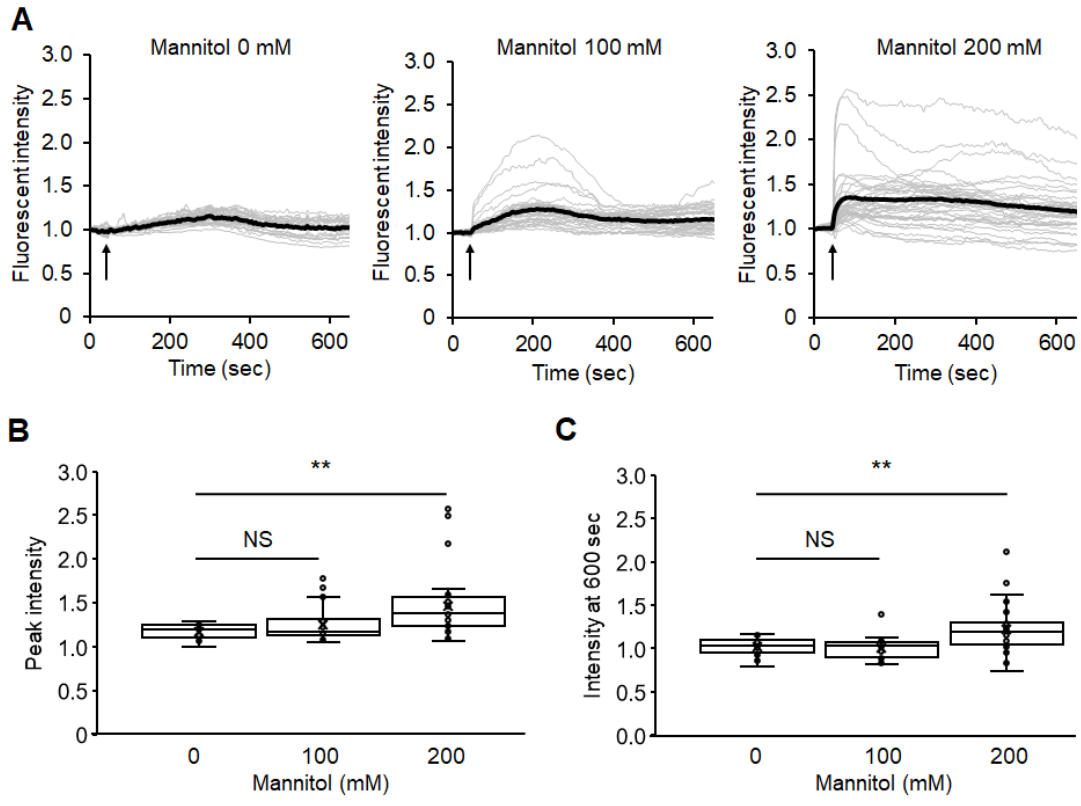

Fig. 3-2 Quantification of hyperosmotic stress on the calcium influx of NRK-52E cells. (A) Summarized relative fluorescence intensity transients in response to 0, 100, and 200 mM mannitol (n = 27 from 0 mM, n = 26 from 100 mM, n = 34 from 200 mM). Individual data is represented by thin gray lines, while averages are represented by bold black lines. The arrows denote the start of the hyperosmotic stimulation. (B, C) A summary of Fluo-4/AM fluorescence signal data from (A), displaying the peak intensity (B) and the amplitude at 600 sec (C). The peak intensity was measured as the highest value of fluorescence intensity transients. The amplitude at 600 sec was calculated as the value of 600 sec after stimulation. Data are presented as box and whisker plots with average, median, interquartile range (IQR), and minimum and maximum values. **P < 0.01; NS, not significant from the data of 0 mM (Dunnett's test).

3.3.2 Treatment with cytochalasin D promotes Ca^{2+} influx

Based on the results shown in Sections 2.3.2 and 3.3.1, the author hypothesized that the disruption of the actin cytoskeleton caused by hyperosmotic stress involves the increase in Ca^{2+} influx. To test this hypothesis, the effect of cytochalasin D, an actin-depolymerizing agent, alone on the Ca^{2+} influx of NRK-52E cells were examined. As expected, treatment with cytochalasin D resulted in an increase in intracellular Ca^{2+} concentration (Fig. 3-3 A). Quantitatively, similar to the 200 mM mannitol treatment, a significant increase in peak values was observed (Fig. 3-3 B; 200 mM mannitol, 1.46 ± 0.06; Cytochalasin D, 1.56 ± 0.11). These results suggest that disruption of the actin cytoskeleton could contribute to Ca^{2+} influx in response to hyperosmotic mannitol stress.

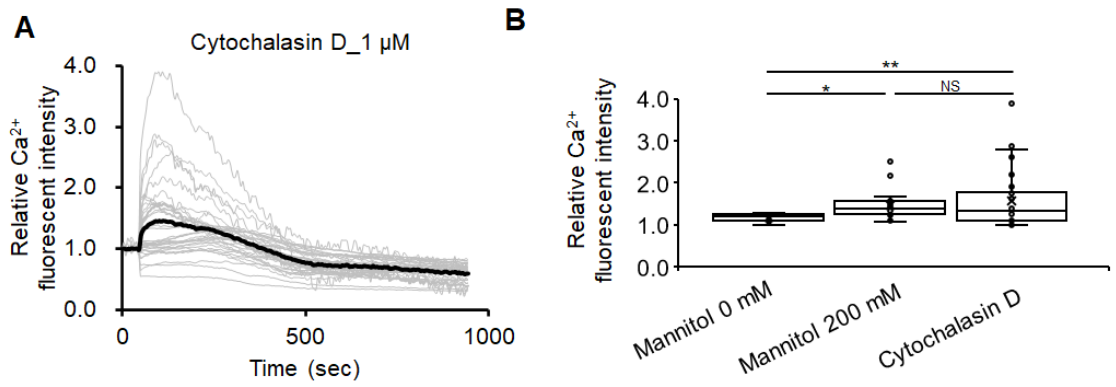

Fig. 3-3 Effects of cytochalasin D on calcium influx of NRK-52E cells. (A) Relative fluorescence intensity transients of Fluo-4/AM loaded cells in response to treatment with 1 μM cytochalasin D (n = 35). Individual data is represented by thin gray lines, while the average is represented by a bold black line. The arrows denote the start of the hyperosmotic stimulation. (B) A comparison of the peak intensity between 200 mM mannitol alone and treatment with 1 μM cytochalasin D. The data of 200 mM mannitol alone (left) were identical to those in Figure 3-2B, which were shown for comparison. Data are presented as box and whisker plots with average, median, interquartile range (IQR), and minimum and maximum values. *P < 0.05; **P < 0.01; NS, not significant (Turkey's test).

3.3.3 Cotreatment with HC-067047 suppresses hyperosmolarity-induced Ca^{2+} influx

To elucidate the pathways involved in the increase of intracellular Ca^{2+}, cells were pre-treated with 4 mM EGTA (extracellular Ca^{2+} chelator) before being stimulated with 200 mM mannitol. The pretreatment with EGTA completely eliminated the change in fluorescent intensity caused by hyperosmotic stress (200 mM mannitol, 1.46 ± 0.06; EGTA, 1.06 ± 0.01 (P < 0.01)) (Figs. 3-4A and B), indicating that extracellular Ca^{2+} influx participates in the accumulation of intracellular Ca^{2+}.

TRPV4 has been identified as a mechanosensor involved in the effect of hyperosmotic stress [13], and it is expressed in NRK-52E cells [14]. Therefore, the author investigated the potential role of TRPV4 channels in hyperosmotic mannitol-mediated Ca^{2+} influx in NRK-52E cells. Pre-treated with 10 μM HC-067047, a TRPV4 antagonist, significantly reduced the increase in Ca^{2+} fluorescent signals caused by 200 mM mannitol hyperosmotic stress (200 mM mannitol, 1.46 ± 0.06; HC-067047, 1.17 ± 0.03 ($P < 0.01$)) (Figs. 3-4C and D). This suggests that TRPV4 channels are involved in hyperosmotic mannitol-mediated Ca^{2+} influx.

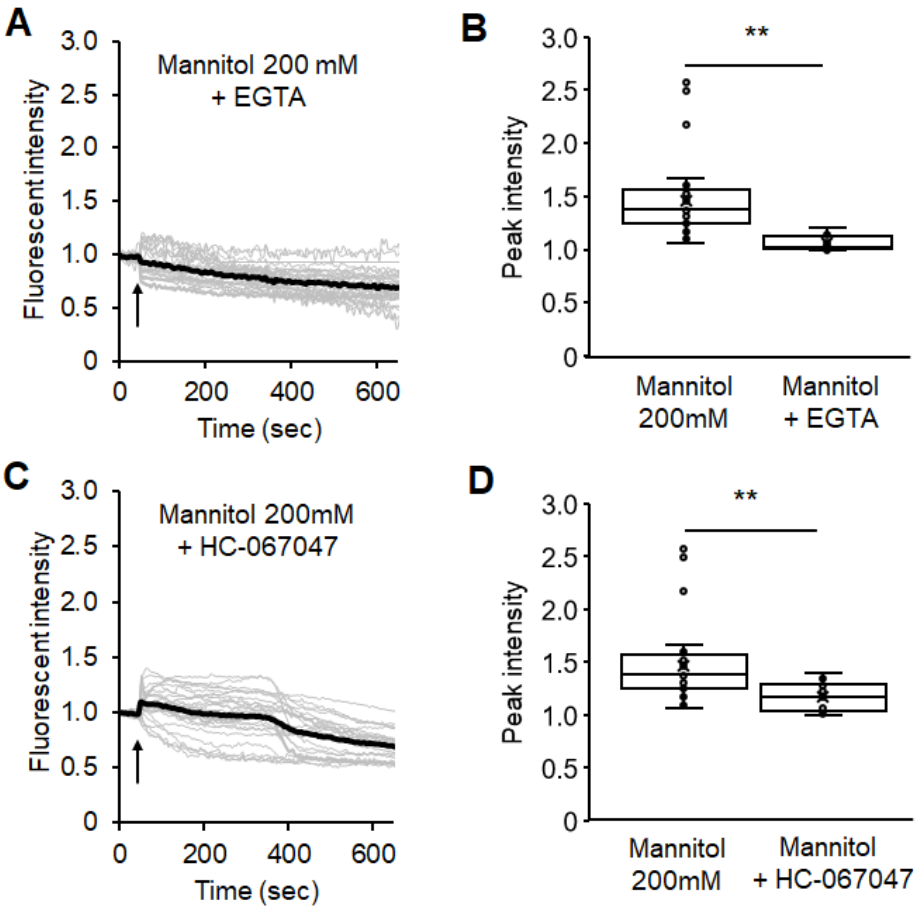

Fig. 3-4 Effects of EGTA and TRPV4 antagonist on the hyperosmotic mannitol-induced calcium influx of NRK-52E cells. (A, C) Relative fluorescence intensity transients of Fluo-4/AM loaded cells in response to cotreatment with 200 mM mannitol and 4 mM EGTA (n = 29) (A) or 10 μM HC-067047 (n = 25) (C). Individual data is represented by thin gray lines, while the average is represented by a bold black line. The arrows denote the start of the hyperosmotic stimulation. (B, D) A comparison of the peak intensity between 200 mM mannitol alone and cotreatment with EGTA (B) or HC-067047 (D). The data of 200 mM mannitol alone (left) were identical to those in Figure 3-2B, which were shown for comparison. Data are presented as box and whisker plots with average, median, interquartile range (IQR), and minimum and maximum values. **P < 0.01 from the data of 200 mM mannitol (Student's t-test).

3.3.4 Enhancement of calcium influx by TRPV4 channel activation

To further investigate whether hyperosmotic mannitol stress-induced Ca^{2+} influx is associated with TRPV4 channels, NRK-52E cells were treated with the selective TRPV4 agonist GSK1016790A (hereafter GSK-101; 100 nM). As expected, compared to 200 mM mannitol treatment (Fig. 3-5A), GSK-101 treatment increased intracellular Ca^{2+} concentration (Fig. 3-5B). The calcium dynamics, on the other hand, differed slightly. Although there was no statistically significant difference between treatments of GSK-101 and 200 mM mannitol in the response latency, defined as the time from the stimulation to the peak fluorescent intensity (GSK-101, 87 ± 21 sec; 200 mM mannitol, 121 ± 20 sec) (Figs. 3-5C), the Fluo-4 fluorescence levels for GSK-101 treated cells returned faster to the initial level and was significantly lower than that for 200 mM mannitol treated cells at 600 sec after hyperosmotic stimulation (GSK-101, 1.02 ± 0.03; 200 mM mannitol, 1.20 ± 0.04 ($P < 0.01$)) (Fig. 3-5D). Furthermore, GSK-101 treatment significantly increased the peak Ca^{2+} fluorescence intensity when compared to 200 mM mannitol (the peak fluorescent intensity: GSK-101, 1.77 ± 0.07; 200 mM mannitol, 1.46 ± 0.06 ($P < 0.01$)) (Fig. 3-5E). This could be due to the difference in TRPV4 activation levels between the GSK-101 treatment and hyperosmotic stress.

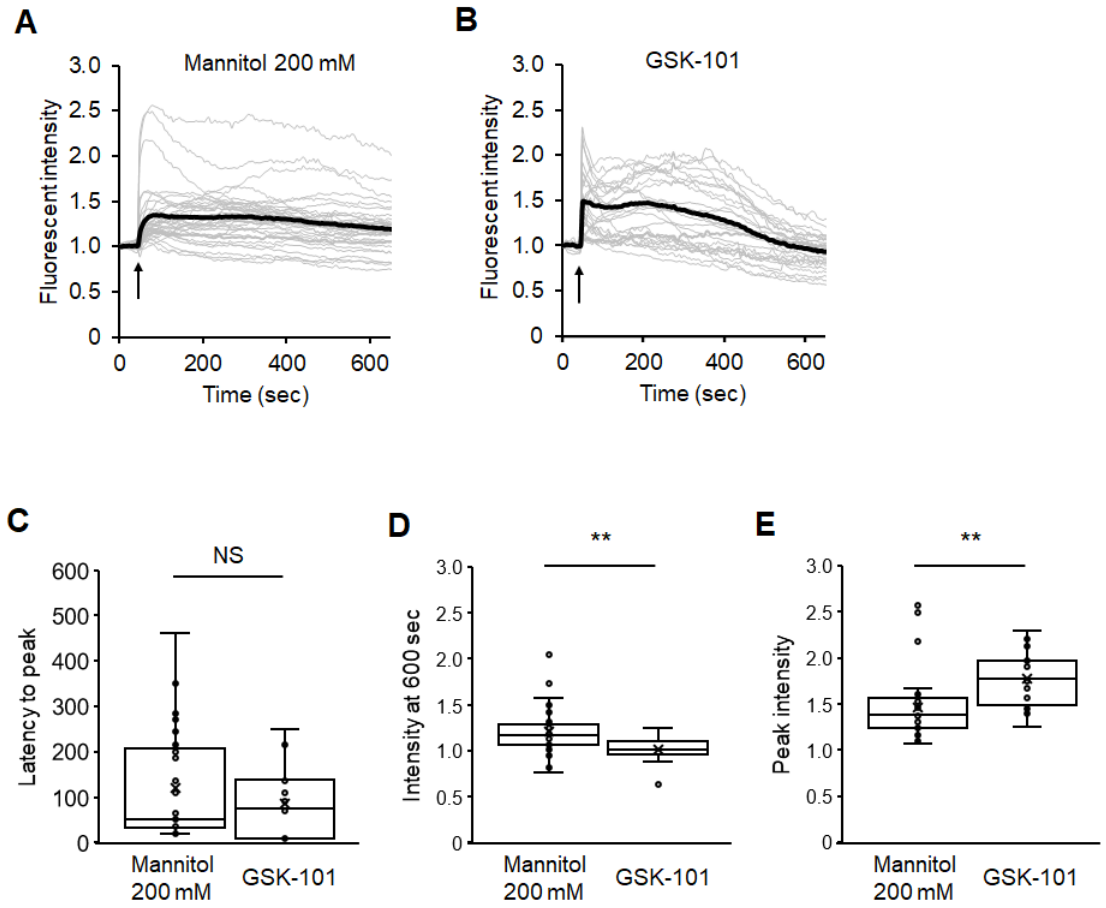

Fig. 3-5 Effects of TRPV4 agonist on the calcium influx of NRK-52E cells. (A, B) Relative fluorescence intensity transients of Fluo-4/AM loaded cells in response to treatment with 200 mM mannitol (n = 34) (A) or 100 nM GSK-1016790A (n = 16) (B). Individual data is represented by thin gray lines, while the average is represented by a bold black line. The arrow denotes the start of the stimulation of mannitol or GSK-101. The data of 200 mM mannitol (A) were identical to those in Fig. 3-2A, which were shown for comparisons. (C–E) A summary of Fluo-4/AM fluorescence signal data from (B), displaying the latency to peak (C), the amplitude at 600 sec (D), and the peak intensity (E). The latency to the peak was calculated as the time between stimulation and the peak value. The amplitude at 600 sec was calculated as the value of 600 sec after stimulation. The peak intensity was calculated as the highest value of fluorescence intensities. The

data of 200 mM mannitol alone (black bar) were identical to those in Figure 2, which were shown for comparison. Data are presented as box and whisker plots with average, median, interquartile range (IQR), and minimum and maximum values. **P < 0.01; NS, not significant from the data of control (Student's t-test).

3.4 Discussion

TRPV4 has been identified as an osmotically-activated channel [15]. The effect of hyperosmotic stress on the TRPV4 channel activation has been controversial, with some reports indicating that treatment of hyperosmotic stress induces TRPV4 channel activation in dorsal root ganglion neurons [15,16], while others suggest that it does not in corneal epithelial cells and some other tissues [17,18]. In this chapter, the author confirmed that hyperosmotic mannitol stress could induce a transient Ca^{2+} influx in NRK-52E, implying the involvement of TRPV4 channel activation.

Although a significant increase in intracellular Ca^{2+} concentration was observed with 200 mM mannitol treatment, there was a wide variation in results between cells, with some cells responding and others not. This may be due to differences in TRPV4 expression, cell shape, and cell cycle among cells. Synchronizing the cell cycle by serum starvation prior to hyperosmotic stress may be one effective way to limit variability.

Chelating extracellular Ca^{2+} with EGTA prevented hyperosmotic-induced cytoplasmic Ca^{2+} entry (Figs. 3-4A and B), emphasizing the importance of extracellular Ca^{2+} through the plasma membrane. TRPV4 activation may account for some of this phenomenon, as a TRPV4 antagonist, HC-067047, significantly reduced hyperosmotic mannitol-induced Ca^{2+} influx (Figs. 3-4C and D). Despite the lack of statistics, the initial Ca^{2+} levels after hyperosmotic stimulation remained slightly higher in the TRPV4 inhibition condition

compared to the EGTA treatment (Figs. 3-4A and C). Furthermore, the cells treated with the TRPV4 activator GSK-101 did not exhibit a sustained Ca^{2+} response induced by hyperosmotic mannitol stress. Other Ca^{2+} channels may thus be involved in mediating or compensating for the increased intracellular Ca^{2+} [2]. TRPV1 is also found to be expressed in renal tubules [19] and indicated as a mechanosensor responsible for the effect of hyperosmotic stress [10,11]. Importantly, knocking out this channel abolished the susceptibility to hyperosmolar conditions [20], suggesting that TRPV1 mediation of the change in intracellular Ca^{2+} might be the first step of this series of changes. On one hand, TRPV4 signaling is important in mechanosensory transduction; for example, when bladder filling activates TRPV4 in epithelial cells, adenosine triphosphate (ATP) is released and acts on P2X receptors, one of the Ca^{2+} channels [21]. The effects of hyperosmolarity on the effects of other Ca^{2+} channels can help to clarify the mechanism underlying changes in intracellular Ca^{2+} concentration in proximal tubular epithelial cells.

Although the findings of this chapter suggest that TRPV4 channels are involved in the initial step of calcium influx caused by hyperosmotic mannitol treatment, it is still unclear how TRPV4 is activated by hyperosmotic stress. TRPV4 interacts with the actin cytoskeletal network [8,22], so it will be interesting to determine if TRPV4 is stimulated by cytoskeletal remodeling and/or feed-forward mechanisms. The Ca^{2+} response of NRK-52E cells to hyperosmotic mannitol stress may be due to cell shrinkage disrupting actin filaments. Cytoskeletal networks, such as actin filaments are directly molecularly bound to the C-terminus of the TRPV4 channel [8], and hyperosmotic stress increased intracellular Ca^{2+} concentration while disrupting the actin cytoskeleton [23]. When actin filaments were disrupted by treatment with Cytochalasin D, a transient increase in intracellular Ca^{2+} fluorescence was observed (Fig. 3-3). Thus, actin filaments may be

involved in the hyperosmotic stress-induced Ca^{2+} influx. Moreover, it is known that structural changes in the plasma membrane, such as changes in membrane tension, contribute to the activation of ion channels on the plasma membrane concomitant with cell volume changes [18]. Changes in actin cytoskeletal tension due to cell swelling induced by hypoosmotic stress affect TRPV4 channel activity [24]. Since, in Chapter 2, the author showed that hyperosmotic mannitol stress causes cell shrinkage in NRK-52E cells (Fig. 2-3A), it is possible that the TRPV4 channel is activated (opened) by the changes in the plasma membrane structure associated with the cell contraction. Investigating the mechanisms of Ca^{2+} influx induced by hyperosmotic mannitol will also help to clarify the mechanisms underlying the effects of Ca^{2+} dynamics on various phenotypes, including EMT and autophagy, which are discussed in Chapters 4 and 5.

3.5 Conclusion

In the present chapter, the author showed that the hyperosmotic mannitol stress induces a transient Ca^{2+} influx in NRK-52E, implying the involvement of TRPV4 channel activation.

Reference

1. Carafoli E, Krebs J. Why calcium? How calcium became the best communicator. Journal of Biological Chemistry. 2016;291: 20849–20857.
2. Bagur R, Hajnóczky G. Intracellular Ca2+ Sensing: Its Role in Calcium Homeostasis and Signaling. Molecular Cell. 2017;66: 780–788.
3. Mooren FC, Kinne RKH. Intracellular calcium in primary cultures of rat renal inner medullary collecting duct cells during variations of extracellular osmolality. Pflugers Arch. 1994;427: 463–472.
4. O'Neil RG, Heller S. The mechanosensitive nature of TRPV channels. Pflugers Arch. 2005.193–203.
5. Thodeti CK, Matthews B, Ravi A, Mammoto A, Ghosh K, Bracha AL, et al. TRPV4 channels mediate cyclic strain-induced endothelial cell reorientation through integrin-to-integrin signaling. Circulation Research. 2009;104: 1123–1130.
6. Grace MS, Bonvini SJ, Belvisi MG, McIntyre P. Modulation of the TRPV4 ion channel as a therapeutic target for disease. Pharmacology & therapeutics. 2017;177: 9–22.
7. Berrout J, Jin M, Mamenko M, Zaika O, Pochynyuk O, O'Neil RG. Function of transient receptor potential cation channel subfamily V member 4 (TRPV4) as a mechanical transducer in flow-sensitive segments of renal collecting duct system. Journal of Biological Chemistry. 2012;287: 8782–8791.
8. Goswami C, Kuhn J, Heppenstall PA, Hucho T. Importance of non-selective cation channel TRPV4 interaction with cytoskeleton and their reciprocal regulations in cultured cells. PLoS ONE. 2010;5: 19–21.

9. Chiong M, Parra V, Eisner V, Ibarra C, Maldonado C, Criollo A, et al. Parallel activation of Ca2+-induced survival and death pathways in cardiomyocytes by sorbitol-induced hyperosmotic stress. Apoptosis. 2010;15: 887–903.

10. Pan Z, Wang Z, Yang H, Zhang F, Reinach PS. TRPV1 activation is required for hypertonicity-stimulated inflammatory cytokine release in human corneal epithelial cells. Invest Ophthalmol Vis Sci. 2011;52: 485–493.

11. Khajavi N, Reinach PS, Skrzypski M, Lude A, Mergler S. L-carnitine reduces in human conjunctival epithelial cells hypertonic-induced shrinkage through interacting with TRPV1 channels. Cell Physiol Biochem. 2014;34: 790–803.

12. Jiang LB, Cao L, Yin XF, Yasen M, Yishake M, Dong J, et al. Activation of autophagy via Ca2+-dependent ampk/ mtor pathway in rat notochordal cells is a cellular adaptation under hyperosmotic stress. Cell Cycle. 2015;14: 867–879.

13. Liedtke W. TRPV4 as osmosensor: a transgenic approach. Pflugers Archiv : European journal of physiology. 2005;451: 176–180.

14. Zhang X, Mao Z, Huang Y, Zhang Z, Yao J. Gap junctions amplify TRPV4 activation-initiated cell injury via modification of intracellular Ca 2+ and Ca 2+-dependent regulation of TXNIP. Channels (Austin, Tex). 2020;14: 246–256.

15. Strotmann R, Harteneck C, Nunnenmacher K, Schultz G, Plant TD. OTRPC4, a nonselective cation channel that confers sensitivity to extracellular osmolarity. Nature cell biology. 2000;2: 695–702.

16. Alessandri-Haber N, Joseph E, Dina OA, Liedtke W, Levine JD. TRPV4 mediates pain-related behavior induced by mild hypertonic stimuli in the presence of inflammatory mediator. Pain. 2005;118: 70–79.

17. Sidhaye VK, Güler AD, Schweitzer KS, D'Alessio F, Caterina MJ, King LS.

Transient receptor potential vanilloid 4 regulates aquaporin-5 abundance under hypotonic conditions. PNAS. 2006;103: 4747–4752.

18. Le Roux AL, Quiroga X, Walani N, Arroyo M, Roca-Cusachs P. The plasma membrane as a mechanochemical transducer. Philosophical transactions of the Royal Society of London Series B, Biological sciences. 2019;374: 20180221.

19. Feng NH, Lee HH, Shiang JC, Ma MC. Transient receptor potential vanilloid type 1 channels act as mechanoreceptors and cause substance P release and sensory activation in rat kidneys. AJP - Renal Physiology. 2008;294: 316–325.

20. Naeini RS, Witty MF, Séguéla P, Bourque CW. An N-terminal variant of Trpv1 channel is required for osmosensory transduction. Nature Neuroscience. 2006;9: 93–98.

21. Wang ECY, Lee JM, Ruiz WG, Balestreire EM, Von Bodungen M, Barrick S, et al. ATP and purinergic receptor-dependent membrane traffic in bladder umbrella cells. Journal of Clinical Investigation. 2005;115: 2412–2422.

22. Jiao R, Cui D, Wang SC, Li D, Wang YF. Interactions of the Mechanosensitive Channels with Extracellular Matrix, Integrins, and Cytoskeletal Network in Osmosensation. Frontiers in molecular neuroscience. 2017;10: 96.

23. Pritchard S, Erickson GR, Guilak F. Hyperosmotically induced volume change and calcium signaling in intervertebral disk cells: the role of the actin cytoskeleton. Biophysical journal. 2002;83: 2502–2510.

24. Erickson GR, Northrup DL, Guilak F. Hypo-osmotic stress induces calcium-dependent actin reorganization in articular chondrocytes. Osteoarthritis Cartilage. 2003;11: 187-197.

Chapter 4

The effects of hyperosmotic stress on EMT of renal tubular epithelial cells

4.1 Introduction

The epithelial-mesenchymal transition (EMT) of tubular epithelial cells is a widely accepted mechanism for the transformation of injured tubular epithelial cells into myofibroblasts. EMT is characterized by the loss of epithelial markers like E-cadherin and the upregulation of mesenchymal markers such as α-smooth muscle actin (α-SMA) [1]. A growing body of evidence suggests that renal tubular EMT plays an important role in the progression of acute and chronic kidney damage [1-4]. The exact mechanism of mannitol-induced AKI has not been clarified yet but changes in tubular osmolarity and the osmolar gap may be the contributing factors [5]. Besides, previous studies have reported that interstitial α-SMA-positive myofibroblasts appear around the proximal tubules in the AKI model [6,7]. Therefore, hyperosmotic stress could be involved in the induction of EMT.

EMT occurs in response to numerous factors such as cytokines, hormones, and autacoids [1,8-10]. Interestingly, recent studies have demonstrated that mechanical stresses such as fluid shear stress and cyclic stretch could also induce EMT [11,12]. Changes in osmotic conditions of proximal tubular epithelial cells can generate not only osmotic but also mechanical stresses in cells by altering cell volume and cytoplasm membrane tension [13]. Cells sense the mechanical stresses through cell–extracellular matrix (ECM) adhesion structures known as focal adhesions (FAs), which are connected

to the actin structure through FA-associated binding proteins [14] and transmit force-induced signals between the ECM and cytoskeleton [15,16]. The cytoskeleton and FAs are not static structures that simply transmit force, but they are always dynamically reorganized [15]. It is also known that the induction of EMT causes a dynamic remodeling of the actin cytoskeleton from the cortical organization of actin filaments to thick actin stress fibers, which is a hallmark of mesenchymal cells [17,18]. Although it has been reported that hyperosmotic stress induces depolymerization and rearrangement of actin filaments [19], to the best of our knowledge, there are no studies regarding the effects of hyperosmolarity on FAs. In fact, it has been proposed that the size of FAs controls the recruitment of α-SMA to actin stress fibers [20-22]. Therefore, FAs could be involved in the induction of EMT by controlling the expression of α-SMA.

The aim of this chapter was to investigate the mechanisms involved in hyperosmolarity-induced EMT. For this purpose, the author examined the effects of hyperosmotic stress on α-SMA expression and FA dynamics in proximal tubular epithelial cells. Moreover, based on the Chapter 3 results, the author investigated the effects of TRPV4-mediated calcium influx on EMT to better understand the mechanisms of hyperosmolarity-induced EMT.

4.2 Materials and methods

4.2.1 Cell lines and reagents

NRK-52E cells, mannitol, a TRPV4 antagonist HC-067047, and a TRPV4 agonist GSK-1016790A were obtained as described in Section 3.2.1. Y-27632, ROCK (Rho-associated protein kinase) inhibitor, was obtained from FUJIFILM Wako Pure Chemical. Antibodies for α-SMA, vinculin, E-cadherin, and GAPDH were purchased from DAKO

(Glostrup, Denmark), Invitrogen (Carlsbad, CA), Abcam (Cambridge, MA), and Cell Signaling Technology (Danvers, MA), respectively.

4.2.2 Cell culture and hyperosmotic stimulation

Culture of NRK-52E cells and application of hyperosmotic mannitol were performed as described in Section 2.2.2.

4.2.3 RNA extraction and quantitative real-time PCR

NRK-52E cells were lysed in ISOGEN (NIPPON GENE, Toyama, Japan), and to obtain cDNA, the reverse transcription reaction was performed using the ReverTra Ace qPCR RT Master Mix (TOYOBO, Osaka, Japan). Quantification of cDNA was performed using THUNDERBIRD SYBR qPCR Mix (TOYOBO) and the Thermal Cycler Dice Real-Time System Tp800 (TaKaRa Biomedicals, Shiga, Japan). PCR was conducted in 5 μM of cDNA, 10 μM of master mix, and 5 pM of sense, and antisense primers. Table 4-1 shows the primer sets used for PCR. The relative mRNA expression levels of the target genes in each sample were calculated as the CT value, which is the cycle number at which the fluorescence signal is greater than a defined threshold. The expression of each gene was normalized with the housekeeping gene GAPDH, and the relative mRNA levels were analyzed by the ΔΔCT method and compared to those of untreated, time-matched control samples.

Table 4-1: Primers used in this study

Gene Name	Sense	Antisense
Rat GAPDH	TGACAACTTTGGCATCGTGG	GGGCCATCCACAGTCTTCTG
Rat SNAIL	CAGATGGCTGATGGAAGGCA	CAGCTGTGTCCAGAGGCTAC
Rat TWIST	AGAGATTCCCAGAGGCAACG	TGACTGATTGGCAAGACCTC
Rat Collagen-I	ACTGGTACATCAGCCCAAAC	GGAACCTTCGCTTCCATACTC
Rat PAI-1	GACAATGGAAGAGCAACATG	ACCTCGATCTTGACCTTTTG
Rat Fibronectin	GTGATCTACGAGGGACAGC	GCTGGTGGTGAAGTCAAAG
Rat E-cadherin	GAGGTCTTTGAGGGATCTGTTG	GGCAGCATTGTAGGTGTTTATG
Rat vimentin	CTTCCCTGAACCTGAGAGAAAC	GTCTCTGGTTTCAACCGTCTTA
Rat α-SMA	AGGGAGTGATGGTTGGAATG	GGTGATGATGCCGTGTTCTA

4.2.4 Immunofluorescence staining

After the stimulation of hyperosmotic stress with mannitol or urea, the morphology of NRK-52E cells was observed under the phase-contrast microscope (Olympus). For immunofluorescence staining, cells were fixed with 4% paraformaldehyde for 15 min and then permeabilized with 0.5% Triton X-100 for 15 min at room temperature. After blocking with 3% BSA (Sigma-Aldrich) in PBS for 1 h, cells were incubated with E-cadherin, α-SMA, or vinculin antibody (diluted to 1:200 in the blocking solution) for 1 h

at room temperature, followed by staining with Alexa Fluor 488- or 546-conjugated secondary antibody (1:500, Invitrogen) for 1 h. For staining the nuclei and F-actin, cells were also incubated with Hoechst 33342 (Invitrogen) and Alexa Fluor 546-conjugated phalloidin (Invitrogen), respectively, for 15 min. All samples of immunofluorescence staining were imaged by confocal microscopy (Olympus).

4.2.5 Image processing

The ImageJ Fiji software (version 1.52) was used for the processing of images. After removing the background, the cell outline was detected and binarized. In the region excluding the cell edge, a vinculin dot of ≥0.8 μm^2 was defined as FA [23], and "the number of FAs per cell" and "the area of each FA" were obtained for each cell. Relative immunofluorescence intensities of E-cadherin and α-SMA were quantified by using the ImageJ Fiji [24].

4.2.6 Western blotting

Protein samples prepared using whole-cell lysates. After washing with PBS, NRK-52E cells were lysed in lysis buffer (150 mM NaCl, 1 mM EDTA, 50 mM Tris, 1% NP-40, and 1% Triton-X-100) containing 1% protease inhibitor cocktail (Sigma-Aldrich). Protein concentrations were determined using the DC Protein Assay kit (Bio-Rad, Hercules, CA) and absorbance spectrophotometer (Bio-Rad). Equal amounts of protein (from 1 to 5 μg) were separated by SDS-polyacrylamide gel electrophoresis (SDS-PAGE) and transferred to polyvinylidene difluoride (PVDF) membranes. After blocking the PVDF membranes with 5% nonfat milk in TBST (Tris-buffered saline (TBS) containing 0.1% Tween 20) for 1 h, the membranes were incubated with E-cadherin, α-SMA or GAPDH, diluted up to

1:2000, at 4°C overnight. Goat anti-rabbit IgG, horseradish peroxidase-linked secondary antibody (Cell Signaling Technology), diluted up to 1:2000 was detected by adding an enhanced chemiluminescent reagent. Blots were stripped with Restore™ Western Stripping Buffer (Thermo Fisher Scientific) and re-probed with different antibodies. The band intensity was quantified from scanned membrane images using the ImageJ Fiji software.

4.2.7 Statistical analysis

Statistical analyses were performed as described in Section 2.2.6. All results were analyzed using the GraphPad Prism 5 ver. 5.0 software (GraphPad Software) or the R 4.1.2 software (R Foundation for Statistical Computing, Vienna, Austria). Comparison of the two groups was performed using Student's t-test. For multiple group comparisons, one-way analysis of variance (ANOVA), followed by Steel, Steel–Dwass, Dunnett's, and Tukey's post hoc test was used to compare groups with nonparametric and parametric data, respectively.

4.3 Results

4.3.1 Hyperosmolarity induces the EMT of NRK-52E cells

The effect of hyperosmotic stress induced by mannitol on EMT was examined by immunofluorescence staining (Fig. 4-1A). In the absence of extracellular osmolytes, E-cadherin, an epithelial cell marker, was abundantly localized to the plasma membrane. The expression of α-SMA, a mesenchymal cell marker was rarely detected, which is consistent with previous studies investigating the induction of EMT using NRK-52E cells [25-27]. When the cells were stimulated by hyperosmotic stress for 12 h, the expression of E-cadherin was markedly decreased, and the expression of α-SMA was dramatically increased in the cytoplasm in a mannitol-dose-dependent manner (Fig. 4-1A). Quantitatively, the mean fluorescence intensity of E-cadherin and α-SMA was significantly decreased and increased, respectively, by hyperosmotic mannitol stress (Fig. 4-1B). These changes in expression are consistent with the features of EMT.

In Chapter 2, the author described that when NRK-52E cells were exposed to hyperosmotic urea, the reduction in cell volume was markedly smaller than that under hyperosmotic mannitol treatment (Fig. 2-3). Thus, the author next explored the E-cadherin and α-SMA expression of NRK-52E cells under urea-medicated hyperosmolarity to further understand the effect of hyperosmotic stress-induced cell volumetric changes on EMT. Unlike the result obtained with mannitol, treatment with hyperosmotic urea resulted in no changes in the expression of E-cadherin and α-SMA compared with the control (0 mM) (Figs. 4-2A and B).

These results suggest that the hyperosmotic stress-induced EMT in NRK-52E cells requires cell shrinkage concomitant with the osmotic gradient between the intracellular and extracellular compartments as a result of water efflux from the cells.

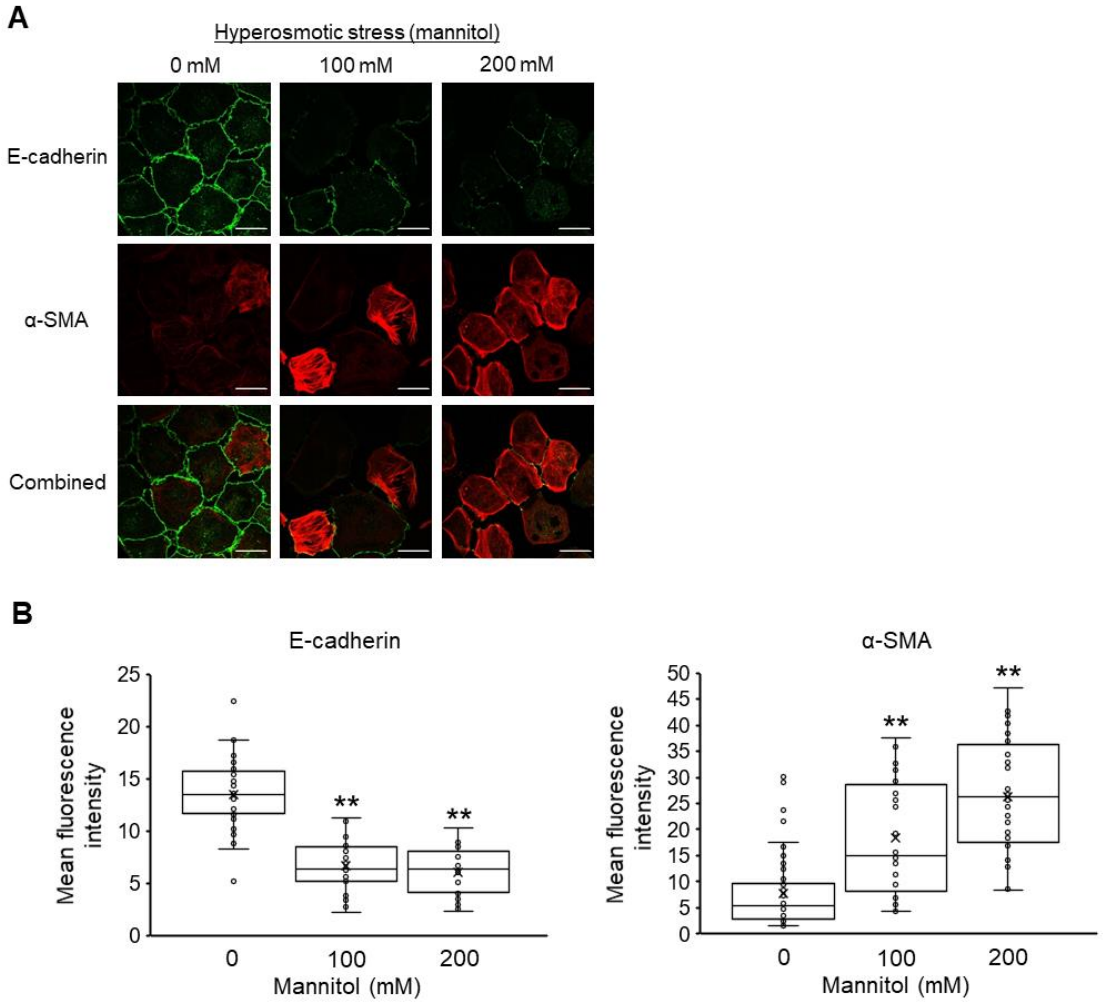

Fig. 4-1 Effects of hyperosmotic mannitol stress on the epithelial-mesenchymal transition (EMT) of NRK-52E cells. (A) Typical fluorescence images of E-cadherin (green), α-SMA (red), and combined (green and red) cultured with 0, 100, and 200 mM mannitol for 12 h. Bar, 25 μm. (B) Quantitation of the changes in the mean fluorescence intensity of E-cadherin and α-SMA (n = 46 from 0 mM, n = 30 from 100 mM, n = 26 from 200 mM) by immunofluorescence staining. Data are presented as box and whisker plots with average (×), median, IQR, and minimum and maximum values. The n indicates the number of independent experiments. $^{**}P < 0.01$ from the data of 0 mM (Dunnett's test).

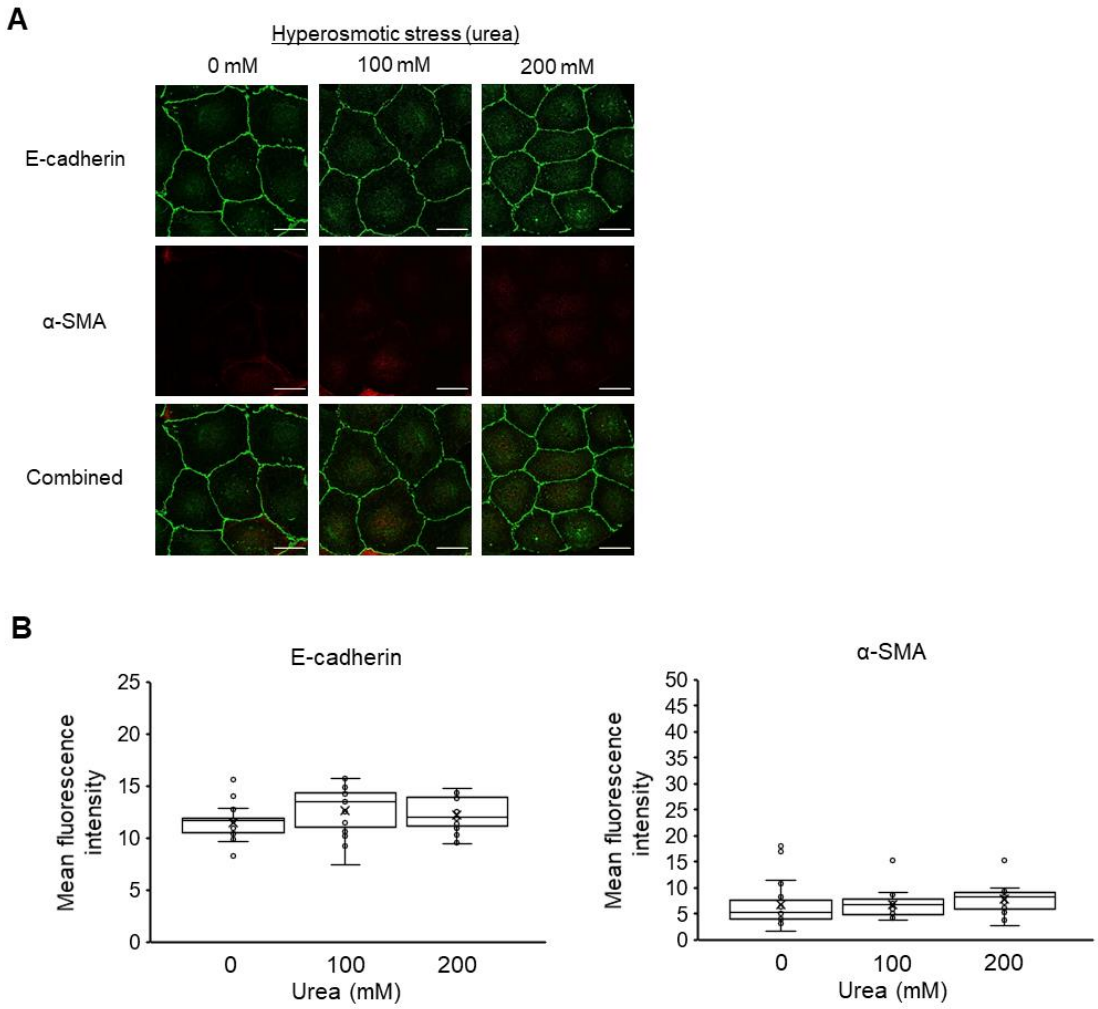

Fig. 4-2 Effects of hyperosmotic urea stress on the epithelial-mesenchymal transition (EMT) of NRK-52E cells. (A) Typical fluorescence images of E-cadherin (green), α-SMA (red), and combined (green and red) cultured with 0, 100, and 200 mM urea for 12 h. Bar, 25 μm. (B) Quantitation of the changes in the mean fluorescence intensities of E-cadherin and α-SMA (n = 19 from 0 mM, n = 19 from 100 mM, n = 19 from 200 mM) by immunofluorescence staining. Data are presented as box and whisker plots with average (×), median, IQR, and minimum and maximum values. The n indicates the number of independent experiments.

4.3.2 Hyperosmolarity induces the upregulation of Snail and Twist.

Since E-cadherin downregulation is an initial hallmark of the differentiation of epithelial cells to the mesenchymal phenotype [28,29], the author measured the expression levels of Snail and Twist, which are the major transcription factors that regulate E-cadherin expression [1,10,30], to verify the mechanism underlying the hyperosmotic stress-induced E-cadherin downregulation. When cells were stimulated by hyperosmotic stress for 12 h, the mRNA expression levels of Snail and Twist were increased in a mannitol-dose-dependent manner (Fig. 4-3). These data suggest that hyperosmotic mannitol stress induces EMT in NRK-52E cells with a reduction of E-cadherin expression by the upregulation of both Snail and Twist.

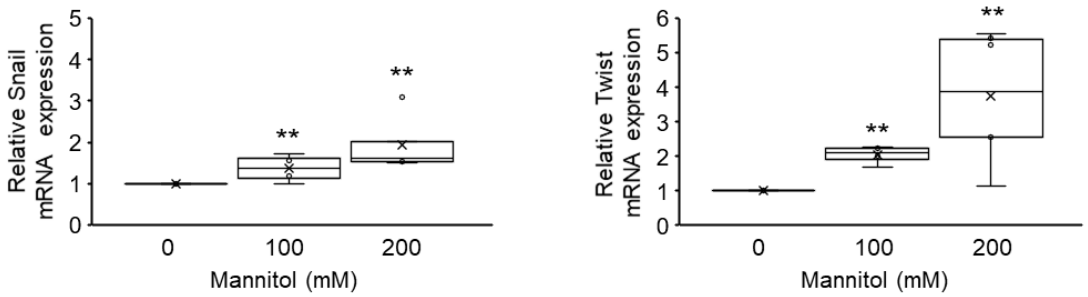

Fig. 4-3 Effects of hyperosmotic mannitol stress on the expression of Snail and Twist. NRK-52E cells were treated with mannitol (0, 100, 200 mM) for 12 h, and mRNA expression was analyzed by qPCR. Quantitation of the changes in the mRNA of Snail (n = 6 from 0 mM, n = 4 from 100 mM, n = 5 from 200 mM) and Twist (n = 7 from 0 mM, n = 4 from 100 mM, n = 6 from 200 mM). Relative gene expression was calculated considering 0 mM as 1. Data are presented as box and whisker plots with average (×), median, IQR, and minimum and maximum values. $^{**}P < 0.01$ from the data of 0 mM (Steel test).

4.3.3 Hyperosmolarity induces the dynamic changes in FAs

Based on the above-described results, the author hypothesized that the cell shrinkage caused by hyperosmotic stress interferes with the structure and organization of the actin cytoskeletal network and FAs by limiting the intracellular space. To test this hypothesis, the author focused on the effect of hyperosmotic stress on actin cytoskeletal structures and FA distribution, which are known to be responsible for mediating various important cellular processes such as cell structural support and functional regulation [19].

Although there was no change in the actin cytoskeleton cultured with 100 mM mannitol (Fig. 4-4A), the actin cytoskeletal structure exhibited drastic time-dependent changes after being treated with 200 mM mannitol (Fig. 4-4B); the actin filaments were disassembled by treatment with 200 mM mannitol for 0.5 h and then reorganized into thick stress fibers at 12 h, as shown in Section 2.3.2. These results are consistent with those of previous studies that demonstrated hyperosmolarity-induced depolymerization and reorganization of the actin cytoskeleton for adaptive responses [19].

The author also evaluated the effect of hyperosmotic treatment on the rearrangement of FAs, which play important roles in the organization and structure of actin filaments. Mannitol-treated cells were examined for their contents of vinculin, an FAs marker, by fluorescence immunostaining. Like the actin cytoskeletal structures, treatment with 100 mM mannitol did not cause any detectable changes in the vinculin fluorescence distribution pattern (Fig. 4-4A), which was similar to control cells demonstrating widespread labeling of FAs (0 h in Fig. 4-4A). In contrast, in the cells treated with 200 mM mannitol, vinculins were disassembled in the central region and almost localized along the edges of cells after 30 min and then recovered to a similar distribution pattern as that of control cells at 12 h (Fig. 4-4B).

To quantify the effect of hyperosmotic stress treatment on FA changes, “the number of FAs per cell” and “the area of each FA” were calculated. Upon treatment with 200 mM mannitol, there was a significant decrease in the number of FAs after 0.25 and 0.5 h (0 h, 23.7 ± 2.0; 0.25 h, 4.7 ± 0.6 ($P < 0.01$); 0.5 h, 3.6 ± 0.6 ($P < 0.01$)) (Fig. 4-4C), which recovered to the control level at 2 h (21.1 ± 3.8) and then significantly increased at 12 h compared with the initial value (46.9 ± 9.0 ($P < 0.01$)) (Fig. 4-4C). The area of each FA was similar to the number of FAs. Within the first 0.5 h of 200 mM mannitol treatment, each FA area gradually decreased (0 h, 2.3 ± 0.1 μm^2; 0.25 h, 1.8 ± 0.2 μm^2; 0.5 h, 1.2 ± 0.1 μm^2 ($P < 0.01$)) (Fig. 4-4D). The value of FA area returned to the level of the untreated cells at 2 h (2.2 ± 0.1 μm^2) and then significantly increased at 12 h (3.0 ± 0.2 μm^2 ($P < 0.01$)) (Fig. 4-4D). Treatment with 100 mM mannitol resulted in no significant changes in both FA number and FA area (Figs. 4-4A, C, and D).

These findings clearly demonstrate that hyperosmotic condition induces the disassembly and subsequent rearrangements of FAs concomitant with actin filament dynamics change in NRK-52E cells.

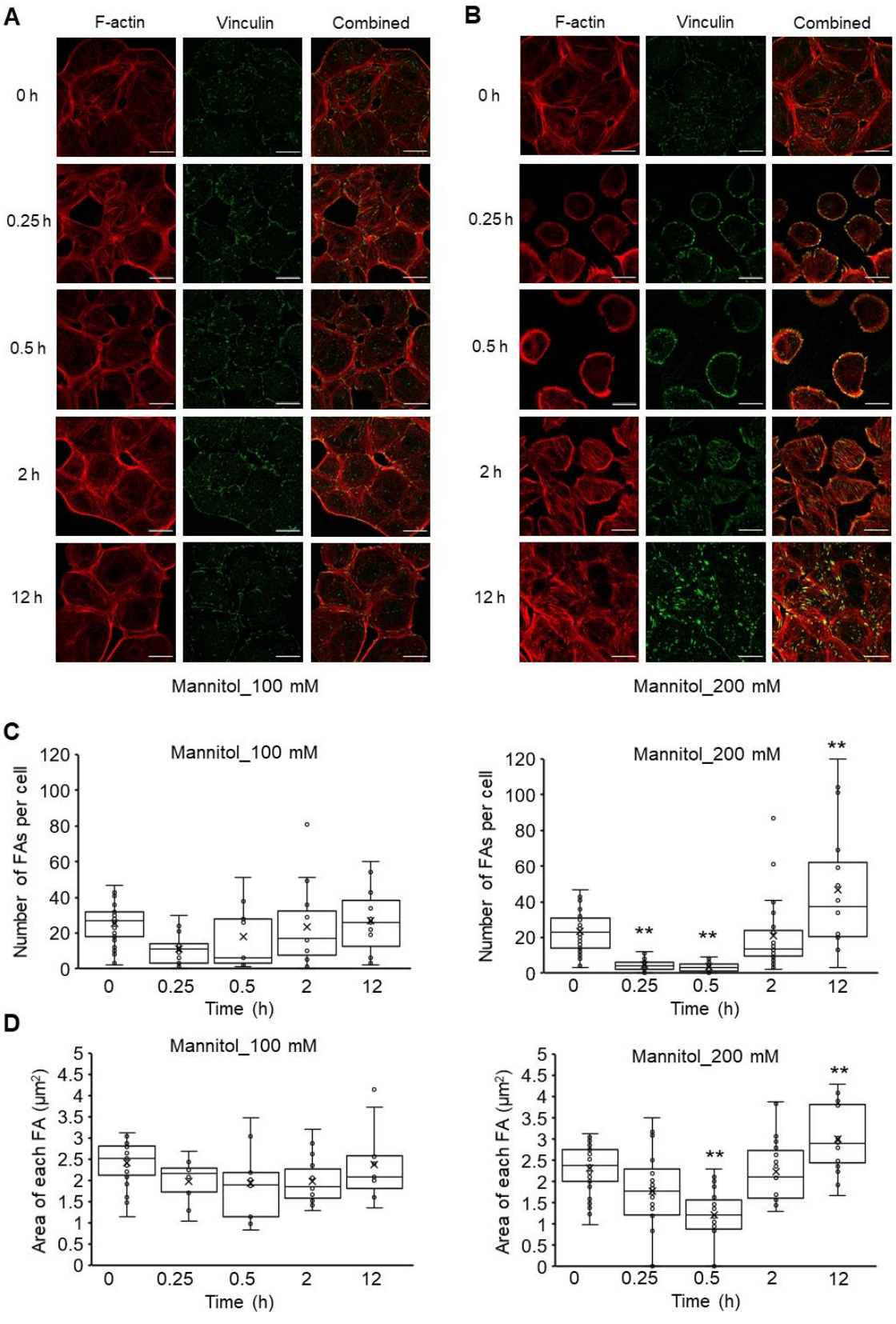
A
F-actin
Vinculin
Combined
0 h
0.25 h
0.5 h
2 h
12 h
Mannitol_100 mM
B
F-actin
Vinculin
Combined
0 h
0.25 h
0.5 h
2 h
12 h
Mannitol_200 mM
C
Mannitol_100 mM
Number of FAs per cell
Time (h)
Mannitol_200 mM
Number of FAs per cell
Time (h)
D
Mannitol_100 mM
Area of each FA (μm²)
Time (h)
Mannitol_200 mM
Area of each FA (μm²)
Time (h)

Fig. 4-4 Effects of hyperosmotic mannitol stress on actin and vinculin distribution in NRK-52E cells. (A, B) Cells were cultured with 100 (A) or 200 mM (B) mannitol for 0, 0.25, 0.5, 2, and 12 h. Typical fluorescence images of F-actin (red), vinculin (green), and combined (red and green). Bar, 25 μm. (C, D) A summary of vinculin staining data from (A) and (B), showing the number of FAs per cell (C) and area of each FA (D) (100 mM; 0 h (n = 25), 0.25 h (n = 13), 0.5 h (n = 9), 2 h (n = 15), 12 h (n = 11): 200 mM; 0 h (n = 33), 0.25 h (n = 28), 0.5 h (n = 27), 2 h (n = 28), 12 h (n = 16)). Data are presented as box and whisker plots with average (×), median, IQR and minimum and maximum values. The n indicates the number of cells analyzed. $^{**}P < 0.01$ from the data of 0 h (Dunnett's test).

4.3.4 Hyperosmolarity promotes the incorporation of α-SMA into actin stress fibers

Treatment with 200 mM mannitol for 12 h significantly increased the area of each FA in NRK-52E cells. Based on the findings of previous studies, FA size controls the recruitment of α-SMA to actin stress fibers [20], the author further hypothesized that hyperosmotic stress promotes the incorporation of α-SMA into actin stress fibers. Strikingly, after treatment with 200 mM mannitol for 12 h, the expression level of α-SMA protein in the cells was significantly increased (Fig. 4-5A), and the association of α-SMA with actin filaments increased cellular anisotropy compared with the control (0 mM) (Fig. 4-5B). Decreased expression of E-cadherin at the same time was also observed, which is consistent with the features of EMT (Fig. 4-5A).

These observations indicate that hyperosmotic conditions could promote the expression and recruitment of α-SMA to the actin stress fibers in NRK-52E cells.

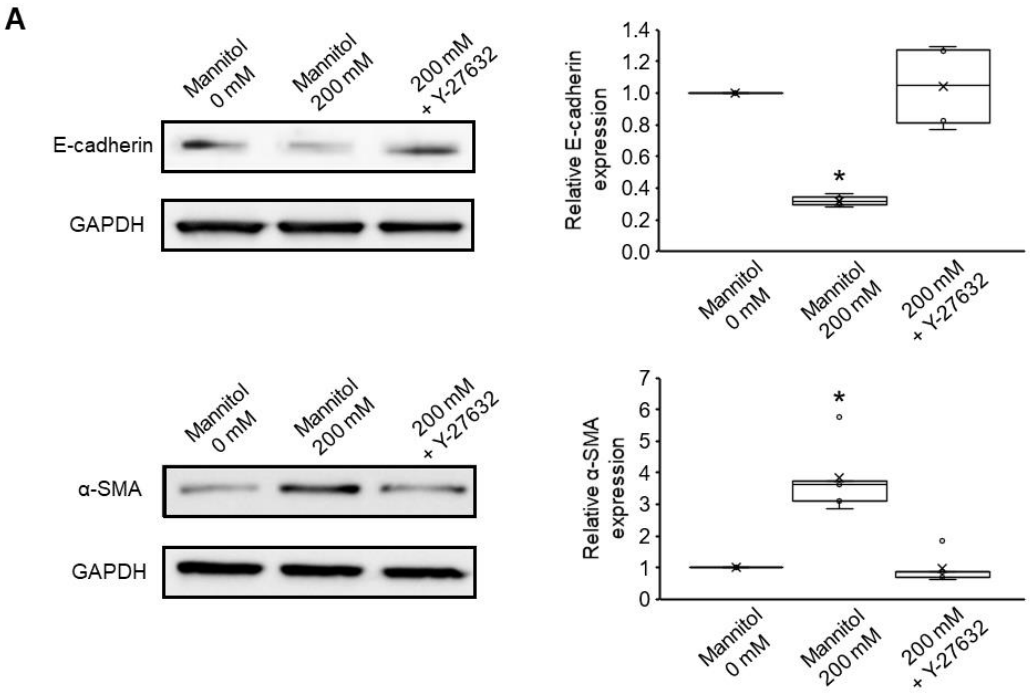
A
Mannitol 0 mM
Mannitol 200 mM
200 mM + Y-27632
E-cadherin
GAPDH
Relative E-cadherin expression
1.4
1.2
1.0
0.8
0.6
0.4
0.2
0.0
*
Mannitol 0 mM
Mannitol 200 mM
200 mM + Y-27632
α-SMA
GAPDH
Relative α-SMA expression
7
6
5
4
3
2
1
0
*
Mannitol 0 mM
Mannitol 200 mM
200 mM + Y-27632

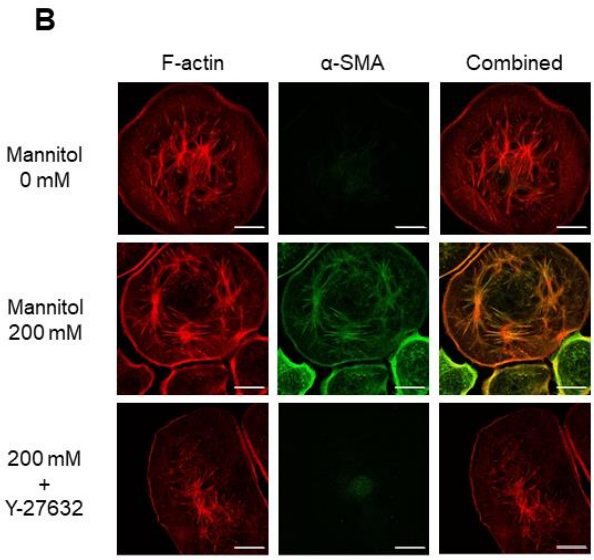
B
F-actin
α-SMA
Combined
Mannitol 0 mM
Mannitol 200 mM
200 mM + Y-27632

Fig. 4-5 Effects of FAs on the recruitment of α-SMA to actin stress fibers. NRK-52E cells were treated with mannitol (200 mM) or cotreated with Y- 27632 (1 μM) for 12 h. (A) Western blot analysis for E-cadherin (n = 4 from mannitol (0 mM), n = 4 from mannitol (200 mM), n = 4 from mannitol (200 mM) + Y-27632) and α-SMA (n = 5 from mannitol (0 mM), n = 5 from mannitol (200 mM), n = 5 from mannitol (200 mM) + Y-27632). Left: The representative bands obtained Western blotting. Right: Quantification analysis of E-cadherin and α-SMA. Relative expression was calculated as normalized to untreated cells (mannitol 0 mM). Data are presented as box and whisker plots with average (×), median, IQR, and minimum and maximum values. The n indicates the number of independent experiments. $^{*}P < 0.05$ from the data of 0 mM (Steel–Dwass test). (B) Typical fluorescence images of F-actin (red), α-SMA (green), and combined (red and green). Bar, 25 μm.

4.3.5 Cotreatment with Y-27632 suppresses hyperosmolarity-induced FA rearrangements and colocalization of F-actin and α-SMA

To investigate whether FA rearrangements directly affect the hyperosmolarity-induced EMT in NRK-52E cells, the author explored the experimental conditions that prevent the rearrangement of FAs.

Treatment with 1 μM Y-27632, a ROCK inhibitor, could suppress FA rearrangements induced by 200 mM mannitol treatment, but it had no appreciable effect on actin filament reorganization (Fig. 4-6A). Quantitatively, the average of FA area of cells cotreated with Y-27632 and mannitol exhibited a significant decrease until 0.5 h (0 h, 2.6 ± 0.1 μm^2; 0.25 h, 1.3 ± 0.3 μm^2 ($P < 0.01$); 0.5 h, 1.4 ± 0.1 μm^2 ($P < 0.01$)) (Fig. 4-6B). Even after 2 h since the beginning of the cotreatment, the significant decrease in the value of FA area continued at 2 and 12 h (1.6 ± 0.2 μm^2 ($P < 0.01$) and 1.9 ± 0.1 μm^2 ($P < 0.05$), respectively) (Fig. 4-6B). The values of FA area at 2 and 12 h after cotreatment with Y-27632 were smaller than those obtained under treatment with 200 mM mannitol alone (Fig. 4-4D) at the same time points; this result was statistically significant (Fig. 4-6C).

These results demonstrated that cotreatment with 200 mM mannitol and 1 μM Y-27632 was an experimental condition that could prevent hyperosmotic stress-induced FA rearrangements without affecting actin cytoskeletal dynamics in NRK-52E cells.

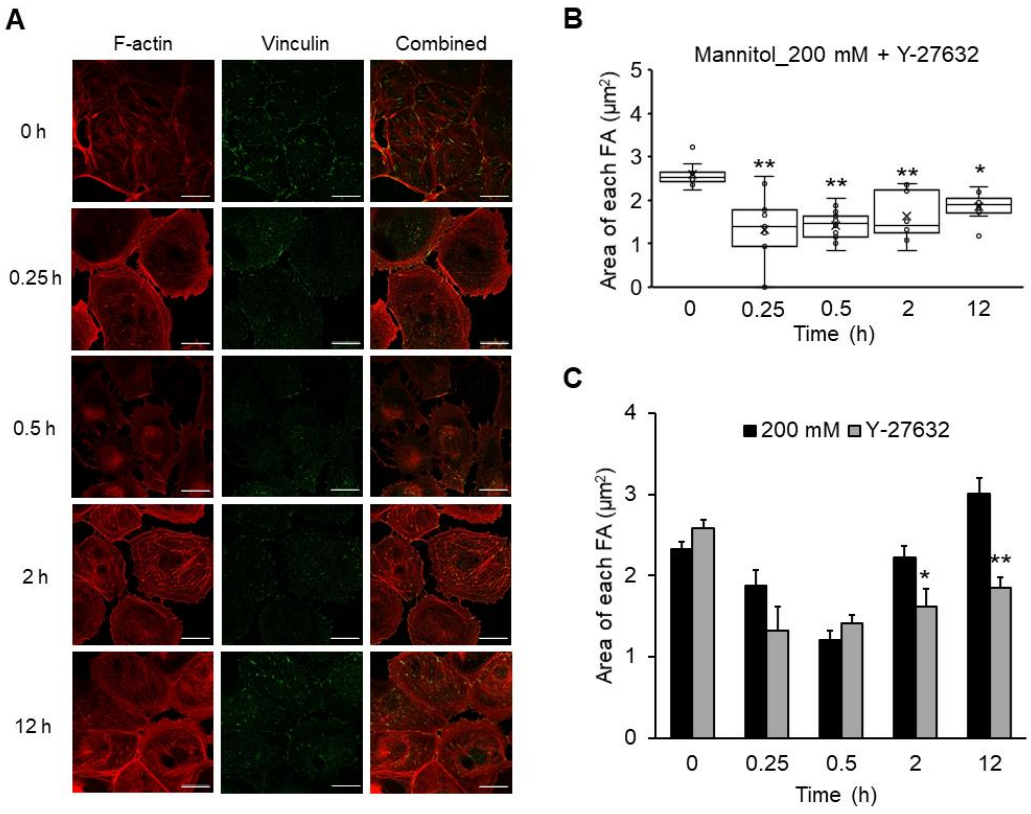

Fig. 4-6 Experimental conditions that prevent the rearrangement of FAs without affecting actin cytoskeleton reorganization. NRK-52E cells were cotreated with mannitol (200 mM) and Y-27632 (1 μM) for 0, 0.25, 0.5, 2, and 12 h. (A) Typical fluorescence images of F-actin (red), vinculin (green), and combined (red and green). Bar, 25 μm. (B) A summary of vinculin staining data from (A), showing the area of each FA (mannitol (200 mM) + Y-27632; 0 h (n = 9), 0.25 h (n = 9), 0.5 h (n = 14), 2 h (n = 8), 12 h (n = 8)). Data are presented as box and whisker plots with average (×), median, IQR, and minimum and maximum values. The n indicates the number of cells analyzed. (C) A comparison between mannitol (200 mM) alone and cotreated with Y-27632 (1 μM) from (B). The data of 200 mM mannitol alone (black bars) were identical to those in Fig. 4-4D, which were shown for comparisons. Data are mean ± SEM. $^{*}P < 0.05$, $^{**}P < 0.01$ from the data of mannitol (200 mM) at the same time point (Student's t-test).

The author then investigated the effects of treatment with 1 μM Y-27632, which prevented the hyperosmolarity-induced FA rearrangements, on the recruitment of α-SMA to actin stress fibers. Preventing the FA rearrangements attenuated the effects of hyperosmolarity. Even under hyperosmotic conditions, treatment with Y-27632 significantly reduced the colocalization of F-actin and α-SMA fluorescence signals similar to the control levels (Fig. 4-5B). These results suggest that the FA rearrangements induced by hyperosmotic stress play an important role in the expression of α-SMA and its incorporation into actin stress fibers in NRK-52E cells.

Furthermore, using Western blotting and immunofluorescence staining, the Y-27632 treatment abolished both the increase in α-SMA and the decrease in E-cadherin expressions induced by mannitol (200 mM) to the control level (Fig. 4-5A and Fig. 4-7A). Similar results were obtained for mRNA levels of the epithelial marker, E-cadherin, and the mesenchymal markers, α-SMA and vimentin (Fig. 4-7B).

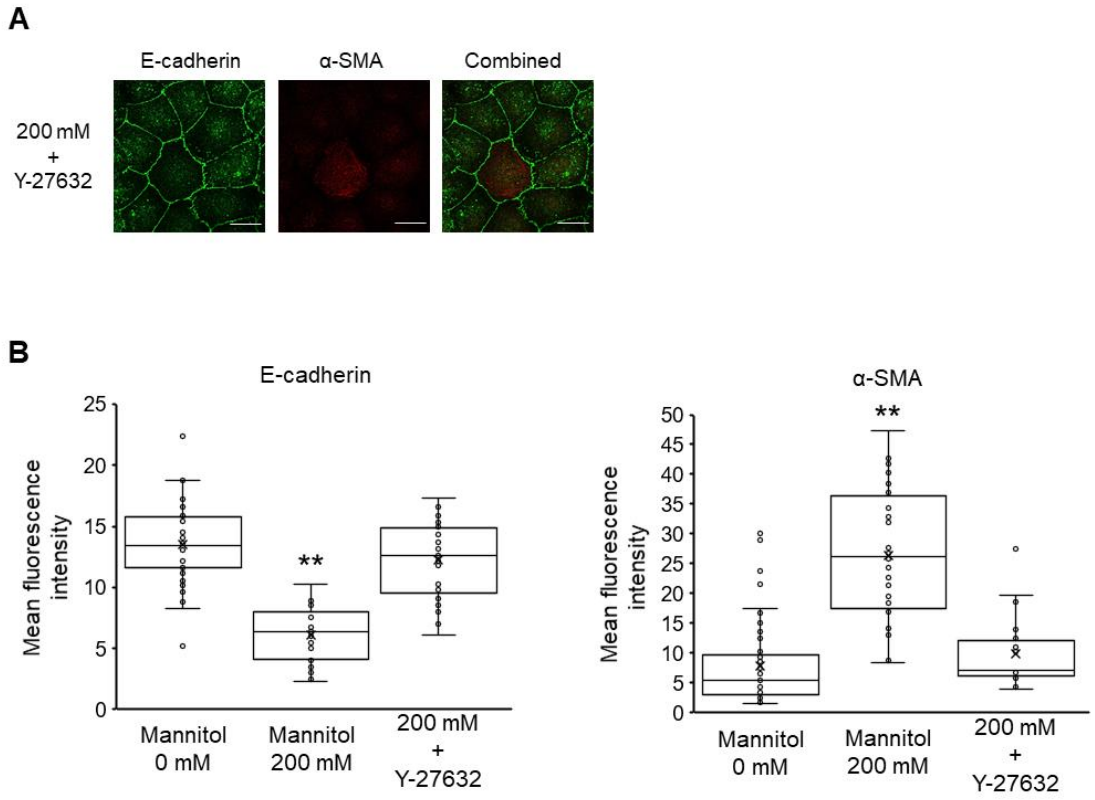

Fig. 4-7 Effects of Y-27632 on the epithelial–mesenchymal transition of NRK-52E cells. (A) Typical fluorescence images of E-cadherin (green), α-SMA (red), and combined (green and red) cotreated with mannitol (200 mM) and Y-27632 (1 μM) for 12 h. Bar, 25 μm. (B) Quantitation of the changes in the mean fluorescence intensity of E-cadherin and α-SMA (n = 34 from 200 mM + Y-27632) by immunofluorescence staining. The data of mannitol (0 and 200 mM) were identical to those in Fig. 4-1B and C, which were shown for comparisons. Data are presented as box and whisker plots with average (×), median, IQR, and minimum and maximum values. $^{**}P < 0.01$ from the data of 0 mM (Tukey's test).

4.3.6 Cotreatment with Y-27632 attenuates the hyperosmolarity-induced production of fibrogenesis-related factors

The differentiation of tubular epithelial cells into α-SMA-positive myofibroblasts ultimately leads to the deposition of the ECM, which contributes to the progression of renal fibrosis [9]. Given that hyperosmotic stress-induced EMT in NRK-52E cells, the author reasoned that the expression of ECM-related genes is promoted in response to hyperosmotic stress.

To test this hypothesis, the author first investigated whether hyperosmotic stress affects the expression of EMT and ECM-related genes using real-time PCR. Upon treatment with 200 mM mannitol for 24 h, not only the expression levels of the EMT maker, but also the expression levels of the ECM marker collagen I and the fibrogenesis factor PAI-1 were changed, but the increase in the expression of ECM fibronectin was not statistically significant (Fig. 4-8). Since PAI-1 is a major inhibitor of plasminogen activator, increased PAI-1 levels are considered to contribute to increased ECM accumulation due to the suppression of plasmin production and matrix metalloproteinase activation [9]. Therefore, these results indicate that hyperosmotic stress induces the expression of fibrosis-related factors through EMT in NRK-52E cells.

Moreover, treatment with Y-27632 abolished the upregulation of the mRNA levels of collagen I, PAI-1, and fibronectin in the presence of mannitol (Fig. 4-8). These results suggest that in NRK-52E cells, the ROCK signaling inhibition attenuates the hyperosmotic stress-induced upregulation of profibrotic factors, and prevention of FAs rearrangements may be involved in part of the mechanism.

EMT-related genes

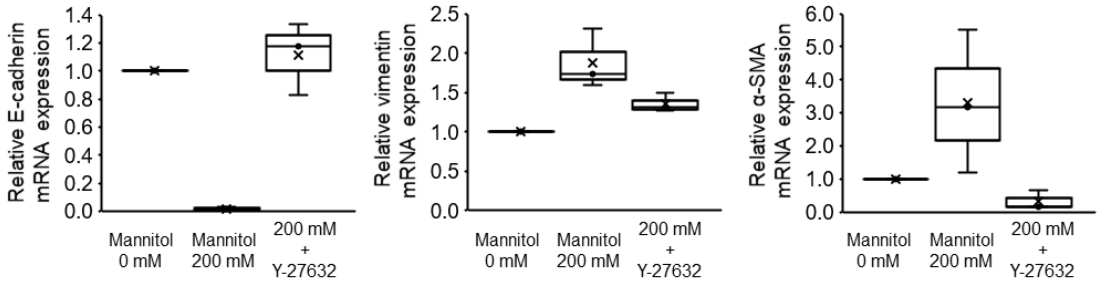

ECM-related genes

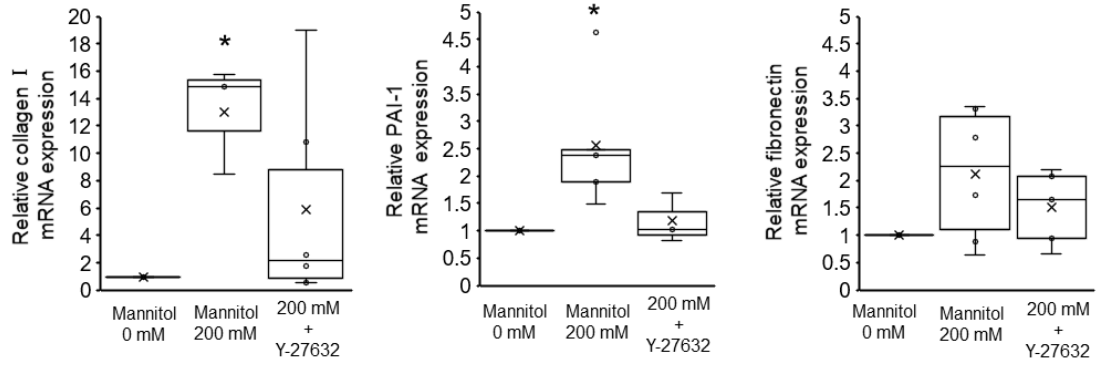

Fig. 4-8 Effects of Y-27632 on the hyperosmotic mannitol stress-induced expression of EMT- and ECM-related genes. NRK-52E cells were cotreated with mannitol and Y-27632, and mRNA expression was analyzed. Quantitation of the changes in E-cadherin (n = 3), vimentin (n = 3), α-SMA (n = 3), collagen-I (n = 6 from 0 mM, n = 3 from 200 mM, n = 6 from 200 mM + Y-27632), PAI-1 (n = 5 from 0 mM, n = 5 from 200 mM, n = 3 from 200 mM + Y-27632) and fibronectin (n = 6 from 0 mM, n = 6 from 200 mM, n = 5 from 200 mM + Y-27632). Relative gene expression was calculated considering 0 mM as 1. Data are presented as box and whisker plots with average (×), median, IQR and minimum and maximum values. T. $^{*}P < 0.05$ from the data of 0 mM (Steel–Dwass test).

4.3.7 TRPV4 channel involves in hyperosmolarity-induced EMT

In Chapter 3, the author described that hyperosmotic mannitol stress could induce a transient Ca^{2+} influx in NRK-52E, implying the involvement of TRPV4 channel activation. Given the growing body of evidence for Ca^{2+} signaling in EMT, the author hypothesized that TRPV4 channels play a role in hyperosmolarity-induced EMT.

When the cells were stimulated with 200 mM mannitol for 12 h, the expression of E-cadherin and α-SMA was significantly decreased and increased, respectively, whereas the HC-067047 treatment abolished both the increase in α-SMA and the decrease in E-cadherin expressions induced by 200 mM mannitol (Fig. 4-9A). To further determine whether TRPV4-mediated Ca^{2+} influx can drive EMT induction, NRK-52E cells were treated with the selective TRPV4 agonist GSK1016790A (hereafter GSK-101; 100 nM). Pharmacological TRPV4 activation by GSK-101 treatment alone resulted in EMT protein marker changes, as evidenced by the upregulation of α-SMA and downregulation of E-cadherin (Fig. 4-9B).

These findings show that TRPV4-mediated Ca^{2+} influx may play an important role in EMT in NRK-52E cells.

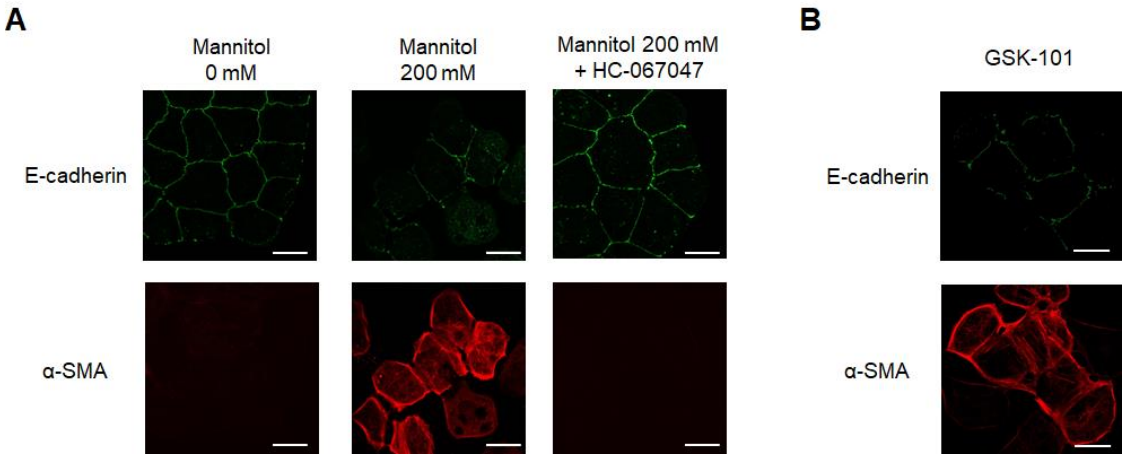

Fig. 4-9 Effects of TRPV4 antagonist and agonist on EMT-related protein expression of NRK-52E cells. (A) Typical fluorescence images of E-cadherin (green) and α-SMA (red) cultured with 0 mM mannitol, 200 mM mannitol, and cotreatment with 200 mM mannitol and 10 μM HC-067047 for 12 h. Bar, 25 μm. (B) Typical fluorescence images of E-cadherin (green) and α-SMA (red) cultured with 100 nM GSK-1016790A (GSK-101) for 12 h. Bar, 25 μm.

4.4 Discussion

The purpose of this chapter was to explore the role of hyperosmolarity in the EMT of proximal tubular epithelial cells. The novel finding was that hyperosmotic mannitol stress could induce EMT, and FAs rearrangements are thought to be partly involved in the mechanism for the hyperosmotic stress-induced EMT.

Considering that using urea, which is a membrane-permeable osmolarity regulator did not induce EMT, the mannitol-induced EMT could be triggered by cell shrinkage due to osmotic differences between the cytosol and extracellular compartment and not by the hyperosmotic condition itself (Figs. 4-1 and 4-2). When NRK-52E cells were exposed to hyperosmotic urea, the reduction in cell volume was markedly smaller than that under hyperosmotic mannitol treatment (Fig. 2-3), which suggests that a reduction of cell-cell contact occurred. Previous studies have demonstrated that disrupting the cell-cell contact induces the proteolytic shedding of E-cadherin, which causes the nuclear translocation of β-catenin, the transcriptional induction of Snail/Slug, and the repression of E-cadherin transcription in NRK-52E cells [31,32]. Mannitol treatment of NRK-52E cells reduced E-cadherin expression (Fig. 4-1) and increased the expression levels of Snail and Twist (Fig. 4-3). Although the author needs further investigate the relationship between the repression of E-cadherin and the up-regulation of Snail/Twist in response to hyperosmotic mannitol, it is reasonable to suppose that the decrease of E-cadherin, followed by the induction of EMT, in hyperosmotic mannitol stress was due to disrupting the cell-cell contact caused by cell shrinkage. To further elucidate the mechanism of hyperosmotic mannitol-induced EMT, it is important to investigate the effects on not only E-cadherin but also various epithelial cell markers, such as zonula occuludens-1 and N-cadherin which is thought to be the predominant classic cadherin in the proximal tubule in vivo

[33-35].

Previous studies have demonstrated that hyperosmotic stress affects cytoskeletal structures such as actin fibers and microtubules [36,37]. The author also observed changes in actin cytoskeletal structure and the arrangements of FAs induced under mannitol-mediated hyperosmotic conditions. It is possible that hyperosmotic conditions affect the synthesis of these proteins [38], which may cause the changes. On the other hand, a previous study demonstrated that hyperosmotic stress even for 10 min activates Rho family small GTPases, Rac/Cdc42, which contribute to volume-dependent cytoskeleton remodeling characterized by disassembly of stress fibers and deposition of peripheral actin filaments [19]. It is also reported that hyperosmotic stress activates Rho/ROCK and shrinkage-induced cofilin phosphorylation, which induces the reorganization of the actin cytoskeleton upon osmotic stress [39]. These results are quite similar to the changes in the actin cytoskeleton in the present study, and our osmotic concentration of 200 mM mannitol (530 mOsmol/L) sufficiently exceeded the threshold for the activation of the ROCK signaling pathway shown by the previous study [40]. Thus, the author thinks that the actin filaments were disassembled by the ROCK signaling pathway under the 200 mM mannitol condition. Since vinculin was observed mostly at the end of actin stress fibers, and FAs act as sites of actin polymerization associating with the reorganization of actin cytoskeletal structure, the author also supposes that hyperosmotic stress induces the disassembly and subsequent rearrangements of FAs concomitant with actin filament dynamics change.

As described in Chapter 2, even the cell volume and the structure of actin cytoskeletons recovered to the initial level under mannitol-mediated hyperosmotic conditions (Figs. 2-2 and 2-3), the number and the area of FAs increased at later time points (Fig. 4-4). The

mechanisms for these cell phenomena are still unclear, but the author hypothesizes a compensatory response of cells causes this. Instead of the decreased E-cadherin expression under hyperosmotic mannitol stress conditions, cells may increase FAs to maintain intracellular force balance [41,42], known as mechanical homeostasis, by remodeling mechanical coupling between cell-cell and cell-substrate adhesion, which is also suggested to play an important role in EMT [43].

Previous studies have reported that the incorporation of α-SMA into stress fibers induces increases in the contractile activity of stress fibers and the FA size [20,24]. It has also been reported that contractile activity correlates with the expression level of α-SMA [22]. The results of this chapter revealed that the application of hyperosmotic stress-induced the increased expression of α-SMA, which is more likely to be incorporated into stress fibers (Fig. 4-5B), as well as the increased size of FA (Fig. 4-4D). These findings provide a strong indication for a hyperosmotic stress-induced positive feedback loop between α-SMA and FAs. The existence of such a feedback loop is further supported by findings in this chapter that cotreatment with a ROCK inhibiter Y-27632 (1 μM), which is known to attenuate the contractile activity of stress fibers based on inhibition of ROCK and MLCK pathways [44,45], inhibited the rearrangement of FAs, α-SMA expression, and recruitment of α-SMA to the actin stress fibers (Fig. 4-5B). Nevertheless, the Rho/ROCK signal also acts on other cytoskeletons, such as tubulin and intermediate filaments and regulates intracellular contractile forces [46-48]. Therefore, one of the limitations of this study is that it could not rule out the effects of Y-27632 on the contractile forces derived from other cytoskeletons except the actin cytoskeleton. Moreover, since Rho/ROCK signal is a pathway that affects both actin and FA dynamics, it cannot be said that the treatment with 1 μM Y-27632 had no effect on actin

reorganization. Indeed, a thinning of the actin skeleton was observed in Figure 4-6A compared to Figure 4-4B. However, present results are potentially important as they demonstrate that the hyperosmolarity-induced cytoskeletal changes may trigger the differentiation of α-SMA-positive myofibroblasts. Investigating the effects of hyperosmolarity on the changes in intracellular contraction forces can further elucidate the mechanism underlying the effects of cytoskeletal changes on EMT.

The importance of EMT in the progression of renal fibrosis has been controversial [49,50]. A previous study has reported that ~5% of the total interstitial α-SMA-positive myofibroblasts arose from an EMT in the unilateral ureteral obstruction model [49]. Thus, the generation of α-SMA-positive myofibroblasts as a consequence of EMT in renal epithelial cells reflects only part of the biological processes of differentiation. However, the present results are believed to be important because recent studies have disclosed that "partial EMT," in which epithelial cells remain attached to the tubular basement membrane but the epithelial cell transformation occurs, plays a vital role in initiating tubular dysfunction and driving fibrosis development [51-53]. It is known that partial EMT causes myofibroblast proliferation, triggering the cell cycle arrest of epithelial cells and promoting the release of fibrogenesis factors [3]. In fact, it has been shown that in animal models of renal fibrosis, several tubular cells are arrested in the cell cycle, and these tubular cells lead to the synthesis and secretion of profibrotic factors through partial EMT [3,54]. In the present study, mannitol treatment of NRK-52E cells increased the expression levels of Snail and Twist, two key transcription factors that regulate partial EMT (Fig. 4-3), and collagen I and PAI-1, major profibrotic factors (Fig. 4-8). Considering the importance of α-SMA-positive myofibroblasts in the pathogenesis of renal disease, the finding of this chapter that hyperosmotic stress-induced the

upregulation of partial EMT markers could have significant implications.

Extracellular signaling factors that drive the EMT require second messengers to transmit their effects to their targets, and Ca^{2+} -permeable ion channels that facilitate the influx of extracellular calcium into the cytosol can modulate EMT [55]. However, these Ca^{2+} channels have been linked to both the promotion and inhibition of the EMT phenomenon [55]. TRPV4 pharmacological inhibition blocked the downregulation of epithelial markers, E-cadherin, and the upregulation of mesenchymal markers, α-SMA, induced by hyperosmotic stress (Fig. 3E) and direct TRPV4 activation with GSK-101 treatment increased α-SMA expression while suppressing E-cadherin expression (Fig. 4-9A). These findings suggest that TRPV4 has the potential to play a direct role in EMT induction. Interestingly, previous studies have demonstrated that TRPV4 and EMT are associated via the ERK, YAP/TAZ, and PI3K/AKT pathways in various cell types in a context-dependent manner [56,57]. To gain a better understanding of the mechanisms underlying hyperosmolarity-induced EMT, the relationship between TRPV4 activation and the involvement of these signals need to be investigated.

4.5 Conclusion

In the present chapter, the FA rearrangement in response to hyperosmotic mannitol is one of the mechanisms responsible for the EMT of proximal tubular epithelial cells. The findings indicate the possibility that hyperosmotic stress, which generates mechanical stress, is a potential risk factor affecting the induction of EMT in proximal tubular cells. Moreover, TRPV4 channels, which are involved in the initial step of calcium influx, could be potential therapeutic targets for controlling the progression of EMT. (Fig. 4-10)

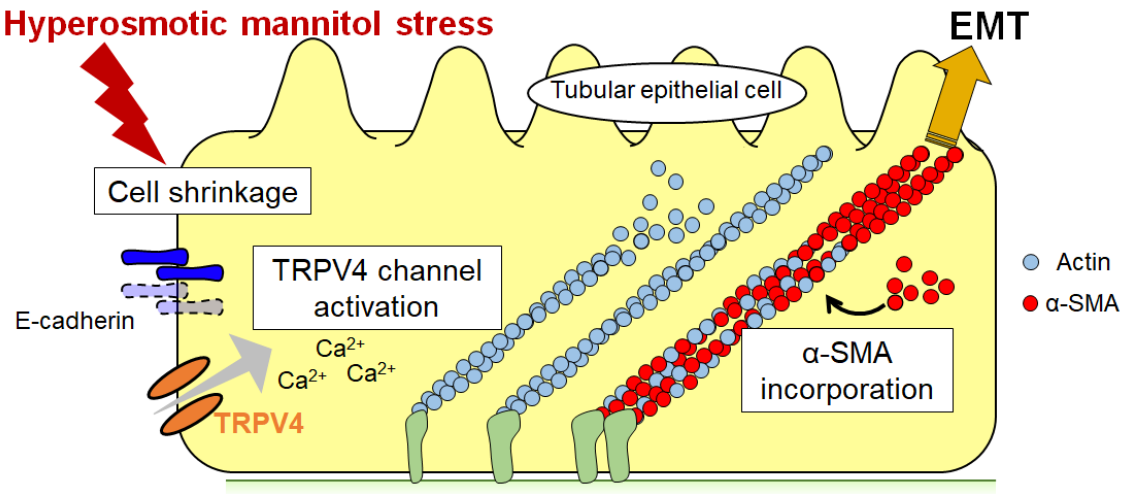

Fig. 4-10 Schematic illustration of the mechanism of hyperosmolarity-induced EMT. Hyperosmotic stress leads to Ca^{2+} influx through TRPV4 channels activation and a reorganization of focal adhesions in tubular epithelial cells. This leads to EMT, as evidenced by a decrease in E-cadherin expression and elevate in the incorporation of α-SMA after mannitol treatment.

References

1. Lamouille S, Xu J, Derynck R. Molecular mechanisms of epithelia mesenchymal transition. Nature Reviews Molecular Cell Biology. 2014;15: 178-196.
2. Ferenbach DA, Bonventre J V. Mechanisms of maladaptive repair after AKI leading to accelerated kidney ageing and CKD. Nature Reviews Nephrology. 2015;11: 264-276.
3. Lovisa S, LeBleu VS, Tampe B, Sugimoto H, Vadnagara K, Carstens JL, et al. Epithelial-to-mesenchymal transition induces cell cycle arrest and parenchymal damage in renal fibrosis. Nature Medicine. 2015;21:998-1009.
4. Humphreys BD. Mechanisms of Renal Fibrosis. Annual Review of Physiology. 2018;80:309-326.
5. Rello J, Triginer C, Sánchez JM, Net A. Acute Renal Failure following Massive Mannitol Infusion. Nephron. 1989;53:377-378.
6. Fujigaki Y, Muranaka Y, Sun D, Goto T, Zhou H, Sakakima M, et al. Transient myofibroblast differentiation of interstitial fibroblastic cells relevant to tubular dilatation in uranyl acetate-induced acute renal failure in rats. Virchows Archiv. 2005;446:164-176.
7. Sun DF, Fujigaki Y, Fujimoto T, Yonemura K, Hishida A. Possible Involvement of Myofibroblasts in Cellular Recovery of Uranyl Acetate-Induced Acute Renal Failure in Rats. The American Journal of Pathology. 2000;157:1321-1335.
8. Miyata Y, Asano Y, Muto S. Effects of P-glycoprotein on cell volume regulation in mouse proximal tubule. Am J Physiol Physiol. 2001;280: F829–F837.
9. Eddy AA. Serine proteases, inhibitors and receptors in renal fibrosis. Thromb Haemost. 2009;101:656-664.

10. Cano A, Pérez-Moreno MA, Rodrigo I, Locascio A, Blanco MJ, del Barrio MG, et al. The transcription factor Snail controls epithelial–mesenchymal transitions by repressing E-cadherin expression. Nature Cell Biology. 2000;2:76-83.

11. Grabias BM, Konstantopoulos K. The physical basis of renal fibrosis: effects of altered hydrodynamic forces on kidney homeostasis. AJP-Renal Physiology. 2014;306: F473-F485.

12. Hamzeh MT, Sridhara R, Alexander LD. Cyclic stretch-induced TGF-β1 and fibronectin expression is mediated by β1-integrin through c-Src- and STAT3-dependent pathways in renal epithelial cells. AJP-Renal Physiology. 2015;308: F425-F436.

13. Pietuch A, Brückner BR, Janshoff A. Membrane tension homeostasis of epithelial cells through surface area regulation in response to osmotic stress. Biochimica et biophysica acta. 2013;1833: 712–722.

14. Burridge K, Guilluy C. Focal adhesions, stress fibers and mechanical tension. Experimental Cell Research. 2016;343:14-20..

15. Saunders RM, Holt MR, Jennings L, Sutton DH, Barsukov IL, Bobkov A, et al. Role of vinculin in regulating focal adhesion turnover. European Journal of Cell Biology. 2006;85: 487-500.

16. Galbraith CG, Yamada KM, Sheetz MP. The relationship between force and focal complex development. Journal of Cell Biology. 2002;159: 695-705.

17. Haynes J, Srivastava J, Madson N, Wittmann T, Barber DL. Dynamic actin remodeling during epithelial–mesenchymal transition depends on increased moesin expression. Molecular Biology of the Cell. 2011;22:4750-4764.

18. Shankar J, Nabi IR. Actin cytoskeleton regulation of epithelial mesenchymal

transition in metastatic cancer cells. PLoS ONE. 2015;10:e0119954.

19. Ciano C Di, Nie Z, Szászi K, Lewis A, Uruno T, Zhan X, et al. Osmotic stress-induced remodeling of the cortical cytoskeleton. AJP Cell physiology. 2002;283:C850-C865.

20. Goffin JM, Pittet P, Csucs G, Lussi JW, Meister J-J, Hinz B. Focal adhesion size controls tension-dependent recruitment of alpha-smooth muscle actin to stress fibers. Journal of Cell Biology. 2006;172:259-268.

21. Hinz B, Celetta G, Tomasek JJ, Gabbiani G, Chaponnier C. Alpha-Smooth Muscle Actin Expression Upregulates Fibroblast Contractile Activity. Molecular Biology of the Cell. 2001;12:2730-2741.

22. Hinz B, Dugina V, Ballestrem C, Wehrle-Haller B, Chaponnier C. Alpha-Smooth Muscle Actin Is Crucial for Focal Adhesion Maturation in Myofibroblasts. Molecular Biology of the Cell. 2003;14:2508-2519.

23. Wang J, Sugita S, Nagayama K, Matsumoto T. Dynamics of actin filaments of MC3T3-E1 cells during adhesion process to substrate. Journal of Biomechanical Science and Engineering. 2016;11:15–00637..

24. Huang H, Zheng F, Dong X, Wu F, Wu T, Li H. Allicin inhibits tubular epithelial-myofibroblast transdifferentiation under high glucose conditions in vitro. Experimental and Therapeutic Medicine. 2017;13:254–262.

25. Bai Y, Wu C, Hong W, Zhang X, Liu L, Chen B. Anti-fibrotic effect of Sedum sarmentosum Bunge extract in kidneys via the hedgehog signaling pathway. Molecular Medicine Reports. 2017;16:737–745.

26. Zhang Y, Li H, Zhu J, Wei T, Peng Y, Li R, et al. Role of artesunate in TGF-β1-induced renal tubular epithelial-mesenchymal transdifferentiation in NRK-52E

cells. Molecular Medicine Reports. 2017;16:8891–8899.

27. Zhu Y-C, Wang Y-K, Bai S-J, Zha F-F, Feng G, Gao C-P, et al. Suppression of CIP4/Par6 attenuates TGF-β1-induced epithelial-mesenchymal transition in NRK-52E cells. International Journal of Molecular Medicine. 2017;40:1165–1171.

28. Birchmeier W. Cell adhesion and signal transduction in cancer. EMBO reports. 2005;6:413–417.

29. Onder TT, Gupta PB, Mani SA, Yang J, Lander ES, Weinberg RA. Loss of E-Cadherin Promotes Metastasis via Multiple Downstream Transcriptional Pathways. Cancer Research. 2008;68:3645–3654.

30. Conacci-Sorrell M, Simcha I, Ben-Yedidia T, Blechman J, Savagner P, Ben-Ze'ev A. Autoregulation of E-cadherin expression by cadherin-cadherin interactions: the roles of beta-catenin signaling, Slug, and MAPK. J Cell Biol. 2003;163: 847–857.

31. Masszi A, Fan L, Rosivall L, McCulloch CA, Rotstein OD, Mucsi I, et al. Integrity of Cell-Cell Contacts Is a Critical Regulator of TGF-β1-Induced Epithelial-to-Myofibroblast Transition. The American Journal of Pathology. 2004;165:1955–1967.

32. Zheng G, Lyons JG, Tan TK, Wang Y, Hsu T-T, Min D, et al. Disruption of E-Cadherin by Matrix Metalloproteinase Directly Mediates Epithelial-Mesenchymal Transition Downstream of Transforming Growth Factor-β1 in Renal Tubular Epithelial Cells. The American Journal of Pathology. 2009;175:580–591.

33. Bolati D, Shimizu H, Higashiyama Y, Nishijima F, Niwa T. Indoxyl sulfate induces epithelial-to-mesenchymal transition in rat kidneys and human proximal tubular cells. American journal of nephrology. 2011;34: 318–323.

34. Prozialeck WC, Lamar PC, Appelt DM. Differential expression of E-cadherin, N-

cadherin and beta-catenin in proximal and distal segments of the rat nephron. BMC Physiology. 2004;4:1–14.

35. Tsuchiya B, Sato Y, Kameya T, Okayasu I, Mukai K. Differential expression of N-cadherin and E-cadherin in normal human tissues. Archives of Histology and Cytology. 2006;69:135–141.

36. Bounedjah O, Hamon L, Savarin P, Desforges B, Curmi PA, Pastré D. Macromolecular Crowding Regulates Assembly of mRNA Stress Granules after Osmotic Stress. Journal of Biological Chemistry. 2012;287:2246–2258.

37. Desforges B, Savarin P, Bounedjah O, Delga S, Hamon L, Curmi PA, et al. Gap junctions favor normal rat kidney epithelial cell adaptation to chronic hypertonicity. AJP-Cell Physiology. 2011;301:C705-C716.

38. Brocker C, Thompson DC, Vasiliou V. The role of hyperosmotic stress in inflammation and disease. BioMolecular Concepts. 2012;3:345-364.

39. Thirone ACP, Speight P, Zulys M, Rotstein OD, Szászi K, Pedersen SF, et al. Hyperosmotic stress induces Rho/Rho kinase/LIM kinase-mediated cofilin phosphorylation in tubular cells: Key role in the osmotically triggered F-actin response. AJP - Cell Physiology. 2009;296:C463–C475.

40. Ciano-Oliveira C Di, Sirokmány G, Szászi K, Arthur WT, Masszi A, Peterson M, et al. Hyperosmotic stress activates Rho: differential involvement in Rho kinase-dependent MLC phosphorylation and NKCC activation. AJP-Cell Physiology. 2003;285:C555–C566.

41. Maruthamuthu V, Sabass B, Schwarz US, Gardel ML. Cell-ECM traction force modulates endogenous tension at cell-cell contacts. Proceedings of the National Academy of Sciences. 2011;108:4708–4713.

42. Paddillaya N, Mishra A, Kondaiah P, Pullarkat P, Menon GI, Gundiah N. Biophysics of Cell-Substrate Interactions Under Shear. Frontiers in Cell and Developmental Biology. 2019;7:251.

43. Scott LE, Griggs LA, Narayanan V, Conway DE, Lemmon CA, Weinberg SH. A hybrid model of intercellular tension and cell–matrix mechanical interactions in a multicellular geometry. Biomechanics and Modeling in Mechanobiology. 2020;19:1997–2013.

44. Amano M. Formation of Actin Stress Fibers and Focal Adhesions Enhanced by Rho-Kinase. Science. 1997;275:1308–1311.

45. Urban NH, Berg KM, Ratz PH. K+ depolarization induces RhoA kinase translocation to caveolae and Ca^{2+} sensitization of arterial muscle. AJP-Cell Physiology. 2003;285:C1377–C1385.

46. Amano M, Nakayama M, Kaibuchi K. Rho-kinase/ROCK: A key regulator of the cytoskeleton and cell polarity. Cytoskeleton. 2010;67:545–554.

47. Koga T, Koga T, Awai M, Tsutsui J, Yue BYJT, Tanihara H. Rho-associated protein kinase inhibitor, Y-27632, induces alterations in adhesion, contraction and motility in cultured human trabecular meshwork cells. Experimental Eye Research. 2006;82:362–370.

48. Schofield A V, Steel R, Bernard O. Rho-associated Coiled-coil Kinase (ROCK) Protein Controls Microtubule Dynamics in a Novel Signaling Pathway That Regulates Cell Migration. Journal of Biological Chemistry. 2012;287:43620–43629.

49. LeBleu VS, Taduri G, O'Connell J, Teng Y, Cooke VG, Woda C, et al. Origin and function of myofibroblasts in kidney fibrosis. Nature Medicine. 2013;19:1047-

1053.

50. Humphreys BD, Lin S-L, Kobayashi A, Hudson TE, Nowlin BT, Bonventre J V, et al. Fate Tracing Reveals the Pericyte and Not Epithelial Origin of Myofibroblasts in Kidney Fibrosis. The American Journal of Pathology. 2010;176:85–97.

51. Grande MT, Sánchez-Laorden B, López-Blau C, De Frutos CA, Boutet A, Arévalo M, et al. Snail1-induced partial epithelial-to-mesenchymal transition drives renal fibrosis in mice and can be targeted to reverse established disease. Nature Medicine. 2015;21:989–997.

52. Ovadya Y, Krizhanovsky V. A new Twist in kidney fibrosis. Nature Medicine. 2015;21:975–977.

53. Zhou D, Liu Y. Renal fibrosis in 2015: Understanding the mechanisms of kidney fibrosis. Nature Reviews Nephrology. 2016;12:68–70.

54. Canaud G, Bonventre J V. Cell cycle arrest and the evolution of chronic kidney disease from acute kidney injury. Nephrology Dialysis Transplantation. 2015;30:575–583.

55. Fang Y, Liu G, Xie C, Qian K, Lei X, Liu Q, et al. Pharmacological inhibition of TRPV4 channel suppresses malignant biological behavior of hepatocellular carcinoma via modulation of ERK signaling pathway. Biomed Pharmacother. 2018;101: 910–919.

56. Sharma S, Goswami R, David, Zhang X, Rahaman SO. TRPV4 regulates matrix stiffness and TGFβ1-induced epithelial-mesenchymal transition. J Cell Mol Med. 2019;23:761-774.

57. Azimi I, Robitaille M, Armitage K, So CL, Milevskiy MJG, Northwood K, et al.

Activation of the ion channel TRPV4 induces epithelial to mesenchymal transition in breast cancer cells. International Journal of Molecular Sciences. 2020;21: 1–14.

Chapter 5

The effects of hyperosmotic stress on autophagy of renal tubular epithelial cells

5.1 Introduction

Macroautophagy, hereafter referred to as autophagy, is a highly conserved "self-eating" pathway that eliminates damaged proteins and organelles and can be activated by pathophysiological stressors [1-3]. The initiation of the autophagic process includes the formation of omegasomes, which expand into double-membrane-bound autophagic vesicles (autophagosomes). Autophagosomes fuse with lysosomes to generate autolysosomes, which degrade harmful cellular components and restore intracellular homeostasis [4,5]. Autophagosomes are tagged by a protein called lipid-conjugated microtubule-associated protein 1 light chain 3 (LC3) [6]. The conversion of soluble LC3-I to lipid-bound LC3-II is considered as an indicator of autophagosome formation [7]. Therefore, the amount of LC3-II correlates with the number of autophagosomes, and is usually used as a marker of autophagy [7]. Autophagy is generally upregulated as a protective response in tubular epithelial cells and podocytes in response to pathogenic cellular stress and damage [8]. Accumulating studies have implicated that autophagy can be induced in AKI, which can arise in response to nephrotoxins, sepsis, and ischemia/reperfusion, and in CKD, including diabetic nephropathy and obstructive nephropathy [8-12]. Targeting the autophagy pathway may show considerable therapeutic potential in the treatment and management of kidney disorders including CKD.

Transcriptional factor EB (TFEB) is a major transcriptional regulator of autophagy-lysosome pathways and positively regulates the expression of autophagy and lysosomal genes, such as LC3, VPS18, Lamp1, and Lamp2 [13,14]. TFEB nuclear translocation is significantly regulated by phosphorylation events [15]. While phosphorylated TFEB is retained in the cytoplasm binding to 14-3-3 proteins, dephosphorylated TFEB travels to the nucleus. Phosphorylation of TFEB is mainly mediated by the mammalian target of rapamycin complex 1 (mTORC1) kinase, a major kinase complex that is a negative regulator of autophagy [16]. When mTORC1 activity is inhibited, TFEB is dephosphorylated and translocated into the nucleus [17]. On the other hand, dephosphorylation of TFEB is mediated by the activity of the calcium-dependent protein phosphatase calcineurin, which is induced by lysosomal specific Ca^{2+}-permeable ion channels, transient receptor potential mucolipin 1 (TRPML1) [17-20]. Since the over-expression of TRPML1 results in a significant increase of the autophagic flux, whereas its mutations can affect the accumulation of autophagosome, TRPML1 has some role in the early steps of autophagy [21].

Several common renal disorders, such as ischemia and inflammation causing tubular epithelial cell injury, induce nuclear translocation of TFEB and consequent activation of autophagy, particularly at the highly metabolically active proximal tubular segment [22]. Tubular epithelial cells are particularly indispensable for autophagy and are required to maintain homeostasis and respond to stressors [23,24]. A previous study demonstrated that mechanical compressive stress could induce autophagy [25]. Proximal tubular epithelial cells are routinely exposed to severe changes in osmolarity, and changes in osmotic conditions can generate not only osmotic but also mechanical stresses in cells by altering the cell shape and cytoplasmic membrane tension [26]. Indeed, as shown in

Chapter 2, rapid cell shrinkage occurs within a few minutes of exposure to hyperosmotic stress [27,28]. Cell compression by hyperosmotic stress may interfere with the organization of cellular cytoskeletal networks [29]. Recent studies have revealed the multiple roles of cytoskeletal elements, such as actin filaments and microtubules, in autophagy [30].

This chapter aimed to investigate the mechanisms involved in hyperosmolarity-induced autophagy. For this purpose, the author examined the relationship between the LC3 upregulation in response to hyperosmotic stress and the reorganization of the actin cytoskeleton. Moreover, I also examined the effects of hyperosmotic stress on TFEB nuclear translocation and its mechanism to better understand the mechanisms of hyperosmolarity-induced autophagy.

5.2 Materials and methods

5.2.1 Cell lines and reagents

NRK-52E cells, mannitol, and cytochalasin D were obtained as described in Sections 2.2.1 and 3.2.1. A microtubule depolymerizing agent, nocodazole, was obtained from FUJIFILM Wako Pure Chemical. Bafilomycin A1, an inhibitor of H^+-ATPase, was obtained from Adipogen Life Sciences (San Diego, CA). Antibodies for tubulin and LC3 were purchased from Abcam (Cambridge, MA). Other antibodies for TFEB, NFAT (nuclear factor of activated T cells), p70S6K, and GAPDH were obtained from Proteintech (Wuhan, China), Invitrogen (Carlsbad, CA), Proteintech, and Cell Signaling Technology (Danvers, MA), respectively. For the inhibitor experiments, cells were pre-treated for 15 min with EGTA (FUJIFILM Wako Pure Chemical), BAPTA-AM (Tokyo Kasei Kogyo, Tokyo, Japan), FK-506 (Cayman Chemical, Ann Arbor, MI), or ML-SI3 (a

TRPML antagonist, MedChemExpress, Monmouth Junction, NJ), before being stimulated with hyperosmotic mannitol.

5.2.2 Cell culture and hyperosmotic stimulation

The culture of NRK-52E cells and application of hyperosmotic mannitol were performed as described in Section 2.2.2.

5.2.3 RNA extraction and quantitative real-time PCR

RNA extraction and quantitative real-time PCR were performed as described in Section 4.2.3. The primer sequences used in this chapter were shown in Table 5-1.

Table 5-1: Primers used in this study.

Gene Name	Sense	Antisense
Rat GAPDH	TGACAACTTTGGCATCGTGG	GGGCCATCCACAGTCTTCTG
Rat LC3	CCTGCTGCTGGCCGTAGT	TGATGAAGTCTTCCTGCCAAAA
Rat VPS18	GCTCCGCATTGACTTGGG	GCCTTCTGTCCATTGCGGT
Rat LAMP1	GCCCGCGTGACTCCTCTTCC	ACGCAGCAGTTCTTCTCCGT
Rat LAMP2	AGCAGGTGGTTTCCGTGTCTCG	AGGGCTGCTCCCACCGCTAT

5.2.4 Immunofluorescence staining and nuclear translocation

Immunofluorescent staining and microscopic observation were conducted as described in Section 4.2.4. In this chapter, primary antibodies (1: 200) against anti-tubulin, anti-TFEB, and anti-NFAT were used.

For the evaluation of TFEB and NFAT nuclear translocation, the cells were incubated with Hoechst 33342 (Invitrogen) in the dark for 20 min to detect nuclei and the quantification of nuclear and cytoplasmic intensity was performed using the ImageJ Fiji software (version 1.52b, NIH) and represents the average intensity/cell with 20–30 cells [31]. TFEB nuclear localization was quantified as the ratio of the average intensity of nuclear TFEB fluorescence divided by the average of the cytosolic intensity of TFEB fluorescence [32].

5.2.5 Western blotting

Western blotting assay was performed as described in Section 4.2.6 "Western blotting". The following primary antibodies (dilution, 1:2000) were used: anti-p70S6K, anti-LC3, and anti-GAPDH serving as an internal control.

5.2.6 Statistical analysis

Statistical analyses were performed as described in Section 2.2.6. In parametric analysis, statistical significance was evaluated by Student's t-test for two-group comparisons, and by one-way analysis of variance (ANOVA) followed by Dunnett's test for multiple-group comparisons. In nonparametric analysis, statistical significance was evaluated by Steel or Steel-Dwass test for multiple group comparisons. The results were analyzed using the R 4.1.2 software (R Foundation for Statistical Computing).

5.3 Results

5.3.1 Hyperosmotic stress promotes the autophagic flux of NRK-52E cells.

Although previous studies have reported that hyperosmotic stress induces autophagy in various cell lines [28,33,34], there is no information on whether hyperosmotic mannitol stress could induce autophagy in NRK-52E cells. Western blot analysis was conducted for the cells stimulated with hyperosmotic stress to evaluate the expression of the autophagosome marker LC3-II. Treatment with 200 mM mannitol increased the expression levels of LC3-II in the NRK-52E cells in a time-dependent manner (1 h, 1.43 ± 0.12; 2 h, 1.90 ± 0.19; 4 h, 1.83 ± 0.09 ($P< 0.05$); 8 h, 2.87 ± 0.12 ($P < 0.05$); and 12 h, 3.82 ± 0.35 ($P < 0.05$); Fig. 5-1A). Likewise, stimulation of the cells with hyperosmotic stress for 12 h significantly ($P < 0.01$) increased the expression of LC3-II in a mannitol-dose-dependent manner (100 mM, 2.80 ± 0.28; 200 mM, 4.16 ± 0.91; Fig. 5-1B).

LC3-II is partly degraded after autophagosome-lysosome fusion because it is present in the outer and inner membranes of the autophagosome. Thus, a high degradation capacity leads to a quick disappearance of LC3-II, which might be misinterpreted as a defect in autophagosome synthesis [35]. The inhibition of lysosomal degradation using bafilomycin A1 (BafA) can aid in differentiating whether the reduction in the level of LC3-II is due to the inhibition of the LC3 processing or the high rate of degradation [35]. Cotreatment with mannitol and BafA, which causes the accumulation of autophagosomes, further enhanced the LC3-II expression (100 mM mannitol + BafA ($P < 0.01$ from 100 mM mannitol), 10.5 ± 0.85; 200 mM mannitol + BafA, 10.6 ± 0.64; Fig. 5-1B). These changes in the expression levels of LC3-II are consistent with the features of autophagic flux, thus confirming that hyperosmotic mannitol stress enhanced the autophagic flux in NRK-52E cells.

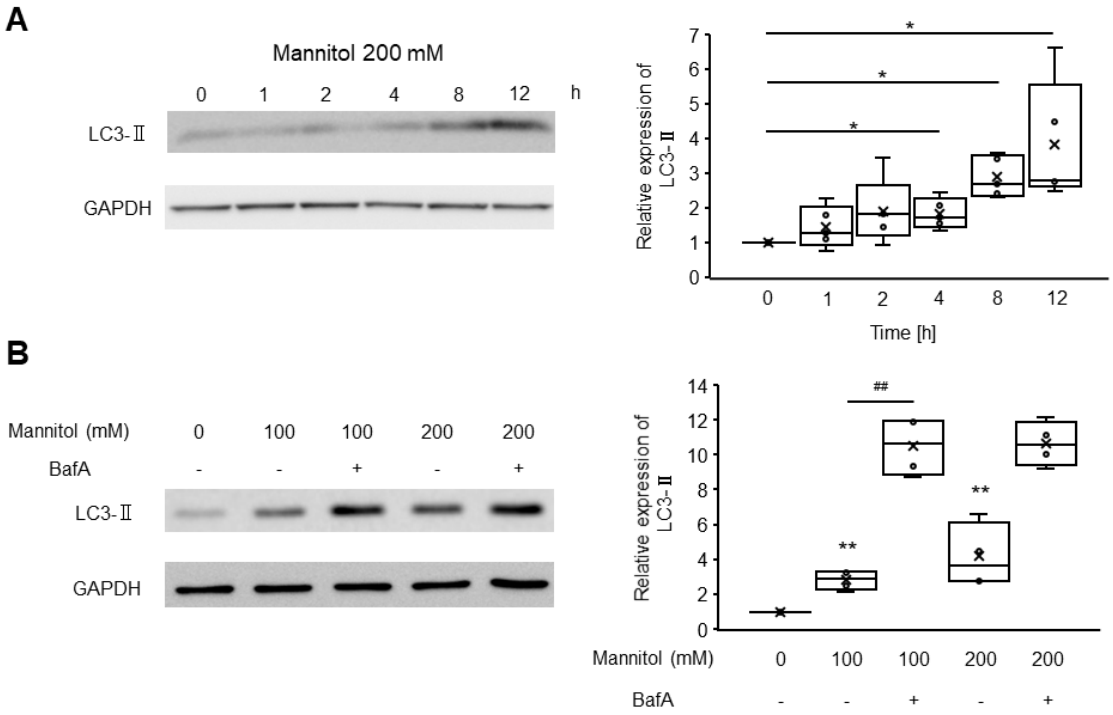

Fig. 5-1 Effects of hyperosmotic mannitol stress on LC3-II expression in NRK-52E cells. NRK-52E cells were treated with mannitol (200 mM) or cotreated with 10 nM bafilomycin A1 (BafA) (A) Western blot analysis for LC3-IIfor 0, 1, 2, 4, 8, and 12 h (n = 5). Left: The representative bands obtained by Western blotting. GAPDH was used as a loading control. Right: Quantification of the relative LC3-II expression normalized by 0 h. *$p < 0.05$ (Steel test). (B) Western blot analysis in cells cultured with mannitol (100 or 200 mM) with or without 10 nM bafilomycin A1 (BafA) for 12 h (n = 4). Left: The representative bands obtained by Western blotting. GAPDH was used as the loading control. Right: Quantification of relative LC3-II expression normalized by the 0 mM mannitol condition. **$p < 0.01$ vs. the data for mannitol (0 mM), $^{\#\#}p < 0.01$ (Steel-Dwass test). Data are presented as box and whisker plots with average (×), median, IQR, and minimum and maximum values.

Unlike the results obtained after using mannitol, treatment with hyperosmotic urea did not lead to any changes in the expression of LC3-II (1 h, 0.84 ± 0.03; 2 h, 1.14 ± 0.14; 4 h, 1.01 ± 0.11; 8 h,1.07 ± 0.03; 12 h, 1.05 ± 0.06) in the current study (Fig. 5-2). These findings indicate that the hyperosmotic stress-induced autophagy in NRK-52E cells requires cell shrinkage concomitant with the osmotic gradient between the intracellular and extracellular compartments as a result of water efflux from the cells.

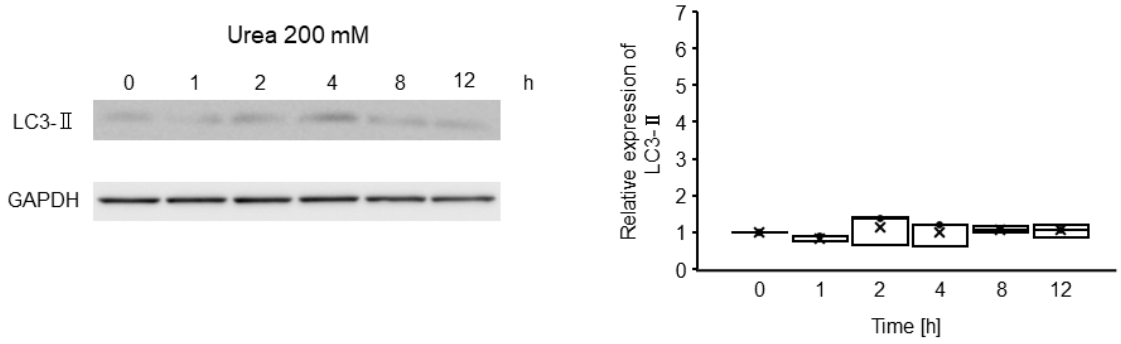

Fig. 5-2 Effect of hyperosmotic urea stress on LC3-II expression in NRK-52E cells. Western blotting analysis of cells cultured with 200 mM urea for 0, 1, 2, 4, 8, and 12 h (n = 3). Left: The representative bands obtained by Western blotting. GAPDH was used as the loading control. Right: Quantification of the relative LC3-II expression normalized by the 0 h. Data are presented as box and whisker plots with average (×), median, IQR, and minimum and maximum values.

5.3.2 Actin cytoskeleton reorganization is required for hyperosmotic stress-induced autophagosome formation.

Based on the results described in the previous section, I hypothesized that cell shrinkage caused by hyperosmotic mannitol stress interferes with the structure and organization of the cytoskeletal network by limiting the intracellular space. This hypothesis was tested by focusing on the effect of hyperosmotic stress on cytoskeletal structures, which are known to be responsible for mediating various important cellular processes such as cell structural support and functional regulation [27]. Recent studies have shown that the biogenesis and trafficking of autophagosomes depend not only on the actin cytoskeleton, which is known to play an essential role in autophagy, but also on the microtubule dynamics [30]. Therefore, I investigated the actin and microtubule cytoskeletal changes in NRK-52E cells in response to hyperosmotic stress. The cells treated with 200 mM mannitol for 0.5 h presented with disassembled actin filaments that were organized concomitant with cell shrinkage, and then reorganized into thick stress fibers at 12 h in the cytoplasm at 12 h (Figs. 5-3A-C). Similar results were observed with regard to changes in the microtubule cytoskeleton (Figs. 5-3F-H). These findings are consistent with those of a previous study, which demonstrated hyperosmolarity-induced depolymerization and reorganization of the cytoskeleton as adaptive responses [27].

Cotreatment of the cells with cytochalasin D, an actin-depolymerizing agent, prevented the reorganization of the actin cytoskeleton induced by mannitol (Fig. 5-3D) without affecting the dynamics of the microtubule cytoskeleton (Fig. 5-3I). A significant ($P < 0.01$) decrease in the level of LC3-II was observed in the cells stimulated with 200 mM mannitol in the presence of cytochalasin D (Fig. 5-4A, Lane 3; 0.38 ± 0.02) when compared to those in the absence of cytochalasin D (Fig. 5-4A, Lane 1). LC3-II levels

were evaluated in the presence and absence of BafA in order to determine the effects of cytochalasin D on hyperosmotic stress-induced autophagic flux. LC3-II accumulation was observed in the hyperosmotic mannitol-stimulated cells treated with BafA (Fig. 5-4A, Lanes 1 and 2; 1.32 ± 0.28); however, the accumulation was prevented following the addition of cytochalasin D (Fig. 5-4A, Lanes 2 [1.32 ± 0.28] and 4 [0.57 ± 0.06]; $P < 0.01$). These results suggest that the actin cytoskeleton reorganization in response to hyperosmotic stress affected the process of autophagosome formation.

As in the case of cytochalasin D, cotreatment with nocodazole prevented the mannitol-induced reorganization of the microtubule (Fig. 5-3J), without affecting the reorganization of the actin cytoskeleton (Fig. 5-3E). The LC3-II levels in cells exposed to 200 mM mannitol were not altered in the presence or absence of nocodazole (Fig. 5-4B, Lanes 1 and 3; 0.97 ± 0.15). Likewise, the LC3-II levels in cells treated with BafA remained unchanged with or without incubation with nocodazole (Fig. 5-4B, Lanes 2 (1.44 ± 0.23) and 4 (1.39 ± 0.32)). These results indicate that reorganization of the microtubule cytoskeleton in response to hyperosmotic stress is not a requisite for hyperosmotic stress-induced autophagy.

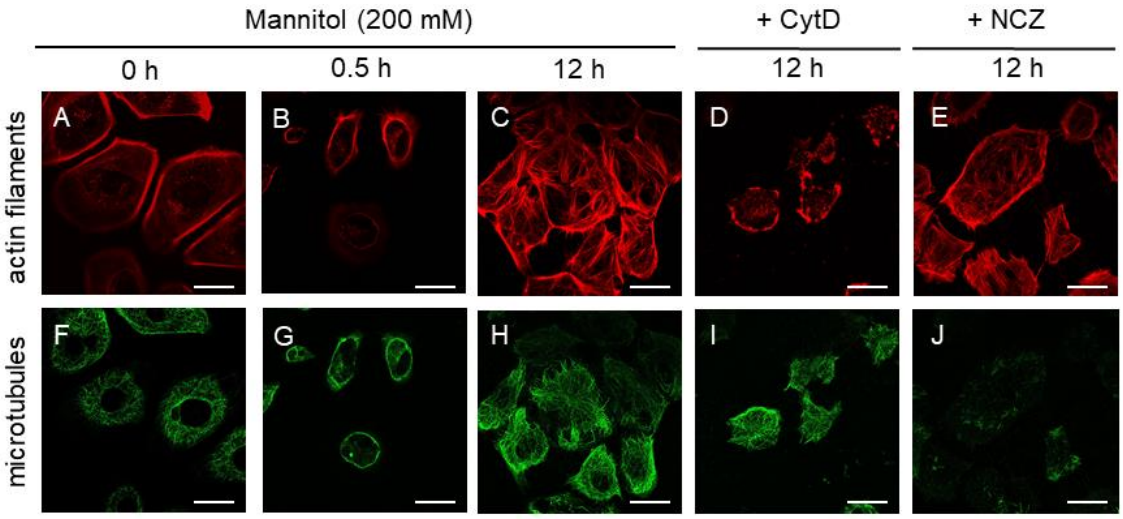

Fig. 5-3 Effect of hyperosmotic mannitol stress on actin and microtubule dynamics in NRK-52E cells. Typical fluorescence images of F-actin (red) and microtubule (green). The NRK-52E cells were treated with 200 mM mannitol for 0, 0.5, and 12 h (A-C; actin filaments, F-H; microtubules). The cells were co-treated with 200 mM mannitol and 0.1 μg/mL cytochalasin D (CytD) (D, actin filaments; I, microtubules) or 1 μM nocodazole (NCZ) (E, actin filaments; J, microtubules) for 12 h. Bar, 25 μm.

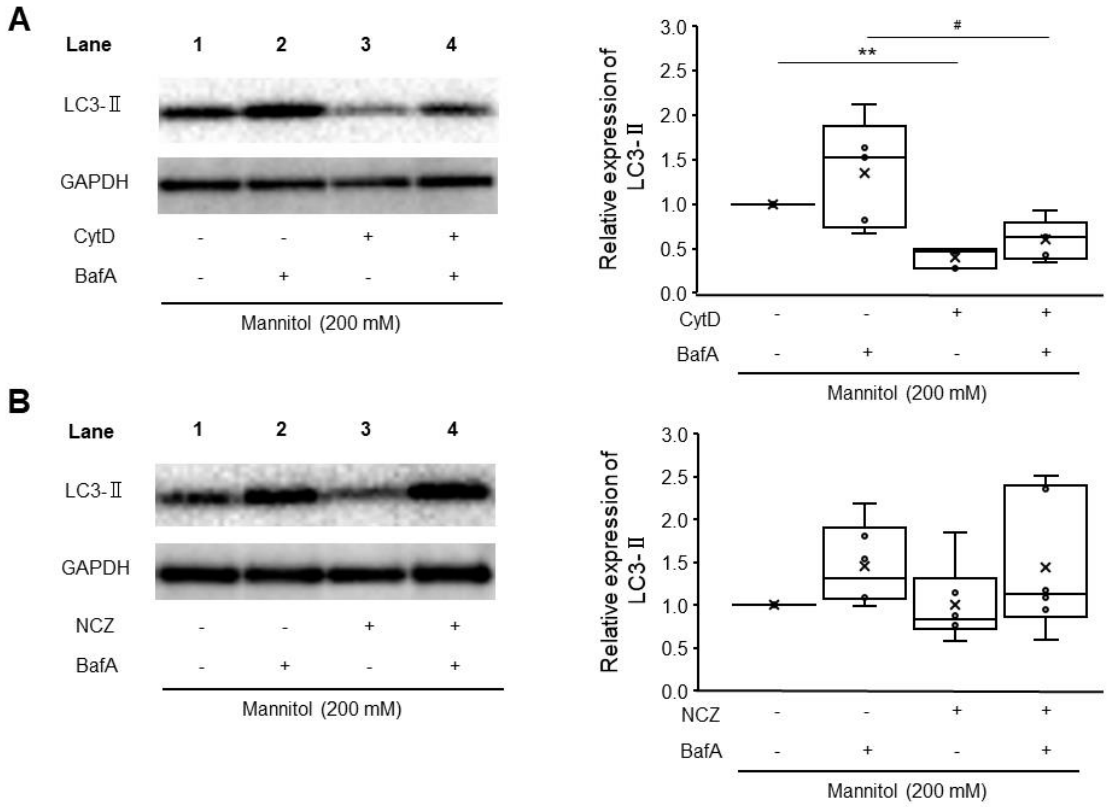

Fig. 5-4 Effect of the cytoskeleton on the hyperosmotic mannitol stress-induced expression of LC3-II. (A) Western blotting analysis of cells cultured with 200 mM mannitol in the presence or absence of 0.1 μg/mL CytD, with or without 10 nM bafilomycin A1 (BafA) for 12 h (n = 5). Quantification of relative LC3-II expression normalized by the 200 mM mannitol condition. Lane 1, 200 mM mannitol; Lane 2, 200 mM mannitol + BafA; Lane 3, 200 mM mannitol + CytD; Lane 4, 200 mM mannitol + CytD + BafA. **$p < 0.01$ and #$p < 0.05$ (Steel-Dwass test). (B) Western blotting analysis of cells cultured with 200 mM mannitol in the presence or absence of 1 μM nocodazole (NCZ), with or without 10 nM BafA for 12 h. (n = 6). Quantification of relative LC3-II expression normalized by the 200 mM mannitol condition. Lane 1, 200 mM mannitol; Lane 2, 200 mM mannitol + BafA; Lane 3, 200 mM mannitol + NCZ; Lane 4, 200 mM mannitol + NCZ + BafA. Data are presented as box and whisker plots with average (×), median, IQR, and minimum and maximum values.

5.3.3 TFEB is localized to the nucleus in response to hyperosmotic mannitol stress.

As TFEB is a key regulator of transcription of autophagy-related genes [13], the author first examined the subcellular localization of TFEB in the cytoplasm and nucleus in response to hyperosmotic stress in NRK-52E cells using immunofluorescence staining (Fig. 5-5). In the absence of extracellular osmolytes (isotonic conditions), the intracellular localization of TFEB was demonstrated to be significantly higher in the cytoplasm compared to the nucleus. When the cells were treated with 100 mM mannitol, TFEB translocated from the cytoplasm to the nucleus (Fig. 5-5A). Similar results were observed when treated with 200 mM mannitol (Fig. 5-5B). Quantitatively, hyperosmotic mannitol stress (100 mM and 200 mM) significantly increased the ratio of nuclear and cytoplasmic TFEB intensity in a time-dependent manner and reached a plateau level at 1 h (100 mM; 0 h (0.51 ± 0.04), 0.25 h (0.74 ± 0.04), 0.5 h (0.97 ± 0.05), 1 h (1.00 ± 0.06), 2 h (0.91 ± 0.05): 200 mM; 0 h (0.57 ± 0.05), 0.25 h (1.03 ± 0.06), 0.5 h (1.47 ± 0.10), 1 h (1.67 ± 0.08), 2 h (1.30 ± 0.07)) (Figs. 5-5C and D).

Next, the author confirmed the TFEB nuclear translocation of NRK-52E cells under urea-medicated hyperosmolarity to further understand the effect of hyperosmotic stress on autophagy (Fig. 5-6). Unlike the result obtained with mannitol, treatment with hyperosmotic urea (200 mM) resulted no change in nuclear fluorescence intensity of TFEB compared with the control 0 h (0.47 ± 0.06), 0.25 h (0.56 ± 0.05), 0.5 h (0.57 ± 0.04), 1 h (0.57 ± 0.05), 2 h (0.45 ± 0.03)) (Figs. 5-6A and B). The ratio of nuclear and cytoplasmic TFEB intensity treated with 200 mM urea was smaller than those obtained under treatment with 200 mM mannitol at the same time point; this result was statistically significant (Fig. 5-6C).

Nuclear TFEB binds to the coordinated lysosomal expression and regulation (CLEAR)

element, which is found in the promoter regions of genes involved in lysosomal biogenesis and autophagy, upregulating the expression of its target genes [17]. In further support of the transactivation of TFEB by hyperosmotic mannitol stress, the author measured the expression levels of the well-known target genes of TFEB, *i.e. LC3*, *VPS18*, *LAMP1*, and *LAMP2*. When the cells were stimulated by hyperosmotic mannitol stress, the mRNA expression levels of LC3 (1 h, 1.24 ± 0.06; 2 h, 1.26 ± 0.06), VPS18 (1 h, 1.28 ± 0.21 ($P < 0.05$); 2 h, 1.50 ± 0.30 ($P < 0.05$)), LAMP1 (1 h, 1.57 ± 0.05; 2 h, 1.74 ± 0.17), and LAMP2 (1 h, 1.59 ± 0.04 ($P < 0.05$); 2 h, 1.82 ± 0.25 ($P < 0.05$)) were increased (Fig. 5-7).

Taken together, hyperosmotic mannitol stress enhanced TFEB nuclear translocation, whereas hyperosmotic urea stress did not. These results suggest that TFEB was localized to the nucleus soon after the application of hyperosmotic mannitol stress, resulting in the activation of its target genes.

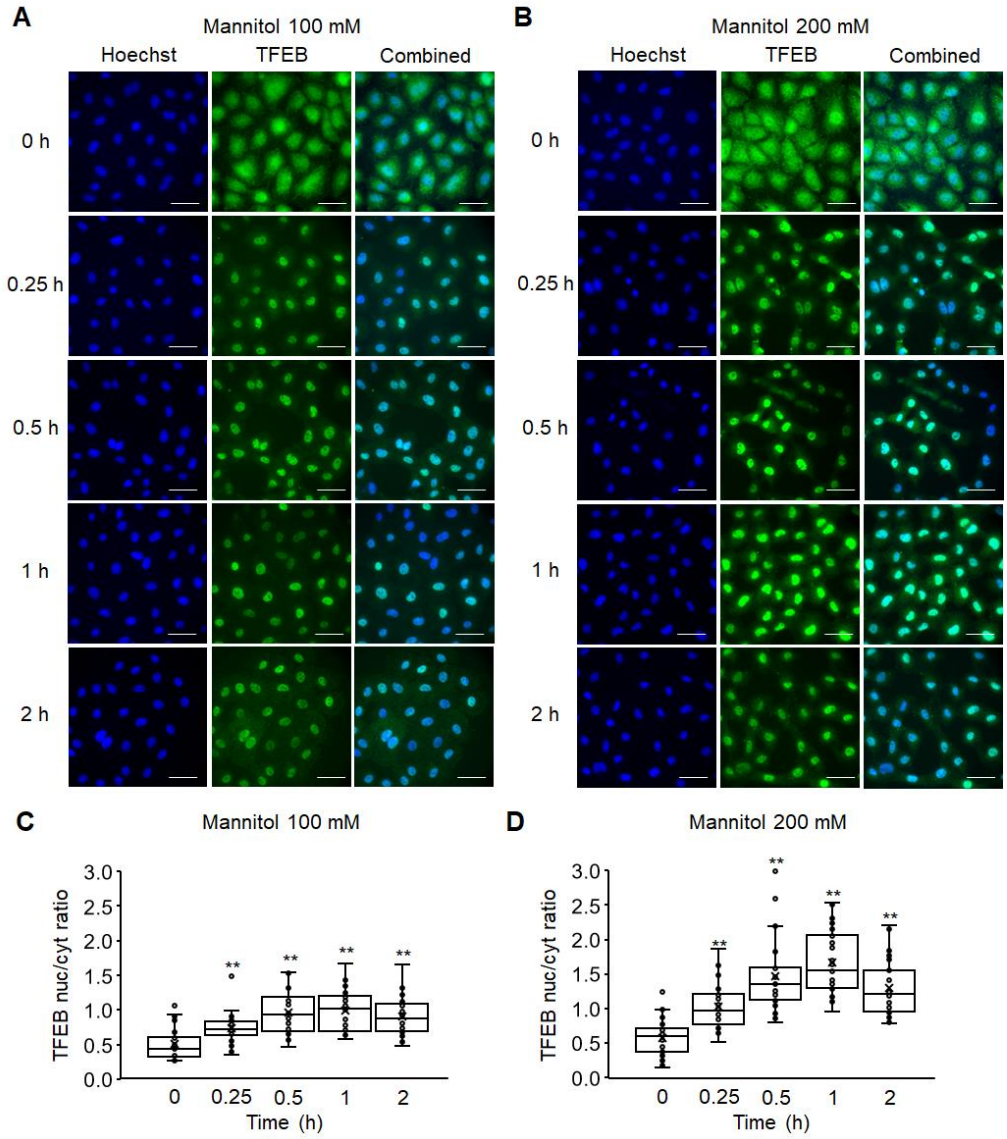

Fig. 5-5 Effects of hyperosmotic mannitol stress on the TFEB nuclear translocation of NRK-52E cells. (A, B) NRK-52E cells were treated with 100 mM (A) or 200 mM (B) mannitol for 0, 0.25, 0.5, 1, and 2 h. Typical fluorescence images of Hoechst 33342 (blue), TFEB (green), and combined (blue and green). Bar, 25 μm. (C, D) Summaries of the ratios between nuclear and cytosolic TFEB fluorescence of NRK-52E cells cultured with 100 (C) and 200 mM (D) mannitol. Data are presented as box and whisker plots with average (×), median, IQR, and minimum and maximum values (100 mM; n = 30, 200 mM; n = 30). $^{**}P < 0.01$ from the data of 0 h (Dunnett's test).

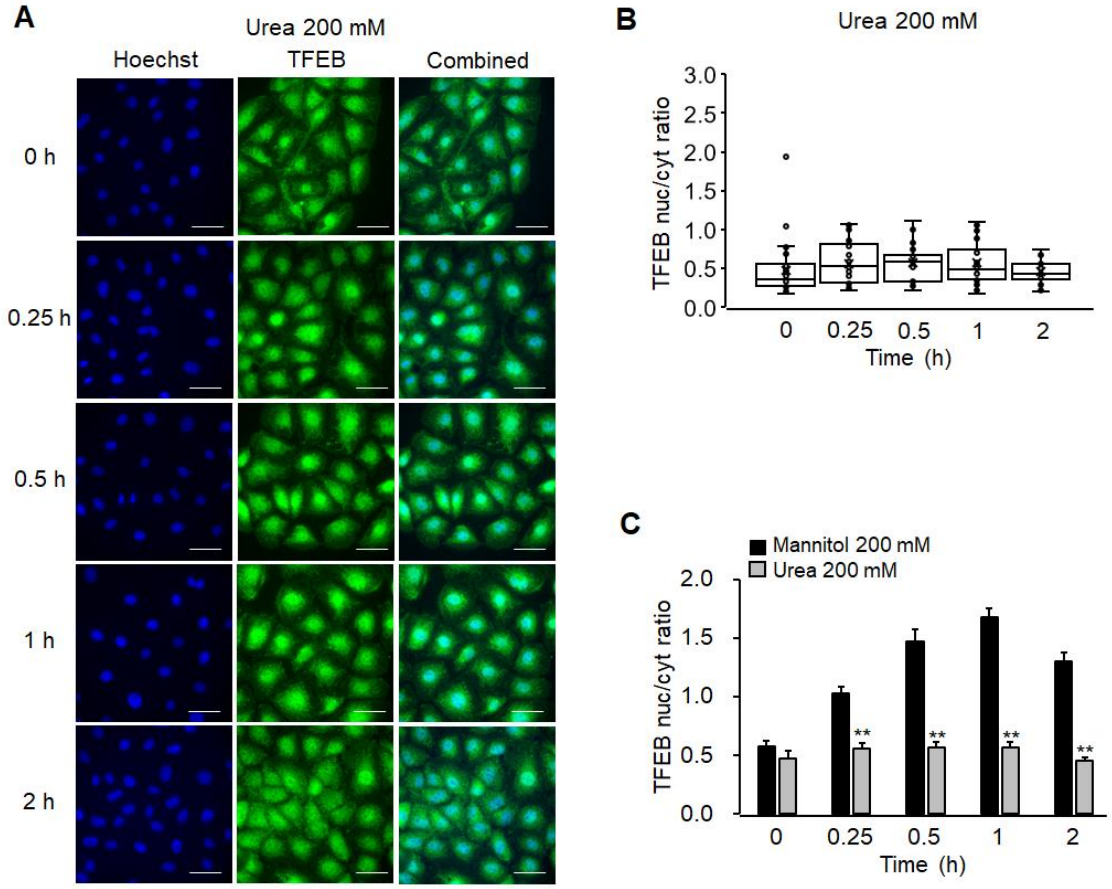

Fig. 5-6 Effects of hyperosmotic urea stress on the TFEB nuclear translocation of NRK-52E cells. (A) NRK-52E cells were treated with 200 mM urea for 0, 0.25, 0.5, 1, and 2 h. Typical fluorescence images of Hoechst 33342 (blue), TFEB (green), and combined (blue and green). Bar, 25 μm. (B) A summary of the ratio between nuclear and cytosolic TFEB fluorescence of NRK-52E cells cultured with 200 mM urea. Data are presented as box and whisker plots with average (×), median, IQR, and minimum and maximum values (n = 30). (C) A comparison between mannitol (200 mM) and treated with urea (200 mM) from (B). The data of 200 mM mannitol (black bars) were identical to those in Fig. 5-5D, which were shown for comparisons. Data are mean ± SEM. $^{**}P < 0.01$ from the data of mannitol (200 mM) at the same time point (Student's t-test).

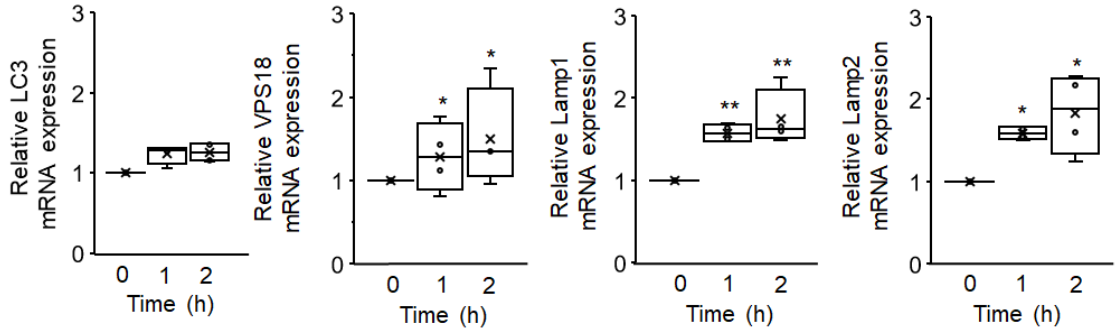

Fig. 5-7 Effects of hyperosmotic mannitol stress on the transcriptional activity of TFEB. NRK-52E cells were treated with 200 mM mannitol, and mRNA expression was analyzed by real-time PCR. Quantitation of the changes in LC3 (n = 4), VPS18 (n = 4), LAMP1 (n = 4) and LAMP2 (n = 4). Relative gene expression levels were calculated considering mannitol (0 h) as 1 and plotted. Data are presented as box and whisker plots with average (×), median, IQR, and minimum and maximum values *P < 0.05, **P < 0.01 from the data of 0 mM (Steel test).

5.3.4 Hyperosmotic stress-induced TFEB nuclear translocation was induced in a calcineurin-dependent manner.

Ca^{2+} is the primary regulator of autophagy and TFEB nuclear translocation [36] and, in Chapter 3, the author reported that hyperosmotic stress increased intracellular Ca^{2+} concentration in NRK-52E cells (Figs. 3-1 and 3-2). To clarify the role of Ca^{2+} in the TFEB localization, NRK-52E cells were treated with Ca^{2+} chelators before the application of hyperosmotic mannitol stress. As a result, the treatment of a specific intracellular Ca^{2+} chelator, BAPTA-AM (50 μM), strongly reduced hyperosmotic stress-induced TFEB nuclear translocation (0.66 ± 0.03 (P < 0.01)), but an extracellular Ca^{2+} chelator EGTA (4 mM) had no effects (1.64 ± 0.10) compared to 200 mM mannitol (1.67 ± 0.08) (Figs. 5-8A and B). These results suggested that intracellular Ca^{2+} was required the

hyperosmolarity-induced TFEB activation.

Since the primary mechanism of TFEB nuclear translocation is the Ca^{2+}-dependent dephosphorylation of TFEB by calcineurin [37], the author investigated whether hyperosmotic stress modulates calcineurin activity. The activity of calcineurin was evaluated by the nuclear localization of a transcription factor NFAT, which is translocated from the cytoplasm into the nucleus on calcineurin-dependent dephosphorylation [38]. Immunofluorescence staining showed that treatment with 200 mM mannitol promoted NFAT translocated from the cytoplasm to the nucleus (Fig. 5-8C). Quantitatively, after incubation of NRK-52E cells with 200 mM mannitol for 0.25 h or 0.5 h, there was a significant increase in the ratio of nuclear and cytoplasmic NFAT intensity (0 h, 0.44 ± 0.04; 0.25 h, 0.92 ± 0.06 ($P < 0.01$); 0.5 h, 0.92 ± 0.06 ($P < 0.01$)) (Fig. 5-8D).

To further prove whether the calcineurin signaling pathway modulates hyperosmotic stress-induced TFEB activation, I assessed the pharmacological impact of FK-506, a calcineurin-specific inhibiter. Cotreatment with FK-506 effectively inhibited hyperosmotic stress-induced TFEB nuclear translocation dose-dependent manner (200 mM mannitol, 1.67 ± 0.08; FK-506 10μM, 0.93 ± 0.06 ($P < 0.01$); FK-506 50μM, 0.69 ± 0.05 ($P < 0.01$)) (Figs. 5-8E and F). These results suggest that calcineurin activation was involved in TFEB nuclear translocation in response to hyperosmotic stress in NRK-52E cells.

Since the localization of TFEB is known as regulated not only by the phosphatase calcineurin but also by a kinase mTORC1, the author further evaluated the effect of hyperosmotic treatment on a mTORC1 substrate, p70S6 kinase (p70S6K), whose phosphorylation levels (P-p70S6K) are consistent with mTORC1 activity [39]. Western blot analysis showed that treatment with 200 mM mannitol did not alter the expression

ratio of P-p70S6K to p70S6K (0.25 h, 1.07 ± 0.14; 0.5 h, 1.02 ± 0.12) (Fig. 5-9). These results suggest that the hyperosmotic stress promoted TFEB nuclear translocation in a mTORC1-independent manner in NRK-52E cells.

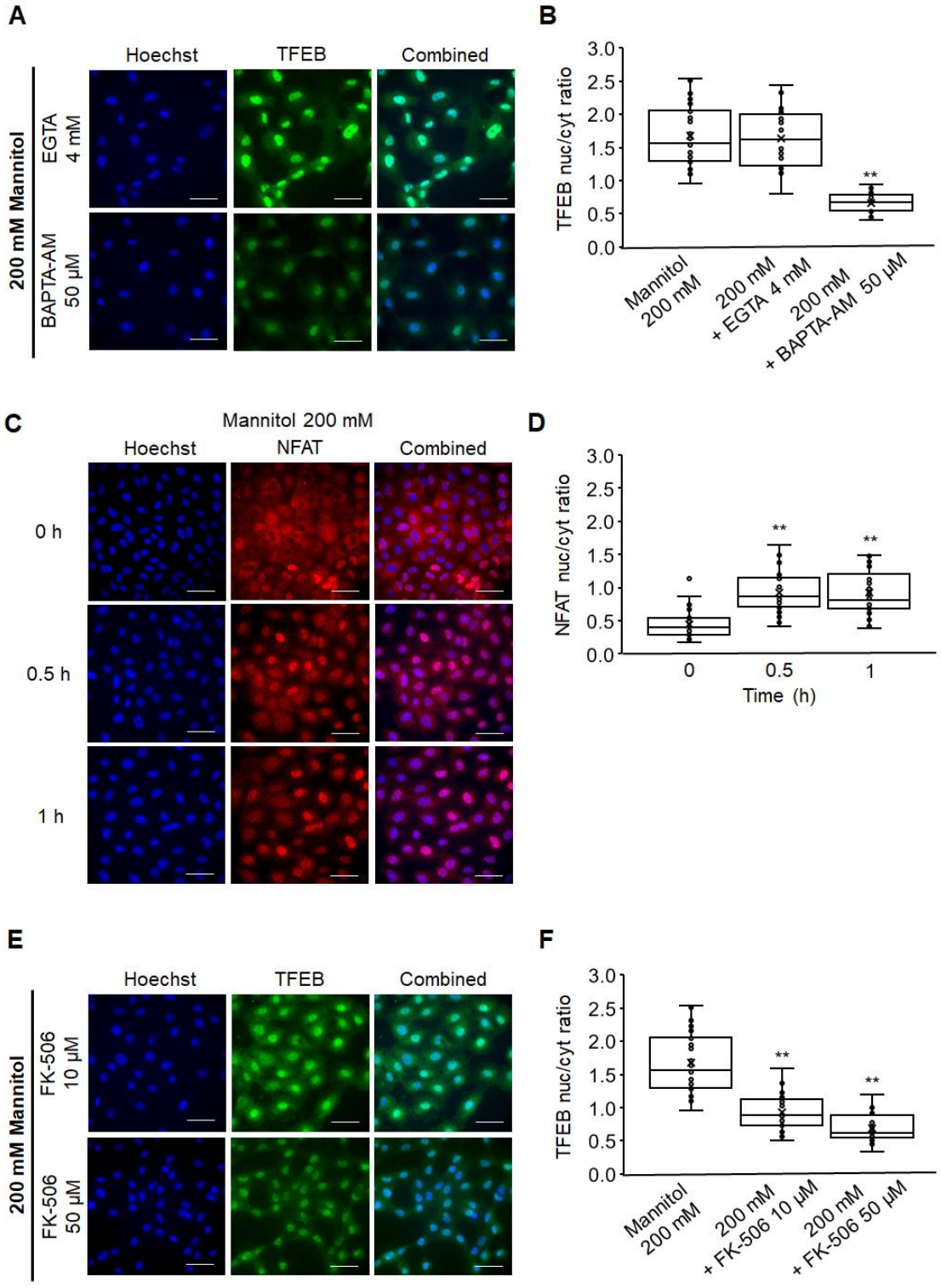
A
Hoechst
TFEB
Combined
200 mM Mannitol
EGTA 4 mM
BAPTA-AM 50 μM
B
TFEB nuc/cyt ratio
3.0
2.5
2.0
1.5
1.0
0.5
0.0
**
Mannitol 200 mM
200 mM + EGTA 4 mM
200 mM + BAPTA-AM 50 μM
C
Mannitol 200 mM
Hoechst
NFAT
Combined
0 h
0.5 h
1 h
D
NFAT nuc/cyt ratio
3.0
2.5
2.0
1.5
1.0
0.5
0.0
**
**
0
0.5
1
Time (h)
E
Hoechst
TFEB
Combined
200 mM Mannitol
FK-506 10 μM
FK-506 50 μM
F
TFEB nuc/cyt ratio
3.0
2.5
2.0
1.5
1.0
0.5
0.0
**
**
Mannitol 200 mM
200 mM + FK-506 10 μM
200 mM + FK-506 50 μM

Fig. 5-8 Effects of hyperosmotic mannitol stress on the calcineurin activity of NRK-52E cells. (A) NRK-52E cells were cotreated with mannitol (200 mM) and EGTA (4 mM) or BAPTA-AM (50 μM) for 1 h. Typical fluorescence images of Hoechst 33342 (blue), TFEB (green), and combined (blue and green). Bar, 25 μm. (B) A summary of the ratios between nuclear and cytosolic TFEB fluorescence intensities of NRK-52E cells. The data of 200 mM mannitol alone were identical to those in Fig. 5-5D, which were shown for comparisons. Data are presented as box and whisker plots with average (×), median, IQR, and minimum and maximum values (200 mM mannitol + 4 mM EGTA (n = 20), 200 mM mannitol + 50 μM BAPTA-AM (n = 21)). **P < 0.01 from the data of 200 mM mannitol (Dunnett's test). (C) NRK-52E cells were treated with 200 mM mannitol for 0, 0.5, and 1 h. Typical fluorescence images of Hoechst 33342 (blue), NFAT (red), and combined (blue and red). Bar, 25 μm. (D) A summary of the ratios between nuclear and cytosolic NFAT fluorescence intensities of NRK-52E cells cultured with 200 mM mannitol. **P < 0.01 from the data of 0 h (Dunnett's test). Data are presented as box and whisker plots with average (×), median, IQR, and minimum and maximum values (n = 30). (E) NRK-52E cells were cotreated with mannitol (200 mM) and FK-506 (10 μM or 50 μM) for 1 h. Typical fluorescence images of Hoechst 33342 (blue), TFEB (green), and combined (blue and green). Bar, 25 μm. (F) A summary of the ratios between nuclear and cytosolic TFEB fluorescence intensities of NRK-52E cells. The data of 200 mM mannitol alone were identical to those in Fig. 5-5D, which were shown for comparisons. Data are presented as box and whisker plots with average (×), median, IQR, and minimum and maximum values (200 mM mannitol + 10 μM FK-506 (n = 24), 200 mM mannitol + 50 μM FK-506 (n = 20)). **P < 0.01 from the data of 200 mM mannitol (Dunnett's test).

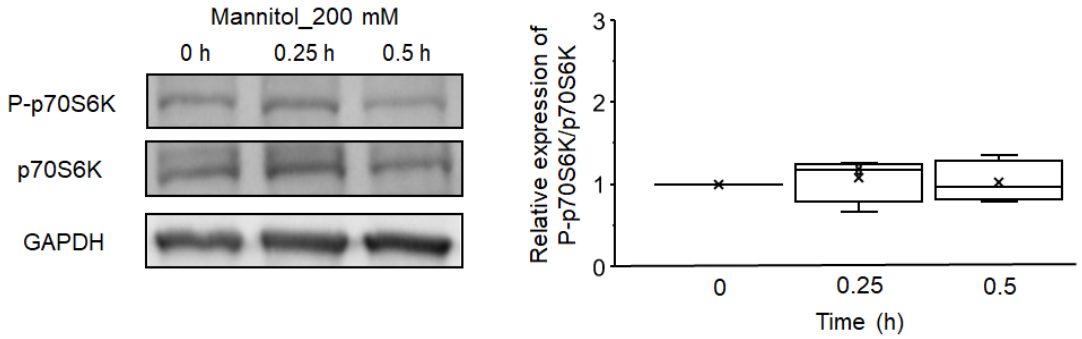

Fig. 5-9 Effects of hyperosmotic mannitol stress on the protein expression levels of P-p70S6K and p70S6K. NRK-52E cells were treated with 200 mM mannitol for 0, 0.25, and 0.5 h. Western blot analysis for P-p70S6K and p70S6K (n = 4). Left: The representative blot images obtained by Western blotting. GAPDH served as a loading control. Right: Quantification analysis of the ratio of P-p70S6K to p70S6K. The expression of P-p70S6K and p70S6K were normalized by that of GAPDH. Relative expression of P-p70S6K/p70S6K was calculated as normalized to 0 h. Data are presented as box and whisker plots with average (×), median, IQR, and minimum and maximum values.

5.3.5 Cotreatment with ML-SI3 inhibits hyperosmotic stress-induced TFEB nuclear translocation.

The TRPML1 channel is predominantly localized on the membranes of late endosomes and lysosomes in NRK-52E cells [40]. Previous studies have reported that TRPML1 plays an important role in the activation of calcineurin and consequent TFEB dephosphorylation [41]. Therefore, I investigated the potential role of TRPML1 channels in hyperosmotic mannitol-induced TFEB nuclear translocation in NRK-52E cells.

Treatment with ML-SI3, a TRPML1 antagonist, attenuated the nuclear localization of TFEB in response to 200 mM mannitol, and the effect was most significant at a high-dose

condition (ML-SI3 1μM, 1.47 ± 0.07; ML-SI3 10μM, 0.89 ± 0.06 ($P < 0.01$)) (Figs. 5-10A and B). Similar results were observed for nuclear translocation of NFAT (ML-SI3 1μM, 0.80 ± 0.06; ML-SI3 10μM, 0.32 ± 0.04 ($P < 0.01$)) (Figs. 5-10C and D).

Moreover, to observe the effects of TRPML1 in autophagy in response to hyperosmotic stress, NRK-52E cells were cotreated with ML-SI3 and mannitol, and Western blotting was used to detect the protein level of LC3-II (Fig. 5-11). When the cells were stimulated with 200 mM mannitol, the expression of LC3-II was significantly increased in a time-dependent manner (1 h, 1.21 ± 0.22; 2 h, 1.88 ± 0.45; 4 h, 1.83 ± 0.3; 8 h, 2.56 ± 0.25 [$P < 0.01$]; and 12 h, 2.09 ± 0.10; Figs. 5-11A and B). Even under the hyperosmotic conditions, treatment with ML-SI3 attenuated the increase of LC3-II expressions similar to the control levels (1 h, 0.97 ± 0.08; 2 h, 0.96 ± 0.10; 4 h, 0.82 ± 0.06; 8 h,0.86 ± 0.05 ($P < 0.05$ from 200 mM mannitol); 12 h, 0.97 ± 0.07 ($P < 0.01$ from 200 mM mannitol); Figs. 5-11A and B). These findings show that TRPML1-mediated TFEB nuclear translocation may play an important role in hyperosmotic stress-induced autophagy in NRK-52E cells.

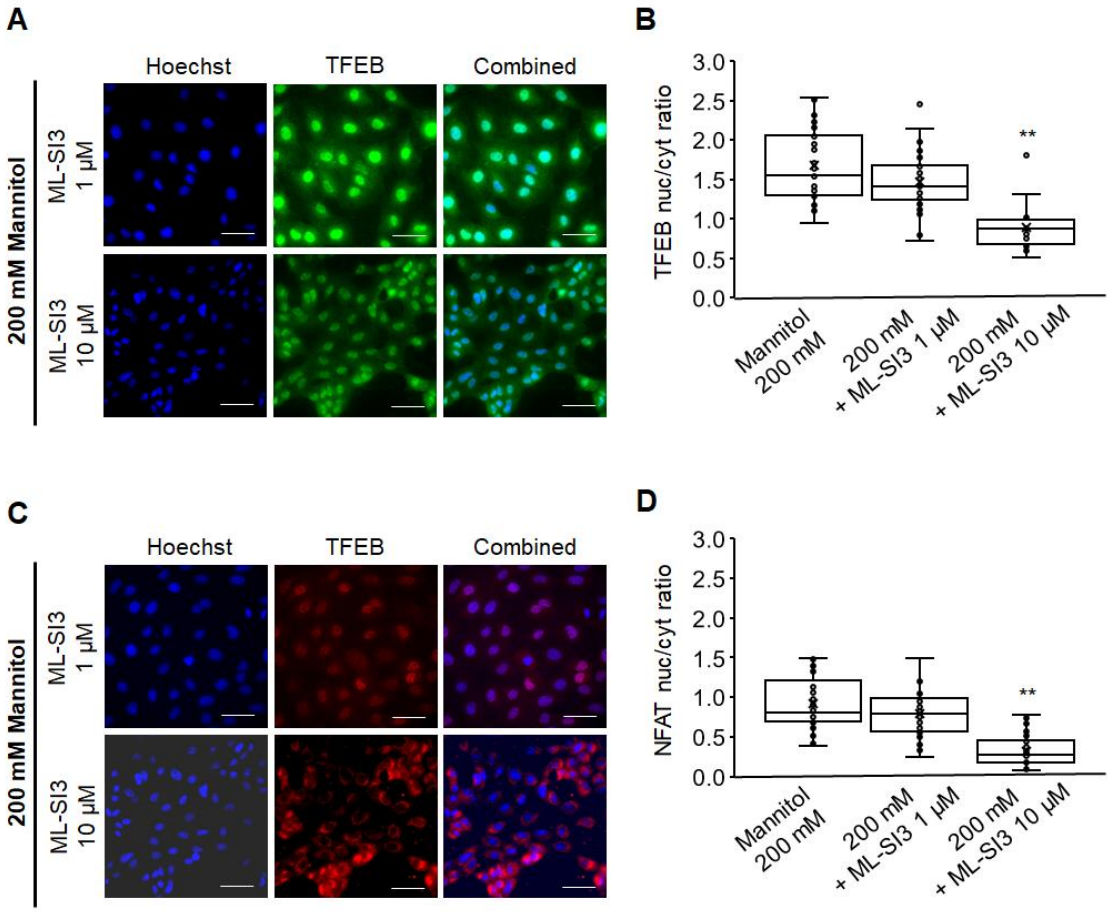

Fig. 5-10 Effects of ML-SI3 on the hyperosmotic mannitol stress-induced TFEB nuclear translocation of NRK-52E cells. (A) NRK-52E cells were cotreated with mannitol (200 mM) and ML-SI3 (1 μM or 10 μM) for 1 h. Typical fluorescence images of Hoechst 33342 (blue), TFEB (green), and combined (blue and green). Bar, 25 μm. (B) A summary of the ratios between nuclear and cytosolic TFEB fluorescence intensities of NRK-52E cells. The data of 200 mM mannitol alone were identical to those in Fig. 5-5D, which were shown for comparisons. Data are presented as box and whisker plots with average (×), median, IQR, and minimum and maximum values (200 mM mannitol + 1 μM ML-SI3 (n = 29), 200 mM mannitol + 10 μM ML-SI3 (n = 20)). **P < 0.01 from the data of 200 mM mannitol (Dunnett's test). (C) NRK-52E cells were cotreated with mannitol (200 mM) and ML-SI3 (1 μM or 10 μM) for 1 h. Typical fluorescence images

of Hoechst 33342 (blue), NFAT (red), and combined (blue and red). Bar, 25 μm. (D) A summary of the ratios between nuclear and cytosolic NFAT fluorescence intensities of NRK-52E cells. The data of 200 mM mannitol alone were identical to those in Fig. 5-8D, which were shown for comparisons. Data are presented as box and whisker plots with average (×), median, IQR, and minimum and maximum values (200 mM mannitol + 1 μM ML-SI3 (n = 28), 200 mM mannitol + 10 μM ML-SI3 (n = 30)). **P < 0.01 from the data of 200 mM mannitol (Dunnett's test).

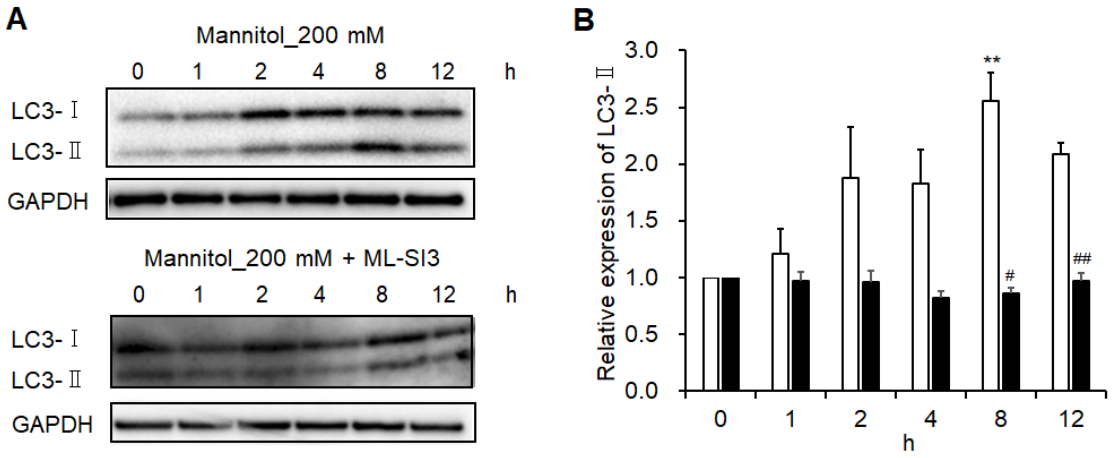

Fig. 5-11 Effects of ML-SI3 on the hyperosmotic mannitol stress-induced LC3-II upregulation of NRK-52E cells. (A, B) NRK-52E cells were treated with 200 mM mannitol or cotreated with ML-SI3 (10 μM) for 0, 1, 2, 4, 8, and 12 h. GAPDH served as a loading control. (A) The representative blot images were obtained Western blot treated with 200 mM mannitol (Top) or cotreated with ML-SI3 (Bottom). (B) Relative LC3-II expression was calculated considering 0 h as 1 and plotted (means ±SEM.). **p < 0.01 vs. the data for 0 h (Steel test), $^{\#}p < 0.05$, $^{\#\#}p < 0.01$ from the data of 200 mM mannitol (Student's t-test).

5.4 Discussion

The purpose of this chapter was to explore the role of hyperosmolarity in the autophagy of proximal tubular epithelial cells. The novel findings are as follows (1) hyperosmotic mannitol stress could induce autophagy, (2) reorganization of the actin cytoskeleton is essential for hyperosmotic stress-induced autophagy, and (3) the TRPML1-calcineurin-TFEB pathway is partly involved in the mechanism for the hyperosmotic stress-induced autophagy (Fig. 5-12). Tubular epithelial cells release Ca^{2+} from lysosomes via TRPML1 in response to hyperosmotic stress. Increased intracellular Ca^{2+} concentration triggers the activation of calcineurin and TFEB was translocated from the cytoplasm to the nucleus, which enhances the expression of autophagy-related genes. Hyperosmotic stress also affects the cytoskeleton, and reorganization of the actin cytoskeleton was essential for the induction of autophagy. In the present study, we have not examined the relationship between TFEB and the actin cytoskeleton. Considering that nuclear translocation of TFEB is an event that precedes the reorganization of the actin cytoskeleton, it would be interesting to examine the relationship between the TRPML1-calcineurin-TFEB pathway and the actin cytoskeleton.

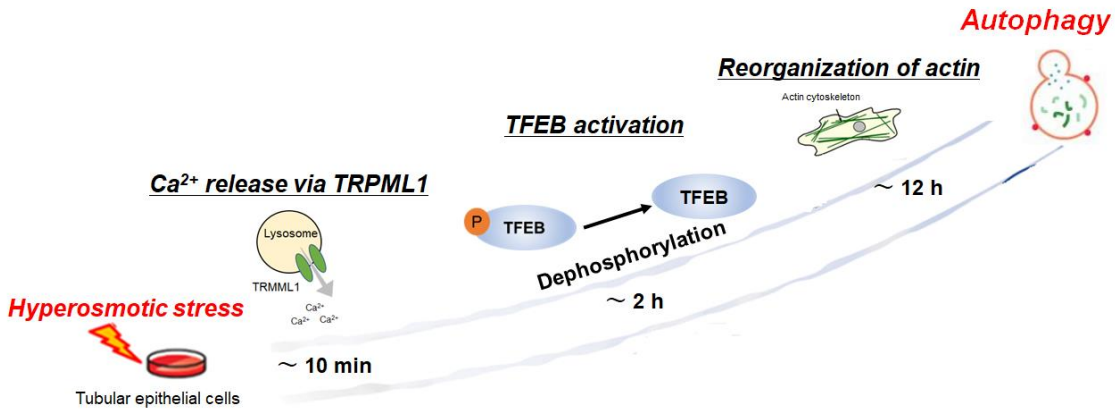

Fig. 5-12 Schematic illustration of the mechanism of hyperosmotic stress-induced

autophagy. Hyperosmotic stress promotes Ca^{2+} release from lysosomes via TRPML1, which then dephosphorylates TFEB via intracellular calcium signaling and promotes TFEB activation (nuclear translocation). Reorganization of actin cytoskeleton observed up to 12 h also contributes to hyperosmotic stimulus-induced autophagy.

The autophagic activity of proximal tubular epithelial cells is very low under physiological conditions [42], whereas higher rates of autophagy are essentially observed in cells under stress. The deletion of the autophagy-related genes Atg5 or Atg7 resulted in proximal tubular cell-specific autophagy defects leading to cell cycle arrest at the G2/M phase, increased tubulointerstitial fibrosis, and progressive renal injury [43-45], thereby suggesting that induction of autophagy is renoprotective during kidney injury.

Reorganization of the cytoskeleton under osmotic stress is critical for the osmo-protective response [46]; nonetheless, the underlying mechanisms involved in this process remain poorly understood. The membrane-permeable osmolarity regulator, urea, did not induce autophagy in the current study; furthermore, the mannitol-induced autophagy was triggered by the shrinkage of the cell (not by the hyperosmotic stress), owing to osmotic differences between the cytosol and the extracellular compartment (Figs. 2-2 and 5-1). Recently, several studies have shown that hyperosmotic stress might be a risk factor for the progression of renal injury [47-50]. The findings of the present study suggest the importance of facilitating the reorganization of the actin cytoskeleton under hyperosmotic conditions to promote autophagy in order to limit the progression of renal injury.

The reorganization of the actin cytoskeleton plays a critical role in the induction of hyperosmotic stress-induced autophagy. The cytoskeleton is thought to be exposed to

compressive stress arising from hyperosmotic stress, which may perturb the actin filaments and lead to their rapid depolymerization. Previous studies have shown that depolymerization of the actin cytoskeleton decreases the degradation of long-lived proteins and prevents the accumulation of autophagosomes [51,52]. In the current study, prevention of the hyperosmotic stress-induced reorganization of the actin cytoskeleton impaired the autophagic flux by reducing the expression of LC3-II (Figs. 5-3 and 5-4). However, the underlying mechanism involved in this process remains unclear. Reorganization of the actin cytoskeleton is thought to be necessary for the biogenesis of autophagosomes [30,52,53]. Actin reorganization, mainly polymerization, affects the first stage of the formation of autophagy vesicles [52]. Then, F-actin is localized on the isolated membranes of the autophagosomes along with omegasome-associated proteins such as DFCP1 (double FYVE-containing protein 1), ATG5 (autophagy-related 5), and ATG16; this indicates that the assembly of an actin scaffold inside the isolation membrane (the autophagosomal precursor) is essential for the shaping of the autophagosomal membrane [54]. Furthermore, the Arp2/3 (actin-related protein 2/3) complex regulates the initiation of actin polymerization and formation of branched actin networks, which provide mechanical forces for autophagosome biogenesis [30]. Inhibition of the Arp2/3 complex with CK-666, a small molecule inhibitor, results in a decrease in LC3-II expression levels and the number of autophagosomes [55]. In addition, several reports have demonstrated the roles of JMY (junction-mediating and regulatory protein) and WHAMM (WASP homolog-associated protein with actin, membranes, and microtubules) in the activation of the Arp2/3 complex relating the accumulation of actin in autophagosome [55]. Hyperosmotic stress-induced reorganization of the actin cytoskeleton in the present study may be involved in the formation of autophagic vesicles

and the early events of autophagy via the Arp2/3 complex for autophagosome biogenesis.

Microtubules have been implicated in the formation of autophagosomes and their fusion with lysosomes [30,51]. In a previous study, the disassembly of both labile and stable microtubule networks induced by extensive nocodazole treatment led to complete inhibition of the autophagic flux, whereas limited treatment with nocodazole resulted in labile microtubule disassembly and prevented the formation of starvation-induced autophagosomes [56]. Interestingly, inhibition of the microtubule dynamics by nocodazole did not alter the expression of LC3-II under mannitol-induced hyperosmotic conditions in the present study (Fig. 5-4B). Although the role of microtubule dynamics in starvation-induced autophagy may be fundamentally different from that in hyperosmotic stress-induced autophagy, additional studies are required to elucidate the role of microtubule reorganization in autophagy under hyperosmotic conditions.

Autophagy deletion in proximal tubules worsened tubular injury and renal function, highlighting that enhanced autophagic activities are renoprotective in various pathological models [57-59]. In addition, both mRNA and protein expression levels of TFEB are decreased and misfolded proteins accumulate due to reduced TFEB-mediated autophagy activity in the kidneys of patients with diabetic kidney disease [60]. Thus, pharmacological approaches to modulate autophagy focused on TFEB could hold promise for treating kidney disease. One class of candidate drugs that enhance autophagic activities are mTORC1 inhibitors. Indeed, previous studies have shown that the abnormal mTORC1 hyperactivation, leading to TFEB inactivation, is involved in the pathogenesis of tubular damage in diabetic kidney disease [61]. However, according to a meta-analysis of randomized clinical trials, the relative risk of all grades of AKI in patients taking mTOR inhibitors is significantly higher than in patients not taking mTOR inhibitors,

indicating that renal toxicity is a potential complication of mTOR inhibitor use [62]. Our data revealed that hyperosmotic stress promotes TFEB nuclear translocation independent of mTORC1 inhibition (Fig. 5-9). The activation of calcineurin by hyperosmotic stress could potentially lead to TFEB activation, as calcineurin is known to enhance the nuclear translocation of TFEB (Fig. 5-8). Several positive effects of calcineurin activation have been reported so far, including enhancement of β-cell function or muscle endurance capacity, preserving organelle function, and improvement of the metabolic profile [63-65]. Although this study only focused on calcineurin as the activation mechanism of TFEB, further elucidation of the mechanism in response to hyperosmotic stress may provide a significant insight into drug development targeting mTORC1-independent autophagy pathway for the treatment of kidney disease.

TRPML1 channels localized to lysosomes may account for some of this phenomenon, as a TRPML1 antagonist, ML-SI3, significantly reduced hyperosmotic mannitol-induced TFEB nuclear translocation (Fig. 5-10). Since the main compartmentalized Ca^{2+} stores in cells are the endoplasmic reticulum and mitochondria as well as lysosomes [66], other Ca^{2+} release mechanisms may thus be involved in mediating or compensating for the increased intracellular Ca^{2+} and in activating calcineurin. The effects of hyperosmolarity on the effects of other Ca^{2+} channels can help to clarify the mechanism underlying changes in the TFEB activation in proximal tubular epithelial cells.

ML-SI3, a chemical compound that acts as an antagonist of the TRPML family, abolished hyperosmotic-induced TFEB nuclear translocation (Fig. 5-10). ML-SI3 is a potent inhibitor of TRPML1 (IC50: 1.6 μM) and TRPML2 (IC50: 2.3 μM); it is also a less effective inhibitor (IC50: 12.5 μM) of TRPML3 [67]. TRPML1 is ubiquitously expressed in mammalian cells and mainly localized to lysosomes, whereas TRPML2 and

TRPML3 are expressed in specialized cells (e.g. immune cells and melanocytes) [18], emphasizing the importance of Ca^{2+} release through the activation of TRPML1 channel in the present results. TRPML1 activation could account for some of TFEB activation in response to hyperosmolarity, which is consistent with previous studies that TRPML1 contributes to autophagy by inducing the nuclear translocation of TFEB during starvation [68,69]. Although there is still a lot of uncertainty about the mechanisms by which TRPML1 is activated under hyperosmotic conditions, one of the first topics to be addressed is the endogenous ligand of TRPML1. TRPML1 can be activated by phosphatidylinositol 3,5-bisphosphate (PI(3,5)P2) [66]. PI(3,5)P2 is generated from PI(3)P through a PI5 kinase and its deficient cells exhibit enlarged endolysosomes and trafficking defects in endocytic pathways [70-72]. Thus, both TRPML1 and PI(3,5)P2 involves in membrane-fusion processes such as lysosomal fusion with autophagosomes. Of interest, hyperosmotic stress reportedly increases PI(3,5)P2 levels more than 20-fold within a few minutes [66]. Considering that ML-SI3 can negatively regulate the PI(3,5)P2 activation of TRPML [73], the finding of this chapter that ML-SI3 attenuated hyperosmotic stress-induced autophagy suggests the involvement of calcium signaling, via PI(3,5)P2/TRPML/TFEB in these responses (Fig. 5-11).

5.5 Conclusion

In the present chapter, the activation of TRPML1 in response to hyperosmotic mannitol may be one of the mechanisms responsible for the calcineurin-dependent activation of TFEB of proximal tubular epithelial cells. The present findings suggest that mTORC1-independent autophagy activation mimicking hyperosmotic stress might prove beneficial in providing a protective effect on the kidneys. (Fig. 5-13)

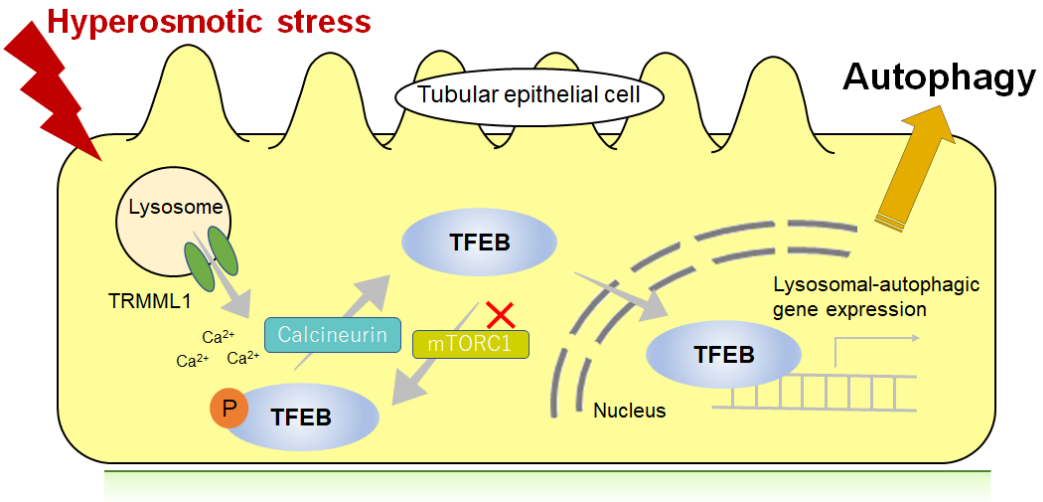

Fig. 5-13 Schematic illustration of the mechanism of hyperosmotic stress-induced autophagy. Under normal conditions, TFEB is phosphorylated and retained in the cytoplasm. During hyperosmotic stress, Ca^{2+} is released from the lysosome through TRPML1 channel, resulting in calcineurin activation which in turn dephosphorylates and activates TFEB independent of mTORC1 inhibition. Dephosphorylated TFEB can translocate from the cytoplasm to the nucleus where it activates the transcription of lysosomal-autophagic gene expression and thereby increases autophagy.

References

1. Mazure NM, Pouysségur J. Hypoxia-induced autophagy: cell death or cell survival? Current Opinion in Cell Biology. 2010;22: 177–180.
2. Galluzzi L, Pietrocola F, Levine B, Kroemer G. Metabolic control of autophagy. Cell. 2014;159: 1263–1276.
3. Russell RC, Yuan HX, Guan KL. Autophagy regulation by nutrient signaling. Cell research. 2014;24: 42–57.
4. Mehrpour M, Esclatine A, Beau I, Codogno P. Overview of macroautophagy regulation in mammalian cells. Cell research. 2010;20: 748–762.
5. Yorimitsu T, Klionsky DJ. Autophagy: molecular machinery for self-eating. Cell death and differentiation. 2005;12 Suppl 2: 1542–1552.
6. Kabeya Y, Mizushima N, Ueno T, Yamamoto A, Kirisako T, Noda T, et al. LC3, a mammalian homologue of yeast Apg8p, is localized in autophagosome membranes after processing. The EMBO journal. 2000;19: 5720–5728.
7. Ravikumar B, Sarkar S, Davies JE, Futter M, Garcia-Arencibia M, Green-Thompson ZW, et al. Regulation of mammalian autophagy in physiology and pathophysiology. Physiological reviews. 2010;90: 1383–1435.
8. Choi ME. Autophagy in Kidney Disease. Annual review of physiology. 2020;82: 297–322.
9. Sureshbabu A, Ryter SW, Choi ME. Oxidative stress and autophagy: crucial modulators of kidney injury. Redox biology. 2015;4: 208–214
10. Sureshbabu A, Patino E, Ma KC, Laursen K, Finkelsztein EJ, Akchurin O, et al. RIPK3 promotes sepsis-induced acute kidney injury via mitochondrial dysfunction. JCI insight. 2018;3: e98411.

11. Suzuki C, Isaka Y, Takabatake Y, Tanaka H, Koike M, Shibata M, et al. Participation of autophagy in renal ischemia/reperfusion injury. Biochemical and biophysical research communications. 2008;368: 100–106.

12. Koch EAT, Nakhoul R, Nakhoul F, Nakhoul N. Autophagy in diabetic nephropathy: a review. International urology and nephrology. 2020;52: 1705–1712.

13. Sardiello M, Palmieri M, Ronza A Di, Medina DL, Valenza M, Gennarino VA, et al. A gene network regulating lysosomal biogenesis and function. Science. 2009;325: 473–477.

14. Settembre C, Di Malta C, Polito VA, Arencibia MG, Vetrini F, Erdin S, et al. TFEB links autophagy to lysosomal biogenesis. Science. 2011;332: 1429–1433.

15. Settembre C, Zoncu R, Medina DL, Vetrini F, Erdin S, Erdin S, et al. A lysosome-to-nucleus signalling mechanism senses and regulates the lysosome via mTOR and TFEB. The EMBO journal. 2012;31: 1095–1108.

16. Peña-Llopis S, Vega-Rubin-De-Celis S, Schwartz JC, Wolff NC, Tran TAT, Zou L, et al. Regulation of TFEB and V-ATPases by mTORC1. The EMBO journal. 2011;30: 3242–3258.

17. Puertollano R, Ferguson SM, Brugarolas J, Ballabio A. The complex relationship between TFEB transcription factor phosphorylation and subcellular localization. The EMBO journal. 2018;37: e98804.

18. Dong XP, Cheng X, Mills E, Delling M, Wang F, Kurz T, et al. The type IV mucolipidosis-associated protein TRPML1 is an endolysosomal iron release channel. Nature. 2008;455: 992–996.

19. Shen D, Wang X, Li X, Zhang X, Yao Z, Dibble S, et al. Lipid storage disorders block lysosomal trafficking by inhibiting a TRP channel and lysosomal calcium

release. Nature communications. 2012;3: 731.

20. Zhang X, Cheng X, Yu L, Yang J, Calvo R, Patnaik S, et al. MCOLN1 is a ROS sensor in lysosomes that regulates autophagy. Nature communications. 2016;7: 12109.

21. Medina DL, Di Paola S, Peluso I, Armani A, De Stefani D, Venditti R, et al. Lysosomal calcium signalling regulates autophagy through calcineurin and TFEB. Nature cell biology. 2015;17: 288–299.

22. Havasi A, Dong Z. Autophagy and Tubular Cell Death in the Kidney. Seminars in nephrology. 2016;36: 174–188.

23. Isaka Y, Kimura T, Takabatake Y. The protective role of autophagy against aging and acute ischemic injury in kidney proximal tubular cells. Autophagy. 2011;7: 1085–1087.

24. Kimura T, Takabatake Y, Takahashi A, Kaimori JY, Matsui I, Namba T, et al. Autophagy protects the proximal tubule from degeneration and acute ischemic injury. Journal of the American Society of Nephrology : JASN. 2011;22: 902–913.

25. King JS, Veltman DM, Insall RH. The induction of autophagy by mechanical stress. Autophagy. 2011;7: 1490–1499.

26. Pietuch A, Brückner BR, Janshoff A. Membrane tension homeostasis of epithelial cells through surface area regulation in response to osmotic stress. Biochimica et biophysica acta. 2013;1833: 712–722.

27. Ciano C Di, Nie Z, Szászi K, Lewis A, Uruno T, Zhan X, et al. Osmotic stress-induced remodeling of the cortical cytoskeleton. AJP Cell physiology. 2002;283.

28. Nunes P, Ernandez T, Roth I, Qiao X, Strebel D, Bouley R, et al. Hypertonic stress promotes autophagy and microtubule-dependent autophagosomal clusters.

Autophagy. 2013;9: 550–567.

29. Zhou EH, Trepat X, Park CY, Lenormand G, Oliver MN, Mijailovich SM, et al. Universal behavior of the osmotically compressed cell and its analogy to the colloidal glass transition. Proceedings of the National Academy of Sciences of the United States of America. 2009;106: 10632–10637.

30. Kast DJ, Dominguez R. The Cytoskeleton-Autophagy Connection. Current biology. 2017;27: R318–R326.

31. Krishan S, Sahni S, Richardson DR. The anti-tumor agent, Dp44mT, promotes nuclear translocation of TFEB via inhibition of the AMPK-mTORC1 axis. Biochimica et biophysica acta Molecular basis of disease. 2020;1866: 165970.

32. Napolitano G, Esposito A, Choi H, Matarese M, Benedetti V, Di Malta C, et al. mTOR-dependent phosphorylation controls TFEB nuclear export. Nature communications. 2018;9.

33. Peña-Oyarzun D, Troncoso R, Kretschmar C, Hernando C, Budini M, Morselli E, et al. Hyperosmotic stress stimulates autophagy via polycystin-2. Oncotarget. 2017;8: 55984–55997.

34. Tamura N, Kageyama S, Komatsu M, Waguri S. Hyperosmotic Stress Induces Unconventional Autophagy Independent of the Ulk1 Complex. Molecular and cellular biology. 2019;39: e00024-19.

35. Mizushima N, Yoshimori T. How to interpret LC3 immunoblotting. Autophagy. 2007;3: 542–545.

36. Shao R, Shi J, Du K, Wang N, Cai W, Liu S, et al. Resveratrol promotes lysosomal function via ER calcium-dependent TFEB activation to ameliorate lipid accumulation. The Biochemical journal. 2021;478: 1159–1173.

37. Napolitano G, Ballabio A. TFEB at a glance. Journal of cell science. 2016;129: 2475–2481.

38. Hogan PG, Chen L, Nardone J, Rao A. Transcriptional regulation by calcium, calcineurin, and NFAT. Genes & development. 2003;17: 2205–2232.

39. Wang C, Niederstrasser H, Douglas PM, Lin R, Jaramillo J, Li Y, et al. Small-molecule TFEB pathway agonists that ameliorate metabolic syndrome in mice and extend C. elegans lifespan. Nature communications. 2017;8: 2270.

40. Wang W, Zhang X, Gao Q, Xu H. TRPML1: an ion channel in the lysosome. Handbook of experimental pharmacology. 2014;222: 631–645.

41. Medina DL. TRPML1 and TFEB, an Intimate Affair. Handbook of experimental pharmacology. 2023;278: 109–126.

42. Kume S, Yamahara K, Yasuda M, Maegawa H, Koya D. Autophagy: emerging therapeutic target for diabetic nephropathy. Seminars in nephrology. 2014;34: 9–16.

43. Li H, Peng X, Wang Y, Cao S, Xiong L, Fan J, et al. Atg5-mediated autophagy deficiency in proximal tubules promotes cell cycle G2/M arrest and renal fibrosis. Autophagy. 2016;12: 1472–1486.

44. Jiang M, Liu K, Luo J, Dong Z. Autophagy is a renoprotective mechanism during in vitro hypoxia and in vivo ischemia-reperfusion injury. The American journal of pathology. 2010;176: 1181–1192.

45. Periyasamy-Thandavan S, Jiang M, Wei Q, Smith R, Yin XM, Dong Z. Autophagy is cytoprotective during cisplatin injury of renal proximal tubular cells. Kidney international. 2008;74: 631–640.

46. Rivero F, Köppel B, Peracino B, Bozzaro S, Siegert F, Weijer CJ, et al. The role

of the cortical cytoskeleton: F-actin crosslinking proteins protect against osmotic stress, ensure cell size, cell shape and motility, and contribute to phagocytosis and development. Journal of cell science. 1996;109 (Pt 1: 2679–2691.

47. Chiang TA, Yang YL, Yang YY, Hu MH, Wu PF, Liu SF, et al. Hyperosmolarity enhanced susceptibility to renal tubular fibrosis by modulating catabolism of type I transforming growth factor-beta receptors. Journal of cellular biochemistry. 2010;109: 663–671.

48. Ly DL, Waheed F, Lodyga M, Speight P, Masszi A, Nakano H, et al. Hyperosmotic stress regulates the distribution and stability of myocardin-related transcription factor, a key modulator of the cytoskeleton. AJP Cell physiology. 2013;304: C115-C127.

49. Mózes MM, Szoleczky P, Rosivall L, Kökény G. Sustained hyperosmolarity increses TGF-ß1 and Egr-1 expression in the rat renal medulla. BMC nephrology. 2017;18: 209.

50. Plischke M, Kohl M, Bankir L, Shayganfar S, Handisurya A, Heinze G, et al. Urine osmolarity and risk of dialysis initiation in a chronic kidney disease cohort--a possible titration target? PloS one. 2014;9: e93226.

51. Aplin A, Jasionowski T, Tuttle DL, Lenk SE, Dunn WA. Cytoskeletal elements are required for the formation and maturation of autophagic vacuoles. Journal of cellular physiology. 1992;152: 458–466.

52. Aguilera MO, Berón W, Colombo MI. The actin cytoskeleton participates in the early events of autophagosome formation upon starvation induced autophagy. Autophagy. 2012;8: 1590–1603.

53. Zhuo C, Ji Y, Chen Z, Kitazato K, Xiang Y, Zhong M, et al. Proteomics analysis

of autophagy-deficient Atg7-/- MEFs reveals a close relationship between F-actin and autophagy. Biochemical and biophysical research communications. 2013;437: 482–488.

54. Mi N, Chen Y, Wang S, Chen M, Zhao M, Yang G, et al. CapZ regulates autophagosomal membrane shaping by promoting actin assembly inside the isolation membrane. Nature cell biology. 2015;17: 1112–1123.

55. Kast DJ, Zajac AL, Holzbaur ELF, Ostap EM, Dominguez R. WHAMM Directs the Arp2/3 Complex to the ER for Autophagosome Biogenesis through an Actin Comet Tail Mechanism. Current biology. 2015;25: 1791–1797.

56. Geeraert C, Ratier A, Pfisterer SG, Perdiz D, Cantaloube I, Rouault A, et al. Starvation-induced hyperacetylation of tubulin is required for the stimulation of autophagy by nutrient deprivation. The Journal of biological chemistry. 2010;285: 24184–24194.

57. Tang C, Livingston MJ, Liu Z, Dong Z. Autophagy in kidney homeostasis and disease. Nature reviews Nephrology. 2020;16: 489–508.

58. Yamamoto T, Takabatake Y, Kimura T, Takahashi A, Namba T, Matsuda J, et al. Time-dependent dysregulation of autophagy: Implications in aging and mitochondrial homeostasis in the kidney proximal tubule. Autophagy. 2016;12: 801–813.

59. Kaushal GP, Shah S V. Autophagy in acute kidney injury. Kidney international. 2016;89: 779–791.

60. Brijmohan AS, Batchu SN, Majumder S, Alghamdi TA, Thieme K, McGaugh S, et al. HDAC6 Inhibition Promotes Transcription Factor EB Activation and Is Protective in Experimental Kidney Disease. Frontiers in pharmacology. 2018;9:

34.

61. Yasuda-Yamahara M, Kume S, Maegawa H. Roles of mTOR in Diabetic Kidney Disease. Antioxidant. 2021;10: 321.

62. Paluri RK, Sonpavde G, Morgan C, Rojymon J, Mar AH, Gangaraju R. Renal toxicity with mammalian target of rapamycin inhibitors: A meta-analysis of randomized clinical trials. Oncology reviews. 2019;13: 170–174.

63. Heit JJ, Apelqvist AA, Gu X, Winslow MM, Neilson JR, Crabtree GR, et al. Calcineurin/NFAT signalling regulates pancreatic beta-cell growth and function. Nature. 2006;443: 345–349.

64. Jiang LQ, Garcia-Roves PM, De Castro Barbosa T, Zierath JR. Constitutively active calcineurin in skeletal muscle increases endurance performance and mitochondrial respiratory capacity. AJP Endocrinology and metabolism. 2010;298: E8-E16.

65. Lim H, Lim Y-M, Kim KH, Jeon YE, Park K, Kim J, et al. A novel autophagy enhancer as a therapeutic agent against metabolic syndrome and diabetes. Nature communications. 2018;9: 1438.

66. Decuypere J-P, Bultynck G, Parys JB. A dual role for Ca(2+) in autophagy regulation. Cell calcium. 2011;50: 242–250.

67. Leser C, Keller M, Gerndt S, Urban N, Chen C-C, Schaefer M, et al. Chemical and pharmacological characterization of the TRPML calcium channel blockers ML-SI1 and ML-SI3. European journal of medicinal chemistry. 2021;210: 112966.

68. Al-Bari MAA, Xu P. Molecular regulation of autophagy machinery by mTOR-dependent and -independent pathways. Annals of the New York Academy of Sciences. 2020;1467: 3–20.

69. Scotto Rosato A, Montefusco S, Soldati C, Di Paola S, Capuozzo A, Monfregola J, et al. TRPML1 links lysosomal calcium to autophagosome biogenesis through the activation of the CaMKKβ/VPS34 pathway. Nature communications. 2019;10: 5630.

70. Mccartney AJ, Zhang Y, Weisman LS. Phosphatidylinositol 3,5-bisphosphate: low abundance, high significance. BioEssays : news and reviews in molecular, cellular and developmental biology. 2014;36: 52–64.

71. Dove SK, Dong K, Kobayashi T, Williams FK, Michell RH. Phosphatidylinositol 3,5-bisphosphate and Fab1p/PIKfyve underPPIn endo-lysosome function. The Biochemical journal. 2009;419: 1–13.

72. Jin N, Mao K, Jin Y, Tevzadze G, Kauffman EJ, Park S, et al. Roles for PI(3,5)P2 in nutrient sensing through TORC1. Molecular biology of the cell. 2014;25: 1171–1185.

73. Schmiege P, Fine M, Li X. Atomic insights into ML-SI3 mediated human TRPML1 inhibition. Structure (London, England : 1993). 2021;29: 1295-1302.

Chapter 6

Concluding remarks

6.1 A review of the study aims and objectives

The purpose of this dissertation is to propose new therapeutic targets for the treatment of chronic kidney diseases (CKD) by revealing the cellular responses to hyperosmotic conditions and their mechanisms from the perspective of cell biomechanics. The author examined the effects of hyperosmotic stress on epithelial-mesenchymal transition (EMT) and autophagy of proximal tubular epithelial cells, which have been identified as key mechanisms involved in the progression and suppression of renal fibrosis. The author also investigated the molecular mechanisms of cellular hyperosmotic responses and attempted to identify key molecules that could lead to new drug targets.

6.2 Synthesis of the main findings

The main findings of this study are as follows (Fig. 6-1): Increased proximal tubular hyperosmotic stress responds to mechanical stress promotes reorganization of focal adhesions (FAs) in proximal tubular epithelial cells and induces EMT. The mechanism of EMT involves Ca^{2+} influx from outside the cell through transient receptor potential (TRP) vanilloid 4 (TRPV4) channels, which are known as mechanoreceptors. Furthermore, changes in the actin cytoskeleton induced by hyperosmotic stress are important for the induction of autophagy, a cytoprotective mechanism, and the activation of calcineurin-TFEB pathway through TRP mucolipin 1 (TRPML1) channels-mediated Ca^{2+} release from lysosomes is thought to be partly involved in the mechanism for the autophagy.

The current study on mechanisms underlying hyperosmotic responses of EMT and autophagy suggests the utility of TRPV4 and TRPML1 channels as potential therapeutic targets for renal protection.

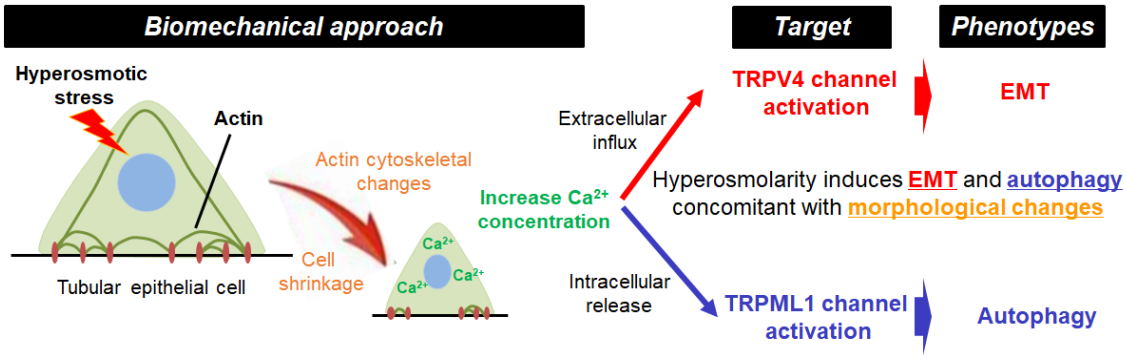

Fig. 6-1 Schematic illustration of the synthesis of the main findings.

6.3 The utility of TRPV4 and TRPML1 channels as new drug targets for CKD

The TRP protein superfamily of ion channels is important in renal physiology [1]. Several subfamilies of TRP channels including TRPC (Canonical), TRPP (Polycystin), TRPM (Melastatin), TRPV, and TRPML have been reported in different parts of nephron (Fig 6-2) [2]. TRPC1, TRPC3, TRPC5, and TRPC6 are expressed in glomeruli, and TRPC1, TRPC3, TRPC5, TRPC6, TRPP2, TRPM6, TRPV4-6, and TRPML1 are expressed in tubules. Moreover, TRPC1, TRPV4, and TRPML1 are expressed in proximal tubules. The distinct distribution of these cation channels along the nephron supports their importance in the regulation of many renal physiological processes.

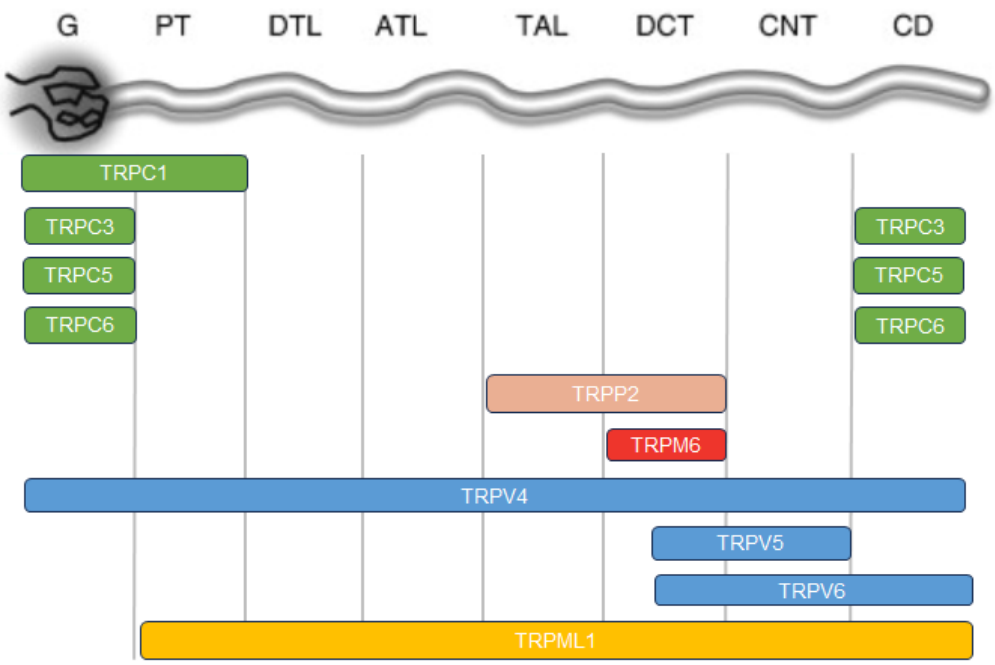

Fig. 6-2 Distribution of TRP channels along the nephron (Modified from Hsu et al., 2007 [2]). Abbreviations: G, glomerulus; PT, proximal tubules; DTL, descending thin limb; ATL, ascending thin limb; TAL, thick ascending limb, DCT, distal convoluted tubule; CNT, connecting tubule; CD, collecting duct.

Several TRP channels are known to be involved in renal disease (Table 6-1). TRPC6 expression is significantly increased in renal fibrosis mouse models [3], and the knockdown of TRPC6 significantly reduced glomerular sclerosis but did not affect tubulointerstitial inflammation and fibrosis [4,5]. The beneficial effects of TRPC5 blockers on renal disease models reveal TRPC5 as a tractable therapeutic target for focal and segmental glomerulosclerosis (FSGS), a common cause of renal failure [6]. In addition, genetics point to two additional TRP channels as plausible therapeutic targets: TRPP2 in autosomal dominant polycystic kidney disease (ADPKD) [7], and TRPM6 in familial hypomagnesemia with secondary hypocalcemia (HSH) [8,9].

Table 6-1 TRP channels related to kidney diseases

Isoform	Proposed function in kidney	Kidney diseases
TRPC5/6	Regulate slit diaphragm function and permeability to protein	FSGS
TRPP2	Interaction with each TRPP1 channels as mechanoreceptors	ADPKD
TRPM6	Renal Mg^{2+} reabsorption	HSH

Abbreviations: FSGS, focal segmental glomerulosclerosis; ADPKD, autosomal dominant polycystic kidney disease; HSH, hypomagnesemia with secondary hypocalcemia

The current status of drug development targeting TRPV4 channels is shown in Table 6-2. The most advanced drug in development for diabetic macular edema is in clinical phase I. However, there are no drugs that target for kidney disease. TRPV4 channels are widely expressed in various renal cells, including renal tubular epithelial cells and endothelial cells [2]. A previous study reported that using an ischemia-reperfusion-induced acute kidney injury model of the renal tubules, serum creatinine levels, that reflect damage to the kidneys, were higher in $trpv4^{-/-}$, as compared to the wild-type animals [10]. Thus, the results of this study suggested that TRPV4 could play a protective role against acute kidney injury. In this study, I showed that TRPV4 activation in response to hyperosmotic stress is one of the mechanisms underlying EMT of proximal tubular epithelial cells. The findings suggest that TRPV4 channels could be useful therapeutic targets for controlling the progression of EMT-mediated renal disease. Further studies will be needed to examine the effects of TRPV4 channels in other nephropathy models to determine whether TRPV4 channel inhibitors can be used in kidney disease in general.

Table 6-2 Development status of TRPV4 channel inhibitor

Originator Company	Active Indications	Status	Technologies	Ref
GlaxoSmithKline Inc	Diabetic macular edema	Phase 1	Small molecule	[11]
GlaxoSmithKline Inc	Pulmonary edema	Preclinical	Small molecule	[12]
AsahiKasei Pharma	Osteoarthritis	Preclinical	Small molecule	[13]
AdAlta Pty Ltd	Unidentified indication	Preclinical	Humanized antibody	[14]

TRPML1 is a lysosomal Ca^{2+} channel involved in the regulation of lysosomal function and intracellular trafficking [15]. To date, there are no reports of clinical trials using TRPML1 channels as a therapeutic target. One reason is that despite the understanding that organelles can play their functions and form a network of organelle interactions in various diseases, drug delivery targeting the organelle has been a research challenge [16]. A drug delivery system that can efficiently deliver drugs to TRPML1-expressing lysosomes may be needed. On the other hand, basic findings on the association between TRPML1 and kidney diseases are being reported.

Ca^{2+} released through TRPML1 channels induces nuclear translocation of TFEB and initiates transcription of lysosomal and autophagy genes [17,18]; TRPML1 and TFEB form a positive feedback loop [18,19]. A previous study reported the reduction in TFEB mRNA and protein levels in the tubulointerstitium in individuals with diabetic kidney disease in comparison to individuals without diabetes and with normal kidney function [20]. According to another study, inadequate renal autophagy was observed histologically in diabetic patients with massive proteinuria, but not in patients with no or minimal proteinuria [21]. In this study, I showed that TRPML1 activation in response to hyperosmotic stress is one of the mechanisms underlying autophagy of proximal tubular epithelial cells. Taken together, I believe that developing drugs that modulate TRPML1 activity or restore its function could have therapeutic potential for renal diseases

associated with autophagy and lysosomal dysfunction. However, it is important to note that TRPML1 is a complex channel with multiple functions, and its precise roles in various renal diseases are still being elucidated. Further research is necessary to determine the therapeutic potential and safety of targeting TRPML1 for renal diseases.

In conclusion, this study conducted from a biomechanical perspective has revealed a novel therapeutic target for the treatment of kidney disease. By investigating the hyperosmotic stress exerted on proximal tubular cells, the author identified the involvement of the TRPV4 and TRPML1 channels in mechanotransduction and cellular response. I believe that the results of this dissertation open up possibilities of targeted interventions to treat CKD by modulating the activity of TRPV4 and TRPML1 channels.

6.4 Limitations of this study

The primary strength of this dissertation is that the author focused on cell biomechanics, which is a different viewpoint from most pharmacological studies, and was able to propose new drug targets for kidney disease. However, there are several limitations.

First, because these were *in vitro* experiments, their experiments typically lack the physiological context that is present in living tissues and organs. The absence of other organ systems, blood circulation, immune responses, and neuronal interactions can limit the understanding of how drugs or biomechanical factors might behave in the context of a whole organism. Additionally, cells in the body are influenced by a variety of factors, including signals from neighboring cells, communication through chemical signaling molecules, and physical forces. *In vitro* experiments often overlook these intricate interactions, which can impact the behavior and response of cells or tissues to drugs or biomechanical stimuli. To overcome this limitation, further studies are needed to evaluate

the potential of the targets *in a* physiological context, such as animal models.

Second, although EMT and autophagy are complex and systemic, the present study investigated only one aspect of the phenomena. For instance, I used only E-cadherin, α-SMA, and LC3 as markers of EMT and autophagy, but the phenomena are regulated by multiple signaling pathways and involve the activation or suppression of numerous genes and proteins. In addition, the localization of LC3-positive puncta has not been confirmed. Investigation of the relationship between the localization of LC3 and the dynamics of the cytoskeleton can further elucidate the mechanism underlying the effects of cytoskeletal changes on autophagy. A systematic analysis of the other markers can capture the diverse aspects of these processes and lead to a more comprehensive understanding of hyperosmotic stress-induced these processes. Nevertheless, the present results are potentially important that the hyperosmolarity-induced cytoskeletal changes may trigger the induction of this phenomenon. Investigating the effects of hyperosmolarity on the changes in intracellular contraction forces can further elucidate the mechanism underlying the effects of cytoskeletal changes on pathogenesis.

Third, the current study focused on mechanisms of EMT and autophagy and proposed TRPV4 and TRPML1 channels as potential therapeutic targets, respectively, but no analysis was performed for the relationship between EMT (TRPV4 channel) and autophagy (TRPML1 channel). A previous study has shown that autophagy induced by rapamycin, an mTOR inhibiter, can alleviate renal fibrosis by inhibiting EMT in obstructive nephropathy fibrosis [22]. For instance, it would be very interesting to examine the effect of autophagy induced by TRPML1 activation on TRPV4-mediated EMT.

References

1. Woudenberg-Vrenken TE, Bindels RJM, Hoenderop JGJ. The role of transient receptor potential channels in kidney disease. Nature reviews Nephrology. 2009;5: 441–449.
2. Hsu Y-J, Hoenderop JGJ, Bindels RJM. TRP channels in kidney disease. Biochimica et biophysica acta. 2007;1772: 928–936.
3. Wu Y-L, Xie J, An S-W, Oliver N, Barrezueta NX, Lin M-H, et al. Inhibition of TRPC6 channels ameliorates renal fibrosis and contributes to renal protection by soluble klotho. Kidney international. 2017;91: 830–841.
4. Kim EY, Shotorbani PY, Dryer SE. TRPC6 inactivation does not affect loss of renal function in nephrotoxic serum glomerulonephritis in rats, but reduces severity of glomerular lesions. Biochemistry and biophysics reports. 2019;17: 139–150.
5. Kim EY, Dryer SE. Effects of TRPC6 Inactivation on Glomerulosclerosis and Renal Fibrosis in Aging Rats. Cells. 2021;10: 856.
6. Zhou Y, Castonguay P, Sidhom E-H, Clark AR, Dvela-Levitt M, Kim S, et al. A small-molecule inhibitor of TRPC5 ion channels suppresses progressive kidney disease in animal models. Science. 2017;358: 1332–1336.
7. Wu G, Somlo S. Molecular genetics and mechanism of autosomal dominant polycystic kidney disease. Molecular genetics and metabolism. 2000;69: 1–15.
8. Schlingmann KP, Weber S, Peters M, Niemann Nejsum L, Vitzthum H, Klingel K, et al. Hypomagnesemia with secondary hypocalcemia is caused by mutations in TRPM6, a new member of the TRPM gene family. Nature genetics. 2002;31: 166–170.

9. Walder RY, Landau D, Meyer P, Shalev H, Tsolia M, Borochowitz Z, et al. Mutation of TRPM6 causes familial hypomagnesemia with secondary hypocalcemia. Nature genetics. 2002;31: 171–174.

10. Mannaa M, Markó L, Balogh A, Vigolo E, N'diaye G, Kaßmann M, et al. Transient Receptor Potential Vanilloid 4 Channel Deficiency Aggravates Tubular Damage after Acute Renal Ischaemia Reperfusion. Scientific reports. 2018;8: 4878.

11. Pero JE, McAtee JJ, Behm DJ, Briand J, Graczyk-Millbrandt G, Erhard K, et al. Identification, Synthesis, and Characterization of a Major Circulating Human Metabolite of TRPV4 Antagonist GSK2798745. ACS medicinal chemistry letters. 2021;12: 1498–1502.

12. Thorneloe KS, Cheung M, Bao W, Alsaid H, Lenhard S, Jian M-Y, et al. An orally active TRPV4 channel blocker prevents and resolves pulmonary edema induced by heart failure. Science translational medicine. 2012;4: 159ra148.

13. Atobe M, Nagami T, Muramatsu S, Ohno T, Kitagawa M, Suzuki H, et al. Discovery of Novel Transient Receptor Potential Vanilloid 4 (TRPV4) Agonists as Regulators of Chondrogenic Differentiation: Identification of Quinazolin-4(3 H)-ones and in Vivo Studies on a Surgically Induced Rat Model of Osteoarthritis. Journal of medicinal chemistry. 2019;62: 1468–1483.

14. Squitti R, Reale G, Tondolo V, Crescenti D, Bellini S, Moci M, et al. Imbalance of Essential Metals in Traumatic Brain Injury and Its Possible Link with Disorders of Consciousness. International journal of molecular sciences. 2023;24: 6867.

15. Pryor PR, Reimann F, Gribble FM, Luzio JP. Mucolipin-1 is a lysosomal membrane protein required for intracellular lactosylceramide traffic. Traffic (Copenhagen, Denmark). 2006;7: 1388–1398.

16. Sakhrani NM, Padh H. Organelle targeting: third level of drug targeting. Drug design, development and therapy. 2013;7: 585–599.

17. Medina DL, Ballabio A. Lysosomal calcium regulates autophagy. Autophagy. 2015;11: 970–971.

18. Medina DL, Di Paola S, Peluso I, Armani A, De Stefani D, Venditti R, et al. Lysosomal calcium signalling regulates autophagy through calcineurin and TFEB. Nature cell biology. 2015;17: 288–299.

19. Settembre C, Di Malta C, Polito VA, Arencibia MG, Vetrini F, Erdin S, et al. TFEB links autophagy to lysosomal biogenesis. Science. 2011;332: 1429–1433.

20. Brijmohan AS, Batchu SN, Majumder S, Alghamdi TA, Thieme K, McGaugh S, et al. HDAC6 Inhibition Promotes Transcription Factor EB Activation and Is Protective in Experimental Kidney Disease. Frontiers in pharmacology. 2018;9: 34.

21. Tagawa A, Yasuda M, Kume S, Yamahara K, Nakazawa J, Chin-Kanasaki M, et al. Impaired Podocyte Autophagy Exacerbates Proteinuria in Diabetic Nephropathy. Diabetes. 2016;65: 755–767.

22. Zhang B, Ru F, Chen X, Chen Z. Autophagy attenuates renal fibrosis in obstructive nephropathy through inhibiting epithelial-to-mesenchymal transition. Zhong Nan Da Xue Xue Bao Yi Xue Ban. 2021;46: 601–608.

Acknowledgment

This research was performed at Department of Mechanical Systems Engineering, Graduate School of Systems Design, Tokyo Metropolitan University, from April 2019 to August 2023. This work was partly supported by Grants-in-Aid for Scientific Research by the MEXT of Japan (No. 17H0277, 18H03521, 18K19934, and 22K19898), Tokyo Metropolitan Government Advanced Research Grant (R2-2), and TMU Research Project for Emergent Future Society.

First of all, I would like to express my deepest gratitude to the dissertation supervisor Assoc. Prof. Naoya Sakamoto of Graduate School of Systems Design, Tokyo Metropolitan University, for their guidance, support, and expertise throughout the entire duration of my doctoral research. His invaluable insights and constructive feedback have significantly shaped this dissertation.

I am indebted to the members of my dissertation committee, Prof. Jiro Nagatomi (Department of Bioengineering, Clemson University), Prof. Hiromichi Fujie (Department of Mechanical Systems Engineering, Tokyo Metropolitan University), and Assoc. Prof. Hiromi Miyoshi (Department of Mechanical Systems Engineering, Tokyo Metropolitan University), for their time, expertise, and valuable feedback. Their rigorous examination and constructive comments have greatly enhanced the quality and rigor of this work. I am thankful for their dedication to my academic growth.

I would like to acknowledge the contributions of my research collaborators and colleagues, Atsushi Suzuki, Yuki Taninaka, and Hisaaki Konta (Tokyo Metropolitan University), for their valuable insights, collaboration, and stimulating discussions. Their expertise and shared passion for the field have been instrumental in shaping my research and broadening my understanding.

The last, but not the least, I extend my deepest appreciation to my family for their unwavering support, encouragement, and understanding throughout this demanding journey.

Takashi Miyano

Tokyo, Japan, August, 2023